Supplementary Materials

LanD-like Flavoproteins Catalyze Aminovinyl-Cysteine Formation through Oxidative Decarboxylation and Cyclization of a Peptide at the C-Terminus

Jingyu Liu[1,#], Yanping Qiu[1,#], Tao Fu[1,#], Miao Li[1], Yuqing Li[1,2], Qian Yang[1], Zhijun Tang[1], Haoyu Tang[1], Guangyu Li[4], Lifeng Pan[1,*] and Wen Liu[1,2,3,*]

[1] State Key Laboratory of Bioorganic and Natural Products Chemistry, Center for Excellence in Molecular Synthesis, Shanghai Institute of Organic Chemistry, University of Chinese Academy of Sciences, 345 Lingling Road, Shanghai 200032, China;

[2] Department of Chemistry, Shanghai Normal University, 100 Guiling Road, Shanghai 200032, China;

[3] Huzhou Center of Bio-Synthetic Innovation, 1366 Hongfeng Road, Huzhou 313000, China.

[4] Nuclear Magnetic Resonance (NMR) Facility, Shanghai Institute of Organic Chemistry, University of Chinese Academy of Sciences, 345 Lingling Road, Shanghai 200032, China

* To whom correspondence should be addressed: Shanghai Institute of Organic Chemistry, Chinese Academy of Sciences, 345 Lingling Rd., Shanghai 200032, China. Lifeng Pan, Email: panlf@sioc.ac.cn, Tel: 86-21-54925561; Wen Liu, Email: wliu@sioc.ac.cn, Tel: 86-21-54925111, Fax: 86-21-64166128.

[#] These authors contributed to this work equally.

Supplementary Methods

1.1 General Materials and Methods.

1.2 Protein Expression and Purification.

1.3 *In vitro* Assays of LanD-like Flavoprotein Activity.

1.4 Peptide Purification and Characterization

1.5 Protein crystallization and related structural elucidation.

1.6 Chemical synthesis of **7-Dha19**.

Supplementary Figures

Supplementary Figure 1. Alignment of the biosynthetic gene clusters of TVAs, CYP and EPI.

Supplementary Figure 2. Purified recombinant enzymes and cofactor analysis.

Supplementary Figure 3. Summary of LanD-like flavoprotein-catalyzed transformations in this study.

Supplementary Figure 4. HPLC-MS analysis of enethiol intermediates and associated shunt aldehyde derivatives in the $TvaA_{S\text{-}87}$-catalyzed conversions of **1** and its variants.

Supplementary Figure 5. Characterization of (ene)thiol and aldehyde peptides in the $TvaF_{S\text{-}87}$-catalyzed conversion of **1** by chemical derivatization.

Supplementary Figure 6. HPLC-MS analysis of enethiol intermediates and associated shunt aldehyde derivatives in the CypD-catalyzed conversions of **7** and its variants.

Supplementary Figure 7. Characterization of (ene)thiol peptides in the CypD-catalyzed conversion of **7** by chemical derivation.

Supplementary Figure 8. 2D-TOCSY f2-slices at related f1 experiments (600 MHz, DMSO-d_6) for residue identification in **7-III**.

Supplementary Figure 9. Overall structural comparison of the monomers of $TvaF_{S\text{-}87}$, CypD, MrsD and the EpiD complex (shown by ribbon diagram).

Supplementary Figure 10. FMN binding interface in the $TvaF_{S\text{-}87}$ structure.

Supplementary Figure 11. FAD binding interface in the CypD structure.

Supplementary Figure 12. Structure-based sequence alignment of CypD, EpiD and $TvaF_{S\text{-}87}$.

Supplementary Figure 13. Structural and biochemical analyses of the binding interface between two trimeric units of the $TvaF_{S\text{-}87}$ dodecamer.

Supplementary Figure 14. Structural analysis of the binding interface between two trimeric subunits of the CypD dodecamer.

Supplementary Figure 15. Structural analysis of the CypD monomer in the CypD complex with the peptide substrate **8**.

Supplementary Figure 16. Structural analysis of the substrate-binding pockets of CypD dodecamer.

Supplementary Figure 17. Structural comparison of the CypD complex and the EpiD H67N mutant complex.

Supplementary Figure 18. *In vitro* assays of CypD activity using the substrates, **7**, **7-C19S** and **7-C19S-D_3**.

Supplementary Figure 19. Characterization of Dha-containing peptides in the CypD-catalyzed conversion of **7-Dha** by chemical derivation.

Supplementary Figure 20. Comparison of the enzymatic activities of CypD with its variants based on examination of the production of **7-I**, **7-II** and **7-III**.

Supplementary Tables

Supplementary Table 1. Related bacterial strains and plasmids used in this study.

Supplementary Table 2. Primers used in this study.

Supplementary Table 3. Gene sequences of *cypD*, *tvaF*$_{S\text{-}87}$, and *3c*.

Supplementary Table 4. HR-MS and HR-MS/MS Data collection of all compounds analyzed in this study.

Supplementary Table 5. The ^{1}H and ^{13}C NMR data of **7** in DMSO-d_6.

Supplementary Table 6. Key data in the 2D-TOCSY f2-slice at f1 experiments.

Supplementary Table 7. Statistics of X-ray crystallographic data collection and model refinements of TvaF$_{S\text{-}87}$ and CypD in their apo-forms.

Supplementary Table 8. Statistics of X-ray crystallographic data collection and model refinement of CypD in complex with **8**.

Supplementary References

Supplementary Methods

1.1 General Materials and Methods

Materials, bacteria strains and plasmids. Biochemicals and media were purchased from Sinopharm Chemical Reagent Co., Ltd. (China), Oxoid Ltd. (U.K.) or Sigma-Aldrich Corporation (USA) unless otherwise stated. Restriction endonucleases were purchased from Thermo Fisher Scientific Co. Ltd. (USA). Chemical reagents were purchased from standard commercial sources. Synthetic peptides were purchased from Genscript Biotech (Nanjing, China). Related bacterial strains and plasmids are summarized in **Supplementary Table 1**. Primers used in this study are listed in **Supplementary Table 2**.

DNA isolation, manipulation, and sequencing. DNA isolation and manipulation in *Escherichia coli* or *Streptomyces* strains were carried out according to standard methods[1]. PCR amplifications were carried out on an Applied Biosystems Veriti™ Thermal Cycler either using Taq DNA polymerase (Vazyme Biotech Co. Ltd, China) for routine genotype verification or PrimeSTAR HS DNA polymerase (Takara Biotechnology Co., Ltd. Japan) for high fidelity amplification. The synthesis of primers and genes were performed at Shanghai Sangon Biotech Co., Ltd. (China). DNA sequencing was performed at Shanghai Biosune Biotech Co., Ltd. (China).

Sequence analysis. Biosynthetic gene clusters (BGCc) were mined from microbial genomes using the AntiSMASH web tool[2]. Open reading frames (ORFs) were identified using the FramePlot 4.0beta program (http://nocardia.nih.go.jp/fp4/)[3]. The deduced proteins were compared with other known proteins in the databases using available BLAST methods (http://blast.ncbi.nlm.nih.gov/Blast.cgi)[4]. Amino acid sequence alignments were performed using Vector NT1 and ESPript 3.0 (http://espript.ibcp.fr/ESPript/ESPript/)[5].

Chemical analysis. Analysis and semi-preparation by High Performance Liquid Chromatography (HPLC) were carried out on an Agilent 1260 HPLC system (Agilent Technologies Inc., USA). Analyses by HPLC-associated Electrospray ionization Mass Spectrometer (ESI-MS) and ESI-high resolution MS (ESI-HR-MS) were performed on a Thermo Fisher LTQ XL ESI-MS spectrometer and a Q Exactive™ Plus Mass Spectrometer (Thermo Fisher Scientific Inc., USA), respectively. Related data were processed using Thermo Xcalibur software. NMR data were recorded on a Bruker AV500 spectrometers (Bruker Co. Ltd., Germany) or on an Agilent PremiumCompact+ 500MHz NMR spectrometer (Agilent Technologies Inc., USA).

1.2 Protein Expression and Purification

Construction and overexpression in *E. coli*. The gene *tvaF*$_{S-87}$ was amplified from the genome of *S.* sp. NRRL S-87 by PCR using the primer pair *tvaF*$_{S-87}$-for/ *tvaF*$_{S-87}$ -rev, in contrast to the gene *cypD*, which was synthesized by Genscript Biotech (Nanjing, China). The gene *tvaF*$_{S-87}$ and *cypD* were cloned individually into pRSFDuet-1 for the expression of the recombinant proteins TvaF$_{S-87}$ and CypD, each of which is tagged by Thioredoxin (TRX) and 6xHis at N-terminus. To prepare the variants of TvaF$_{S-87}$, i.e., TvaF$_{S-87}$-H85A, TvaF$_{S-87}$ -V28D, and TvaF$_{S-87}$-M62D, and the variants of CypD, i.e., CypD-S20A, CypD-S20D, CypD-L23A, CypD-L23Q, CypD-F170A, CypD-F170Q, CypD-H59D, CypD-H59A, CypD-H29R, CypD-H29A, CypD-N80H and CypD-N80D by Site-specific mutagenesis, the Rolling-cycle PCR amplification of each pRSFDuet-1 derivative that contains *tvaF*$_{S-87}$ or *cypD* was conducted by using corresponding primers, and subsequent *Dpn*I digestion was performed according to the standard procedure of the QuickChange Site-Directed Mutagenesis Kit purchased from Stratagene (GE Healthcare, USA) and Multi Express™ II (Vazyme Biotech Co., Ltd., China). For N-terminal tag removal, the protease-encoding gene *3c* was synthesized by Genscript Biotech (Nanjing, China), and cloned into pET28a(+) for the expression of the recombinant 3C protein.

The above derivatives of pRSFDuet-1 and pET28a(+) were introduced into *E. coli* BL21(DE3) individually. The culture of each resulting recombinant *E. coli* strain was incubated in Luria-Bertani (LB) medium (5 g of yeast extract, 10 g of tryptone and 10 g of NaCl per liter) containing 50 μg/mL kanamycin at 37°C and 250 rpm until the cell density reached 0.6-0.8 at OD_{600}. Protein expression was induced by the addition of isopropyl-β-D-thiogalactopyranoside (IPTG) to a final concentration of 0.1 mM, followed by further incubation for 25-30 hr at 25°C or 16°C. The cells were harvested by centrifugation at 3000 × g for 20 min, flash-frozen and then stored at -80°C.

Purification and characterization. *E. coli* cells were re-suspended in lysis buffer (137 mM NaCl, 2.7 mM KCl, 10 mM Na_2HPO_4, 1.8 mM KH_2PO_4, 10% glycerol and 5 mM imidazole, pH 8.0). After disruption by FB-110X Low Temperature Ultra-Pressure Continuous Flow Cell Disrupter (Shanghai Litu Mechanical Equipment Engineering Co., Ltd, China), soluble fractions were collected by centrifugation. Recombinant proteins that contain a 6xHis-tag were purified on a HisTrap HP column (GE Healthcare, USA), which was pre-treated with 10 column volumes (CVs) of lysis buffer followed by 10 CVs of wash buffer (137 mM NaCl, 2.7 mM KCl, 10 mM Na_2HPO_4, 1.8 mM KH_2PO_4, 10% glycerol and 40 mM imidazole, pH 7.4), using elution buffer (137 mM NaCl, 2.7 mM KCl, 10 mM Na_2HPO_4, 1.8 mM KH_2PO_4, 10% glycerol and 250 mM imidazole, pH 7.4). Desired protein fractions were concentrated (to 500 μM-1 mM) using Amicon® Ultra-15 Centrifugal Filter Devices (MILLIPORE, USA) and desalted using a PD-10 Desalting Column (GE Healthcare, USA) according to the manufacturer's protocols, and then quantified in concentration by Bradford assay using

bovine serum albumin as the standard.

The purity of recombinant proteins was determined by sodium dodecyl sulfate polyacrylamide gel electrophoresis (SDS-PAGE). For the determination of the flavin cofactor associated with $TvaF_{S-87}$ and CypD, The UV spectra of recombinant proteins were recorded at a concentration of 30 mg/mL on a DeNovix DS-11 UV/Vis spectrophotometer (DeNovix Inc. Wilmington, DE 19810 USA). Each protein solution was incubated at 100˚C for 5 min for denaturation and then subjected to HR-ESI-MS analysis on a 6230B Accurate Mass TOF LC/MS System (Agilent Technologies Inc., USA) to examine the presence of FMN ($[M+H]^+$ *m/z* calcd. 457.1124; observed 457.1108 from the $TvaF_{S-87}$) and the presence of FAD ($[M+H]^+$ *m/z* calcd. 786.1644; observed 786.1647 from the CypD sample).

1.3 *In vitro* Assays of LanD-like Flavoprotein Activity

Transformations of synthetic peptides. Each conversion was conducted at 30°C for 2 or 5 hr in 60 μL of the reaction mixture that contained 100 μM (or 30 μM) synthetic peptide and 30 μM (or 10 μM) N-terminally TRX-tagged $TvaF_{S-87}$ (or its variant) or CypD (or its variant) along with 50 mM Tris-HCl (pH 8.5), 10 mM TCEP, 5 μM FMN or FAD and 1 μM 3C. Conversions were quenched by adding equal volumes of acetonitrile, and after centrifugation, reaction mixtures were subjected to HPLC-HR-MS and HR-MS/MS analyses. For (ene)thiol determination, 16 μL of each quenched reaction mixture was treated with *N*-ethylmaleimide (NEM) in dark at room temperature for 30 min before 2 μL of 1 M dithiothreitol (DTT) was added to eliminate excessive NEM and prevent side reactions. For aldehyde determination, 16 μL of each quenched reaction mixture was treated with 200 mM 1-(2-hydrazinyl-2-oxoethyl) pyridin-1-ium chloride (HOPI) in dark at 37°C for 2 hr.

HPLC-HR-MS and HR-MS/MS analyses. Reaction mixtures were subjected to HPLC-HR-MS and HR-MS/MS analyses after centrifugation. For HPLC-HR-MS analysis, an Agilent ZORBAX column (300SB-C18, 2.1 mm × 100 mm, 3.5 μm, Agilent Technologies Inc., USA) or an Agilent 300Extend-C18 column (2.1 mm × 100 mm, 3.5 μm, Agilent Technologies Inc., USA) was used on an UltiMate 3000 UHPLC system coupled to a Thermo Scientific Q Exactive Plus Orbitrap mass spectrometer. Gradient elusion was conducted using solvent A (H_2O + 0.1% formic acid) and solvent B (acetonitrile + 0.1% formic acid) with a flow rate of 0.3 mL/min over a 43 min period as follows: T = 0 min, 10% B; T = 2 min, 10% B; T = 20 min, 30% B; T = 25 min, 60% B; T = 30 min, 100% B; T = 35 min, 100% B; T = 38 min, 10% B; and T = 43 min, 10% B. Unless otherwise stated, ESI-MS was performed in positive ion mode, with a spray voltage of 3800 V, a capillary temperature of 375 °C, aux gas heater temperature 350 °C and an S-lens level 60. Full MS was examined at a resolution of 70,000 (AGC target 2e5, maximum IT 50 ms, range 300–1000 or 400-1800 m/z).

Parallel reaction monitoring (PRM) or data-dependent MS^2 was performed at a resolution of 35,000 (AGC target between 1e5 and 1e6, maximum IT between 100 ms and 250 ms, isolation windows in the range of 1.0 to 2.0 m/z) using a stepped NCE of 18, 20 and 28 or an NCE of 25. Scan ranges, inclusion lists, charge exclusions, and dynamic exclusions were adjusted as needed.

1.4 Peptide Purification and Characterization

Production and isolation of 7-III. The *in vitro* enzymatic transformation of **7** into **7-III** was carried out as described above. Each 500 μL of the reaction mixture was then applied to a Thermo C18 HyperSep cartridge coupled with a Vacuum Extraction Manifold system (Agilent Technologies Inc., USA). This cartridge was equilibrated with ACN and the ACN solution (5%) containing 0.1% formic acid. After washing with the same ACN solution to remove polar contaminants and elution with the ACN solution (40%) containing 0.1% formic acid, the collection was freeze-dried using a freeze dryer (Martin Christ Inc., Germany). Further purification was conducted by RP-HPLC on a Agilent ZORBAX column (250 × 4.6 mm, 5 μm, Agilent Technologies Inc., USA) by gradient elution of solvent A (H_2O + 0.01% formic acid) and solvent B (acetonitrile + 0.01% formic acid) with a flow rate of 1 mL/min over a 35 min period as follows: T = 0 min, 15% B; T = 3 min, 15% B; T = 20 min, 60% B; T = 25 min,100% B; T = 30 min, 100% B; and T = 35 min, 15% B (λ at 202 nm). After lyophilization, the collection was subject to HPLC-HR-MS and HR-MS/MS analyses under conditions as described above.

Structural characterization of 7-III. For comparison, the synthetic peptide substrate **7** (Genscript Biotech, Nanjing, China) was subjected to spectral analysis. **7** was obtained as a white amorphous powder: HR-ESI-MS (positive mode) *m/z* $[M+H]^+$, calcd. 795.3739 for $C_{32}H_{58}N_8O_{11}S_2$, obs. 795.3726; ^1H and ^{13}C NMR data (600 and 150 MHz, respectively, recorded in DMSO-d_6), see **Supplementary Table 5**. Clearly, the structure of **7** is characterized as the sequence **G**1-**S**2-**T**3-**I**4-**C**5-**L**6-**V**7-**C**8.

HR-ESI-MS established the molecular formula of **7-III** as $C_{31}H_{54}N_8O_9S$ (*m/z* $[M+H]^+$, calcd. 715.3808, obs. 715.3805). ^1H NMR data of **7-III** were recorded in DMSO-d_6. For structural comparison, the slice spectra from 2D TOCSY were collected using a previously established TOCSY method[6-12], to identify the six residues (i.e., **G**1, **S**2, **T**3, **I**4, **L**6 and **V**7) that are identical to those in **7** and the newly formed AviCys residue that is derived from the two residues **C**5 and **C**8 of **7**. The key signals of each residue (i.e., **S**2, **T**3, **I**4, **L**6, **V**7 or AviCys) were observed according to the 2D-TOCSY f2-slice at the related f1 experiment (S**upplementary Figures 8** and **Supplementary Table 6**). Specifically, a pair of olefin protons were observed by irritating –NH (H) of the 2-aminovinyl group of the AviCys residue. Together with $^3J_{H1/H2}$ = 7.3 Hz ($^3J_{H2/H1}$ = 7.3 Hz), the existence of the vinyl group with a *Z* configuration was indicated by the topspin software (https://www.bruker.com/service/support-upgrades/).

1.5 Protein Crystallization and Structural Elucidation

Size exclusion chromatography coupled with multi-angle light scattering (SEC-MALS). SEC-MALS experiments were performed on a dynamic light scattering detector (DynaPro NanoStar, Wyatt), a static light scattering detector (DAWN HELLOS-II, Wyatt), and a differential refractive index detector (Optilab T-rEX, Wyatt) coupled with an AKTA pure system (GE Healthcare) at 25°C. All the protein samples (concentration above 3 mg/ml) were filtered and loaded into a Superdex 200 Increase 10/300 GL column pre-equilibrated by the buffer containing 20 mM Tris-HCl (pH 7.5), 100 mM NaCl, and 1 mM DTT overnight. The data was analyzed by ASTRA software (version 7.1) and further output to the Origin 9.0 software and aligned with each other.

Protein crystallization and structural elucidation. Crystals of seleno-methionine labeled $TvaF_{S\text{-}87}$ and CypD, CypD fusion proteins were obtained using the sitting-drop vapor-diffusion method at 16°C. Specifically, the freshly purified seleno-methionine labeled $TvaF_{S\text{-}87}$ protein (20 or 10 mg/ml in 20 mM Tris-HCl, 100 mM NaCl, 1 mM DTT, 1 mM EDTA at pH 7.5) was mixed with equal volume of reservoir solution containing 0.1 M amino acids (0.2 M L-Na-Glutamate, 0.2 M Alanine (racemic), 0.2 M Glycine, 0.2 M Lysine HCl (racemic), 0.2 M Serine (racemic)); 0.1 M buffer system at pH 8.5 (Tris (base), Bicine); 50% precipitant mix 3 (40% Glycerol, 20% PEG4000). While, crystals of seleno-methionine labeled CypD and CypD fusion protein (20 or 10 mg/ml in 20 mM Tris-HCl, 100 mM NaCl, 1 mM DTT, 1 mM EDTA at pH 7.5) were grown from 1.8 M Ammonium sulfate, 0.1 M BIS-TRIS pH 6.5, 2% v/v Polyethylene glycol monomethyl ether 550, and 0.15 M DL-Malic acid at pH 7.0, 0.1 M Imidazole at pH 7.0, 22% v/v Polyethylene glycol monomethyl ether 550, respectively. Before diffraction experiments, appropriate glycerol with FAD was added as the cryo-protectant. X-ray data sets were collected at the beamline BL17U1 or BL19U1 of the Shanghai Synchrotron Radiation Facility[13]. The diffraction data were processed and scaled using HKL2000[14].

The phase problems of $TvaF_{S\text{-}87}$ and CypD were solved by single wavelength anomalous diffraction (SAD) method. The phase problem of CypD fusion protein was solved by the molecular replacement method using the structure of CypD with PHASER[15]. The initial structural model was rebuilt manually using COOT[16], and then refined using REFMAC[17] or PHENIX[18]. Further manual model building and adjustment were completed using COOT[16]. The qualities of the final model were validated by MolProbity[19]. The final refinement statistics of solved structures in this study were listed in **Supplementary Tables 7 and 8**. All the structural diagrams were prepared using the program PyMOL (http://www.pymol.org/). Atomic coordinates and structural factors for the reported crystal structures of $TvaF_{S\text{-}87}$ and CypD are deposited in the Protein Data Bank under the accession numbers 6KTP, 6KTT, 6KTI, and 6KT9.

1.6 Chemical synthesis of 7-Dha19

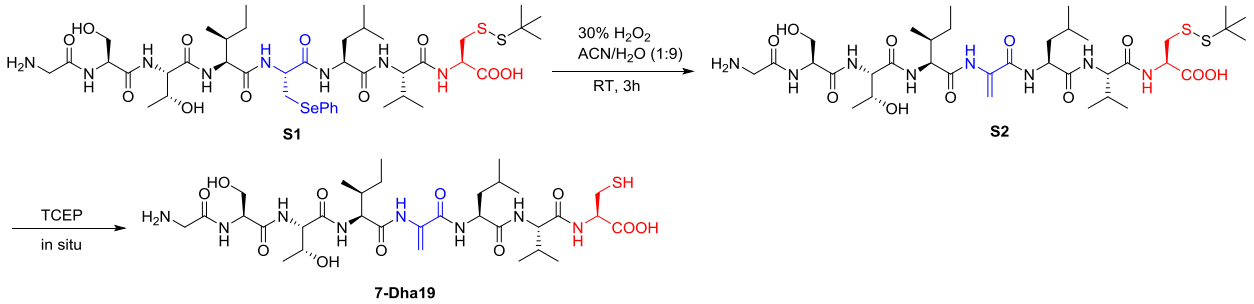

The dehydration of the synthetic substrate **S1** (Genscript Biotech, Nanjing, China) to the intermediate **S2** before *in situ* deprotection with TCEP was conducted in a reaction tube containing 100 µM H_2O_2 (30%, wt/wt) and 25µM **S1** by stirring at room temperature for 3 hr. The reaction mixture was quenched by addition of 10 µl dimethylsulfide. The quenched mixture was freeze-dried and then examined by HR-ESI-MS on a 6230B Accurate Mass TOF LC/MS System (Agilent Technologies Inc., USA) for the production of **S2** (*m/z* $[M+H]^+$ calcd. 849.4209; obs. 849.4214).

Supplementary Figures

Supplementary Figure 1. Alignment of the biosynthetic gene clusters of TVAs, CYP and EPI. Genes coding for precursor peptides and LanD-type flavoproteins are highlighted in blue and red, respectively. Overall, only genes encoding LanD-type flavoproteins are conserved among the *cyp*, *epi* and *tva* clusters. $TvaF_{S-87}$ shares 21.8% and 18.9% with CypD and the archetypal LanD protein EpiD, respectively, while CypD share 17.5% with EpiD. For details in sequence identity, see **Supplementary Figure 12**.

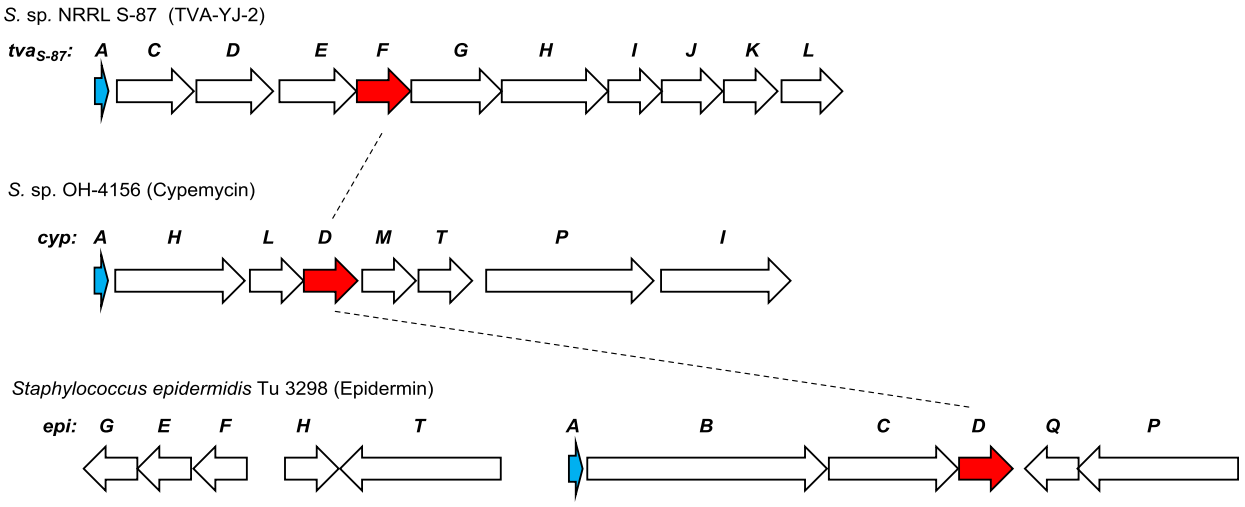

Supplementary Figure 2. Purified recombinant enzymes and cofactor analysis. **(a)** Coomassie-stained SDS-PAGE analysis of TRX-tagged TvaF$_{S-87}$, its variants and 3C with protein standard, TRX-tagged CypD and its variants with protein standard. **(b)** UV-Vis spectra of TRX-tagged recombinant flavoproteins TvaF$_{S-87}$ and CypD. **(c)** Determination of flavin cofactors associated with TvaF$_{S-87}$ and CypD. (i) Authentic FAD; (ii) boiled CypD, (iii) authentic FMN, and (iv) boiled TvaF$_{S-87}$. For examination by HPLC, UV absorbance at 375 nm. **(d)** Multiangle light scattering (MALS) analysis of TvaF$_{S-87}$ and CypD, showing the relative light scattering signal as a function of elution volume. The derived molecular mass of the peak is shown in blue.

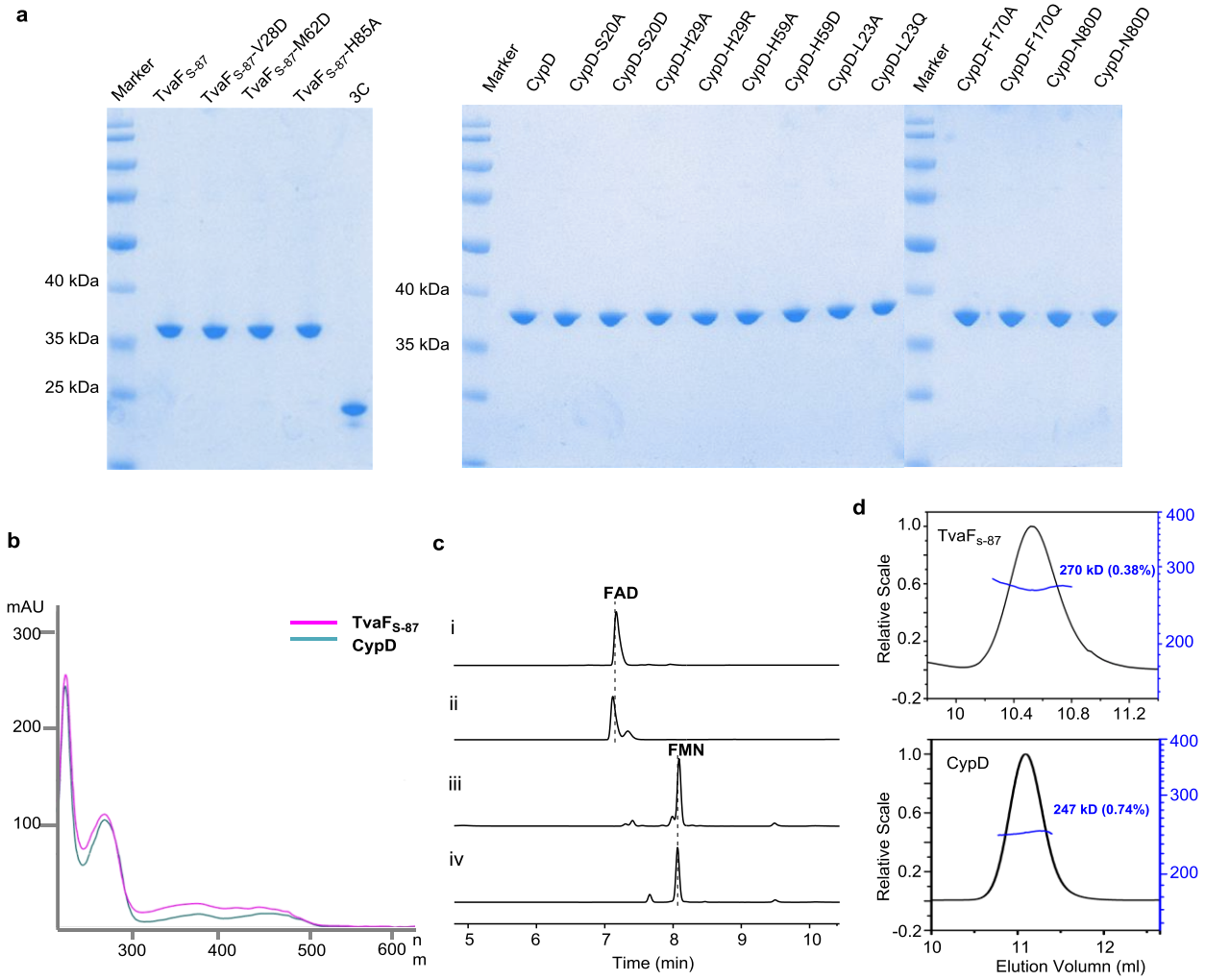

Supplementary Figure 3. Summary of LanD-like flavoprotein-catalyzed transformations in this study. Amino acids corresponding to the two target residues that are processed for Avi(Me)Cys formation and their related structures during each transformation process are colored, e.g., corresponding to the C-terminal L-Cys, red; and corresponding the internal L-Thr/L-Ser or L-Cys, blue. √, observed; ×, not observed; and **N.D.**, not detected. (**a**) $TvaF_{S\text{-}87}$. (**b**) CypD. For variation of the internal residue: X_1, L-[2,3,3-D_3]Ser; X_2, acetylated L-Ser; X_3, glutamylated L-Ser; X_4, phosphorylated L-Ser; X_5, Dha; and X_6, D-Cys.

	Peptidyl Substrate	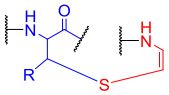 Cyclized Product	Enethiol Intermediate	Aldehyde Shunt Product
a				
1	SPDEEAQGSVMAAAATVAFHC	✓	✓	✓
1-T8A	SPDEEAQGSVMAAAAAVAFHC	✗	✓	✓
1-T8S	SPDEEAQGSVMAAAASVAFHC	✓	✓	✓
1-T8C	SPDEEAQGSVMAAAACVAFHC	✗	✓	✓
1-C13A	SPDEEAQGSVMAAAATVAFHA	✗	✗	✗
1-C13S	SPDEEAQGSVMAAAATVAFHS	✗	✗	✗
1-C13T	SPDEEAQGSVMAAAATVAFHT	✗	✗	✗
2	VMAAAATVAFHC	✓	✓	✓
3	MAAAATVAFHC	✓	✓	✓
4	AAAATVAFHC	✗	✓	N.D.
5	AATVAFHC	✗	✓	N.D.
6	TVAFHC	✗	✓	N.D.
b				
7	GSTI CLVC	✓	✓	✓
7-C19A	GSTI ALVC	✗	✓	✓
7-C19S	GSTI SLVC	✓	✓	✓
7-C19T	GSTI TLVC	✗	✓	✓
7-C22A	GSTI CLVA	✗	✗	✗
7-C22S	GSTI CLVS	✗	✗	✗
7-C22T	GSTI CLVT	✗	✗	✗
7-C19S-D_3	GSTI X_1LVC	✓	✓	✓
7-C19S-Ac	GSTI X_2LVC	✓	✓	✓
7-C19S-Glu	GSTI X_3LVC	✗	✗	✗
7-C19S-P	GSTI X_4LVC	✗	✗	✗
7-Dha19	GSTI X_5LVC	✓	✗	✗
7-d-C19	GSTI X_6LVC	✓	✓	✓

Supplementary Figure 4. HPLC-MS analysis of enethiol intermediates and associated shunt aldehyde derivatives in the $TvaA_{S\text{-}87}$-catalyzed conversions of **1** (the 21-aa C-terminal mimic of the precursor peptide $TvaA_{S\text{-}87}$) and its variants. Reactions were conducted at 30°C for 2 hr in the presence of $TvaF_{S\text{-}87}$ to convert the substrates **1** (i), **1-T8A** (ii), **1-T8S** (iii), **1-T8C** (iv) and **1-C13A** (v), and in the presence of $TvaF_{S\text{-}87}$-V28D (vi), $TvaF_{S\text{-}87}$-M62D (vii) and $TvaF_{S\text{-}87}$-H85A (viii) to convert **1**. (**b**) For detailed HR-MS and HR-MS/MS data, see **Supplementary Table 4**.

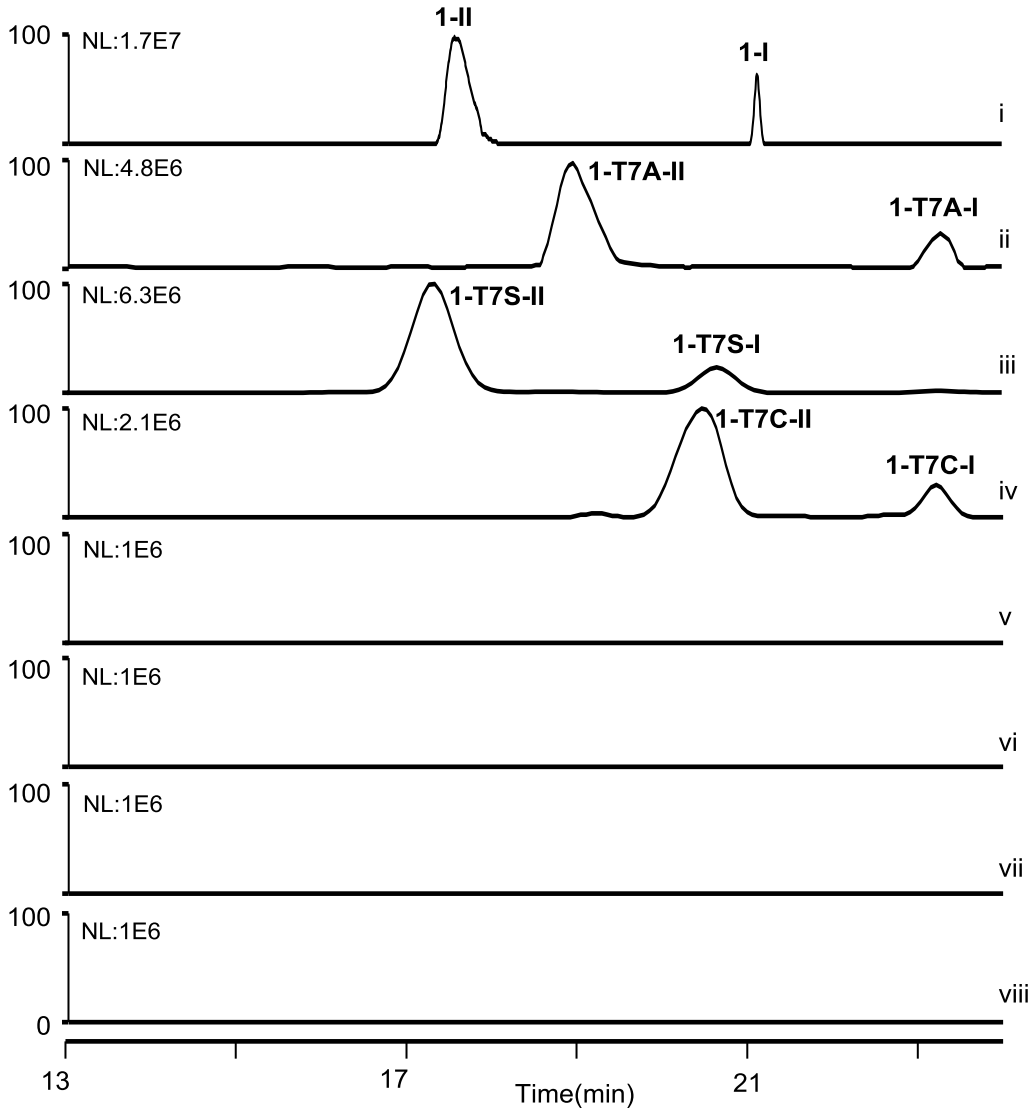

Supplementary Figure 5. Characterization of (ene)thiol and aldehyde peptides in the TvaF$_{S-87}$-catalyzed conversion of **1** by chemical derivatization. (**a**) Examination of **1**, **1-I** and **1-III** by HPLC-MS. i, standard **1**; ii, transformation of **1** at 30°C for 2 hr; iii, treatment of **1** with NEM; and iv, treatment of the reaction mixture of iii with NEM. (**b**) Examination of **1-II** by treating the TvaF$_{S-87}$-catalyzed transformation of **1** with 1-(2-Hydrazinyl-2- oxoethyl)pyridin-1-ium chloride (HOPI). (**c**) HR-MS and HR-MS/MS data for the derivatives **1-NEM**, **1-I-NEM** and **1-II-HOPI** of **1**, **1-I** and **1-II**, respectively.

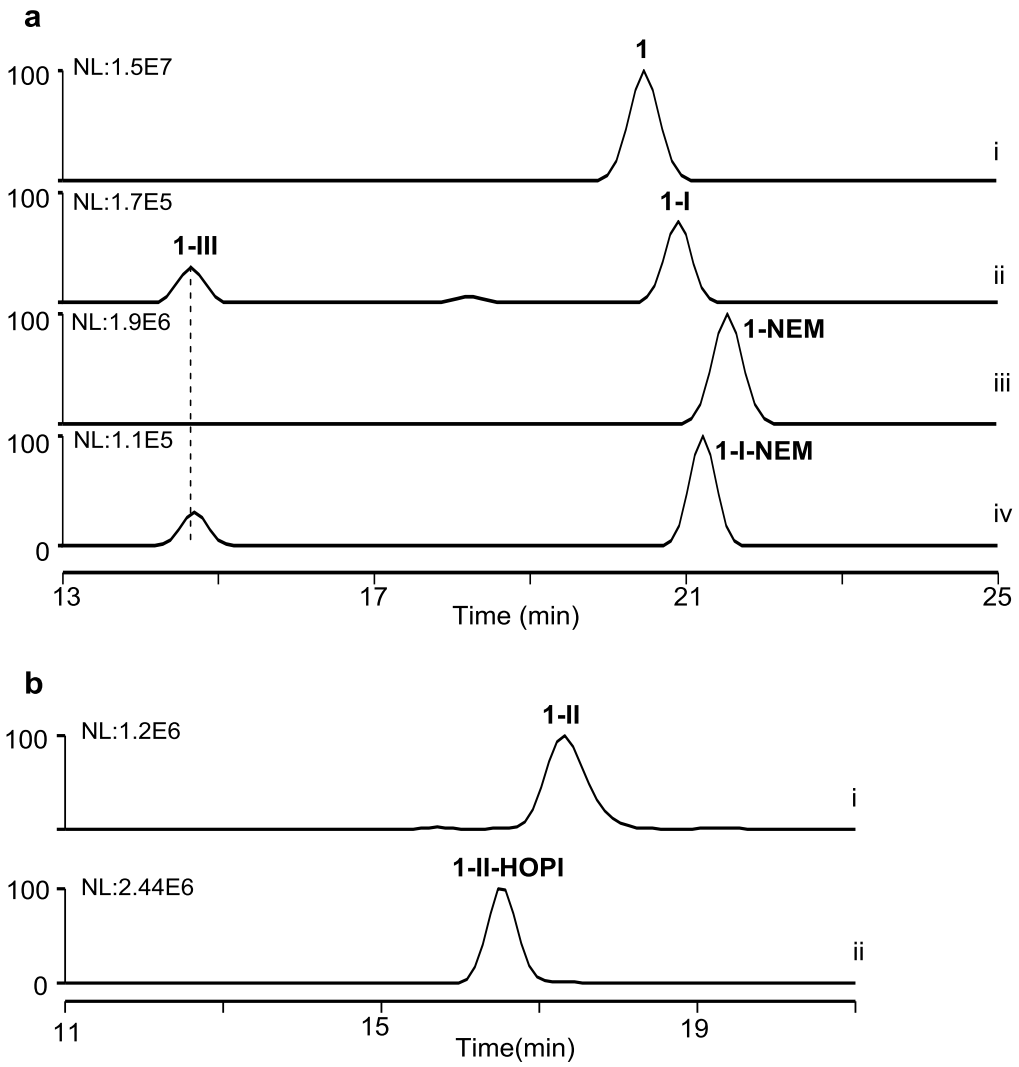

c

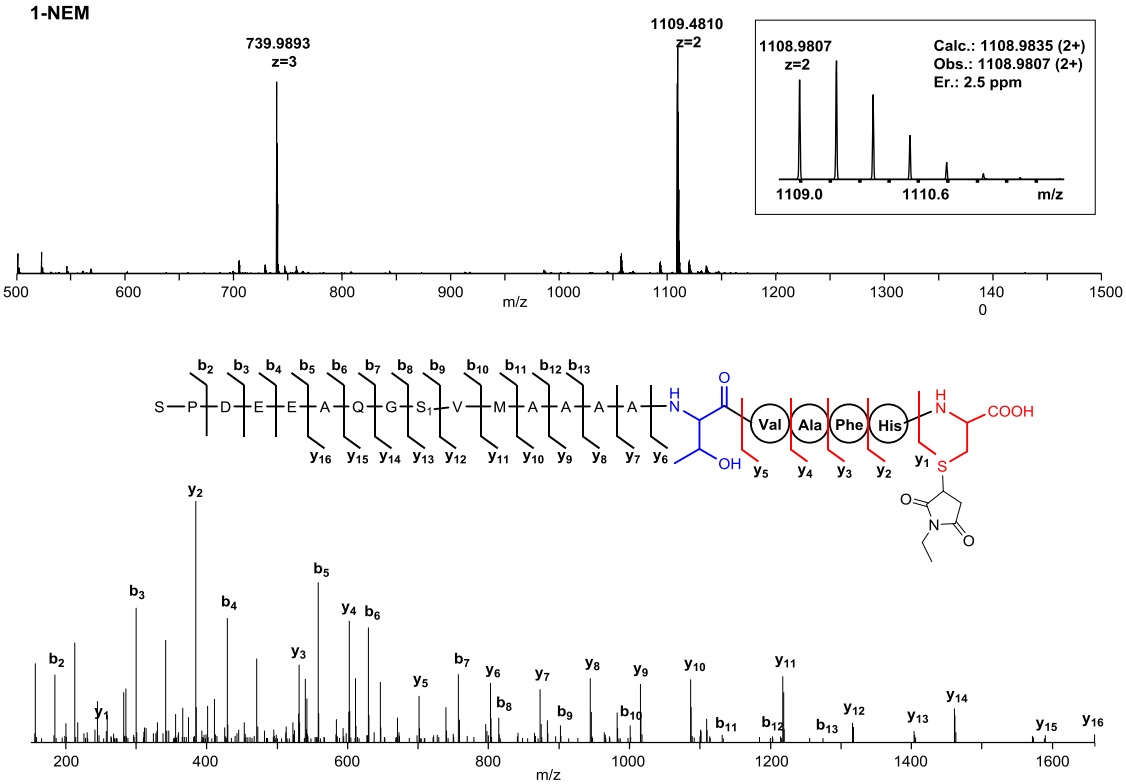

Ions	Calcd.	Obs.	Er. (ppm)	Ions	Calcd.	Obs.	Er. (ppm)
b_2	185.0926	185.0917	4.9	y_1	247.0752	247.0741	4.5
b_3	300.1196	300.1183	4.3	y_2	384.1341	384.1327	3.6
b_4	429.1621	429.1608	3.0	y_3	531.2025	531.2013	2.3
b_5	558.2047	558.2032	2.7	y_4	602.2396	602.2383	2.2
b_6	629.2418	629.2400	2.9	y_5	701.3081	701.3065	2.3
b_7	757.3004	757.2977	3.6	y_6	802.3557	802.3533	3.0
b_8	814.3219	814.3192	3.3	y_7	873.3928	873.3901	3.1
b_9	901.3539	901.3534	0.6	y_8	944.4300	944.4268	3.4
b_{10}	1000.4223	1000.4199	2.4	y_9	1015.4671	1015.4648	2.3
b_{11}	1131.4628	1131.4600	2.5	y_{10}	1086.5042	1086.5013	2.7
b_{12}	1202.4999	1202.4928	5.9	y_{11}	1217.5447	1217.5417	2.5
b_{13}	1273.5371	1273.5386	1.2	y_{12}	1316.6131	1316.6094	2.8
				y_{13}	1403.6451	1403.6471	1.4
				y_{14}	1460.6666	1460.6624	2.9

		y_{15}	1588.7252	1588.7162	5.7
		y_{16}	1659.7623	1659.7634	0.7

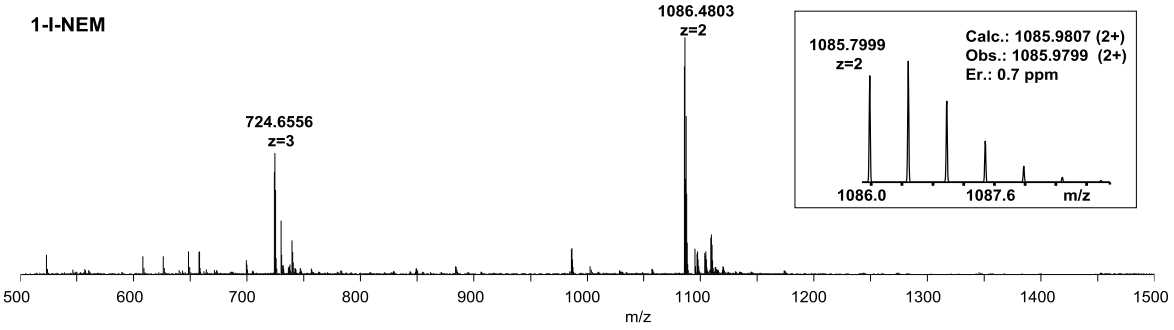

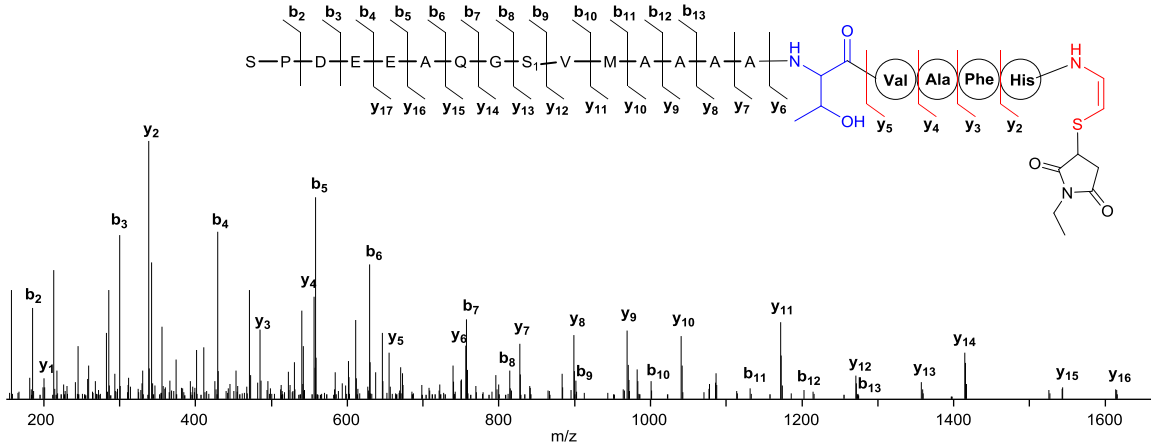

Ions	Calcd.	Obs.	Er. (ppm)	Ions	Calcd.	Obs.	Er. (ppm)
b_2	185.0926	185.0919	3.8	y_1	201.0697	201.0690	3.5
b_3	300.1196	300.1186	3.3	y_2	338.1286	338.1276	3.0
b_4	429.1621	429.1611	2.3	y_3	485.1970	485.1957	2.7
b_5	558.2047	558.2033	2.5	y_4	556.2342	556.2328	2.5
b_6	629.2418	629.2401	2.7	y_5	655.3026	655.3019	1.1
b_7	757.3004	757.2966	5.0	y_6	756.3503	756.3481	2.9
b_8	814.3219	814.3212	0.9	y_7	827.3874	827.3857	2.1
b_9	901.3539	901.3505	3.8	y_8	898.4245	898.4221	2.7
b_{10}	1000.4223	1000.4212	1.1	y_9	969.4616	969.4600	1.7
b_{11}	1131.4628	1131.4642	1.2	y_{10}	1040.4987	1040.4977	1.0
b_{12}	1202.4999	1202.4954	3.7	y_{11}	1171.5392	1171.5377	1.3

b_{13}	1273.5371	1273.5284	6.8	y_{12}	1270.6076	1270.6068	0.6
				y_{13}	1357.6396	1357.6368	2.1
				y_{14}	1414.6611	1414.6575	2.5
				y_{15}	1542.7197	1542.7157	2.6
				y_{16}	1613.7568	1613.7555	0.8

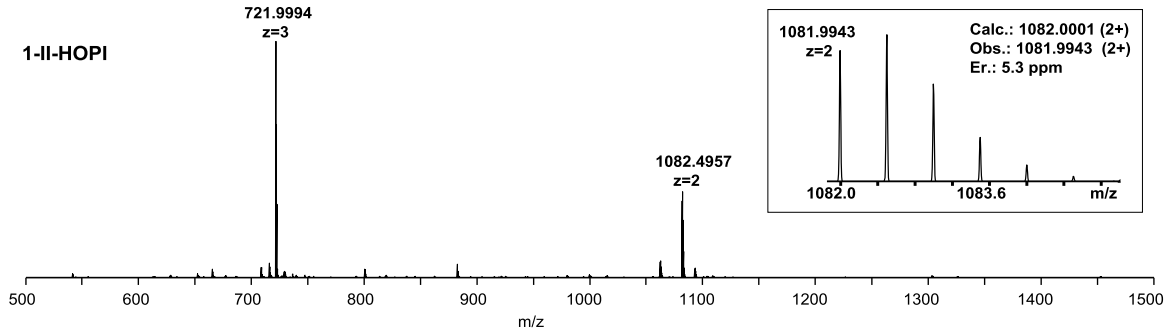

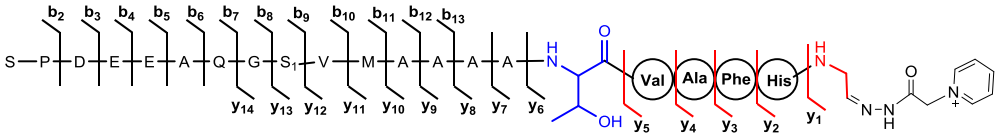

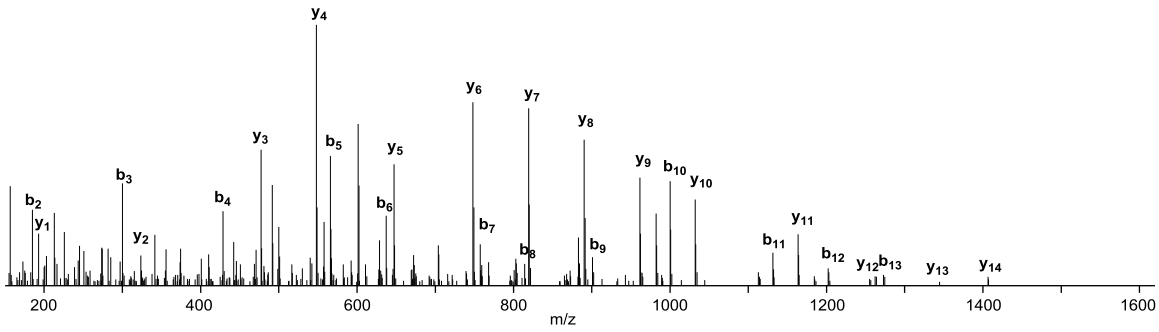

Ions	Calcd.	Obs.	Er. (ppm)	Ions	Calcd.	Obs.	Er. (ppm)
b_2	185.0926	185.0915	5.9	y_1	193.1084	193.1079	2.6
b_3	300.1196	300.1182	4.7	y_2	330.1673	330.1669	1.2
b_4	429.1621	429.1604	3.9	y_3	477.2357	477.2344	2.7
b_5	558.2047	558.2009	6.8	y_4	548.2728	548.2713	2.7
b_6	629.2418	629.2360	9.2	y_5	647.3412	647.3391	3.2
b_7	757.3004	757.2967	4.9	y_6	748.3889	748.3865	3.2
b_8	814.3219	814.3193	3.2	y_7	819.4260	819.4235	3.1

b_9	901.3539	901.3504	3.8	y_8	890.4631	890.4605	2.9
b_{10}	1000.4223	1000.4188	3.5	y_9	961.5002	961.4975	2.8
b_{11}	1131.4628	1131.4590	3.4	y_{10}	1032.5373	1032.5341	3.1
b_{12}	1202.4999	1202.4945	4.5	y_{11}	1163.5778	1163.5741	3.2
b_{13}	1273.5371	1273.5334	2.9	y_{12}	1262.6462	1262.6433	2.3
				y_{13}	1349.6783	1349.6676	7.9
				y_{14}	1406.6997	1406.6971	1.8

Supplementary Figure 6. HPLC-MS analysis of enethiol intermediates and associated shunt aldehyde derivatives in the CypD-catalyzed conversions of **7** (the 8-aa C-terminal mimic of the precursor peptide CypA) and its variants. (**a**) Conversions of **7** (i), **7-C19A** (ii), **7-C19T** (iii), **7-C19S** (iv), **7-C22A** (v) and **7-C22S** (vi). Reactions were conducted at 30°C for 2 hr in 60 μL of the reaction mixture that contained 100 μM synthetic peptide and 30 μM CypD. (**b**) Conversions of **7-Dha19** (i), **7** (ii), **7-d-C19** (iii), **7-C19S** (iv), **7-C19S-Ac** (v), **7-C19S-P** (vi) and **7-C19S-Glu** (vii). Reactions were conducted at 30°C for 2 hr in 60 μL of the reaction mixture that contained 30 μM synthetic peptide and 10 μM CypD. For detailed HR-MS and HR-MS/MS data, see **Supplementary Table 4**.

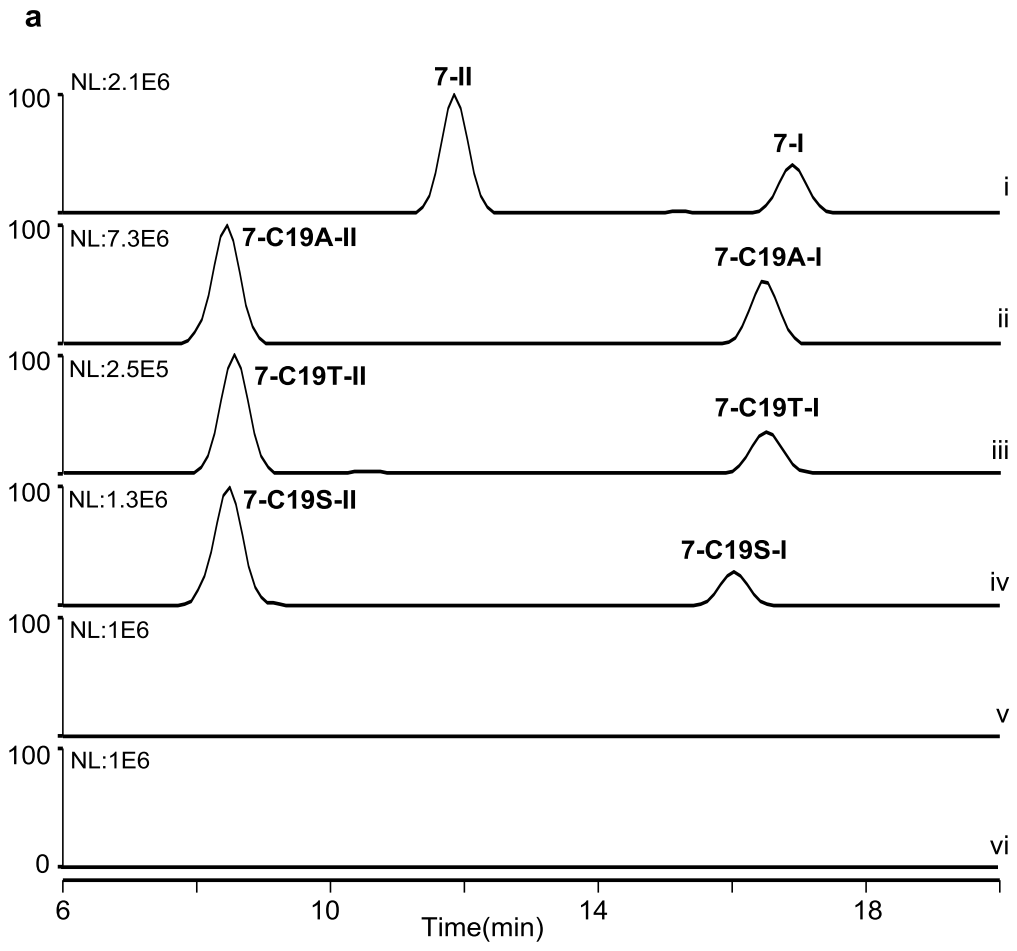

b

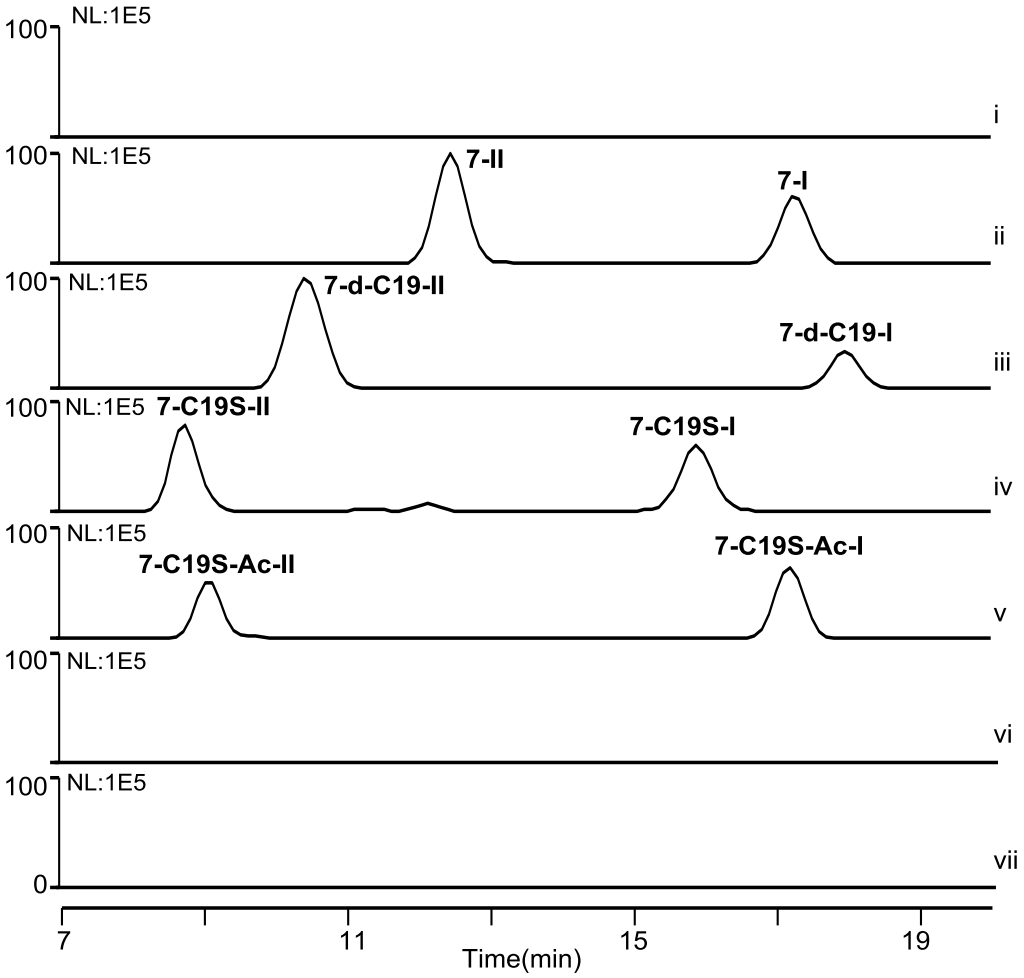
NL:1E5
100
i
NL:1E5
7-II
7-I
ii
NL:1E5
7-d-C19-II
7-d-C19-I
iii
NL:1E5
7-C19S-II
7-C19S-I
iv
NL:1E5
7-C19S-Ac-II
7-C19S-Ac-I
v
NL:1E5
vi
NL:1E5
vii
0
7
11
15
19
Time(min)

Supplementary Figure 7. Characterization of (ene)thiol peptides in the CypD-catalyzed conversion of **7** by chemical derivation. (**a**) Examination of **7**, **7-I** and **7-III** by HPLC-MS. i, standard **7**; ii, transformation of **7** into **7-I** and **7-III** at 30°C for 2 hr; iii, treatment of **7** with NEM; and iv, treatment of the reaction mixture of iii with NEM. (**c**) HR-MS and HR-MS/MS data for the derivatives **7-NEM** and **7-I-NEM** of **7** and **7-I**, respectively.

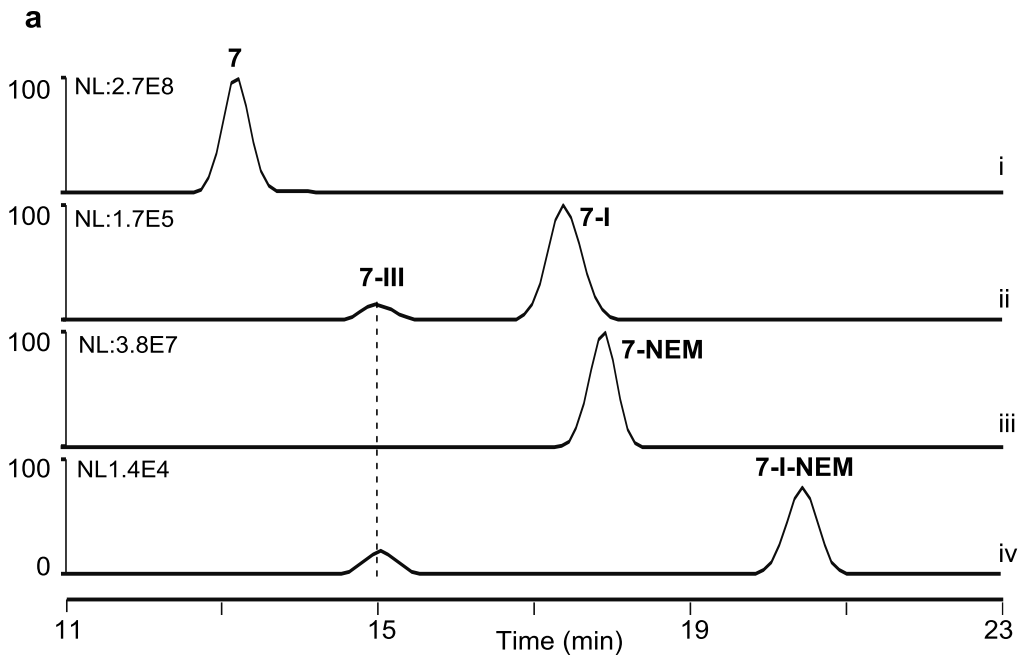

b

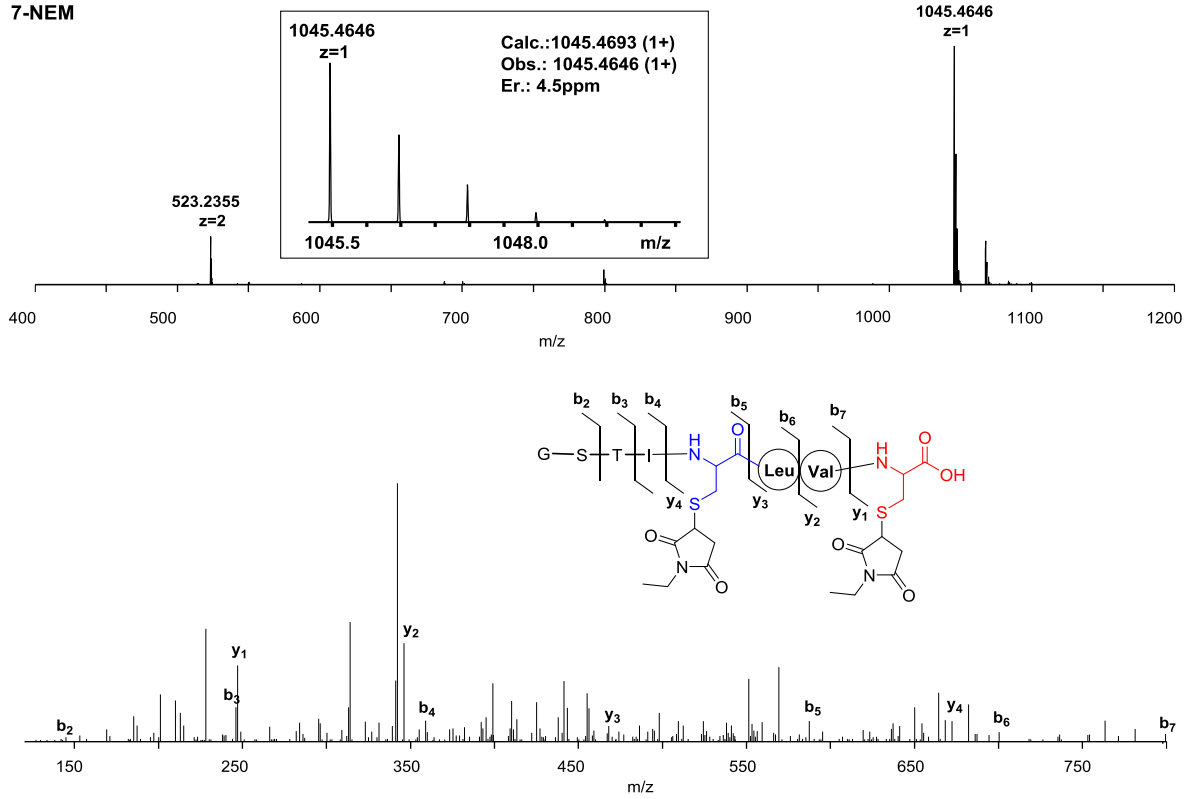

Ions	Calcd.	Obs.	Er. (ppm)
b_2	145.0613	145.0605	5.5
b_3	246.1090	246.1088	0.8
b_4	359.1931	359.1942	3.1
b_5	587.2499	587.2477	3.7
b_6	700.3340	700.3318	3.1
b_7	799.4024	799.3995	3.6
y_1	247.0752	247.0741	4.5
y_2	346.1436	346.1423	3.8
y_3	459.2277	459.2276	0.2
y_4	687.2845	687.2841	0.6

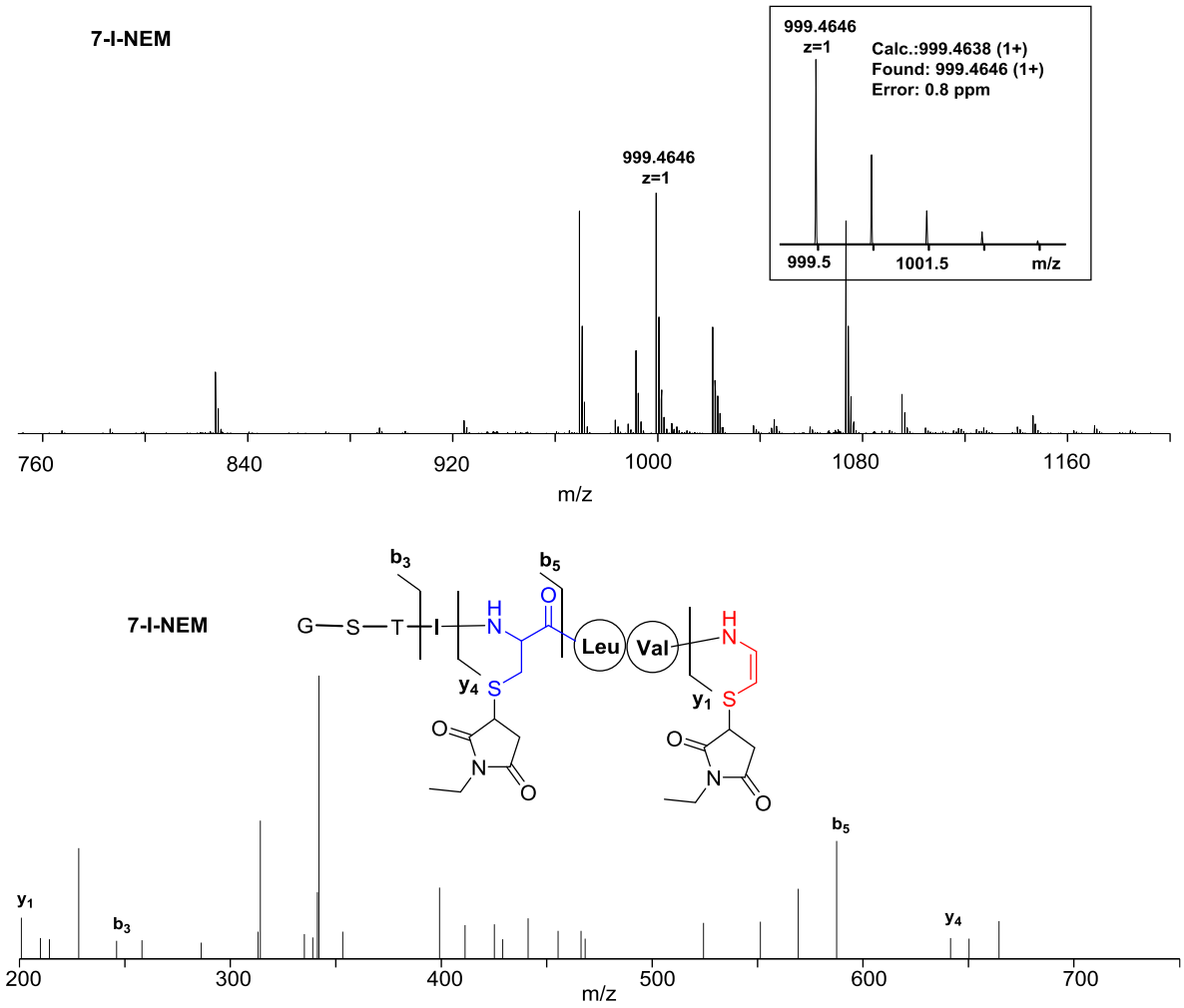

Ions	Calcd.	Obs.	Er. (ppm)
b_3	246.1090	246.1070	8.1
b_5	587.2499	587.2490	1.5
y_1	201.0697	201.0686	5.4
y_4	641.2791	641.2791	0.0

Supplementary Figure 8. 2D-TOCSY f2-slices at related f1 experiments (600 MHz, DMSO-d_6) for residue identification in **7-III**.

Chemical shift of -NH of the L-Ser residue (8.50 ppm).

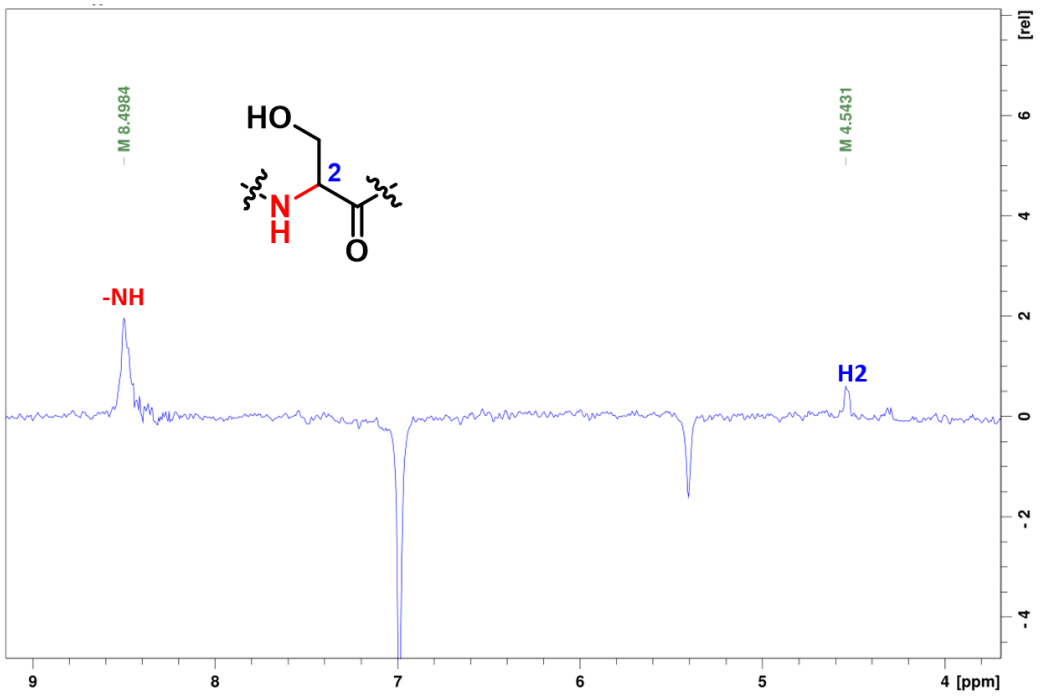

Chemical shift of -NH of L-Thr residue (8.04 ppm).

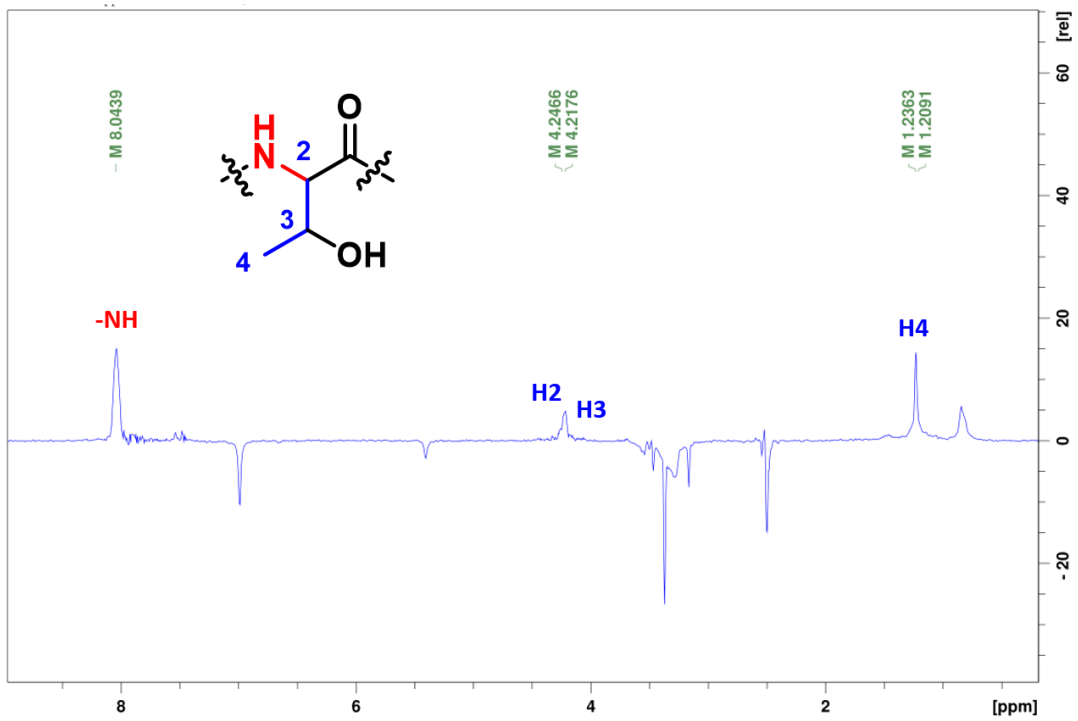

Chemical shift of H2 of L-Ile residue (4.10 ppm).

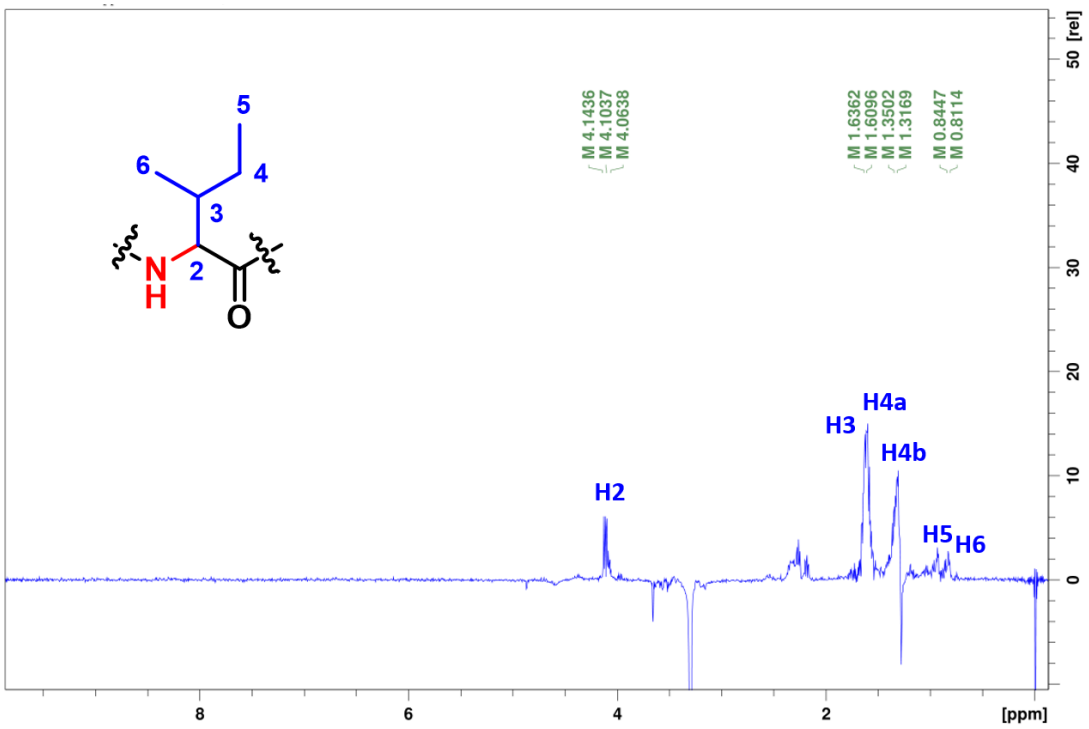

Chemical shift of NH of L-Leu residue (8.21 ppm).

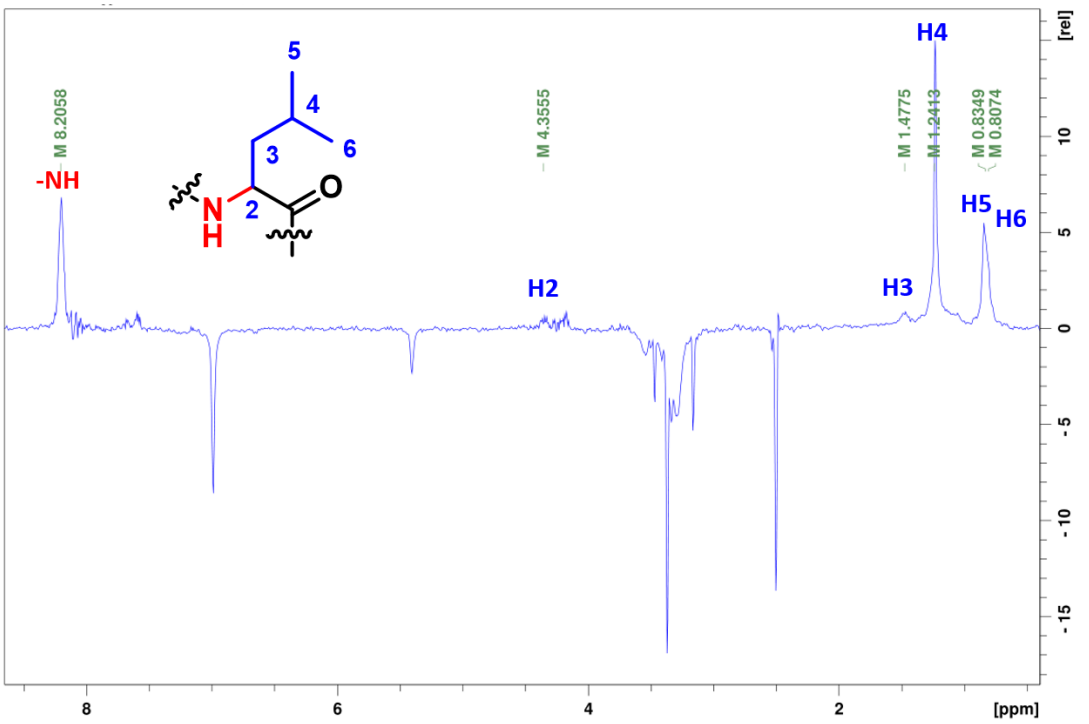

Chemical shift of NH of L-Val residue (7.00 ppm).

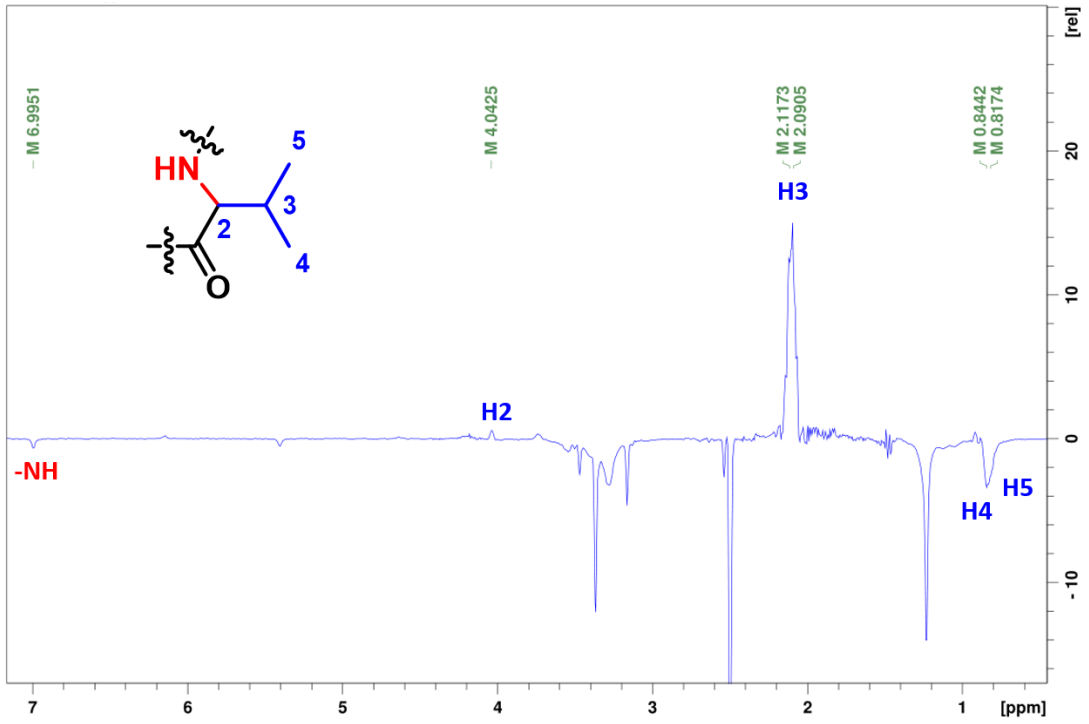

Chemical shift of NH of L-Cys2 residue (7.16 ppm).

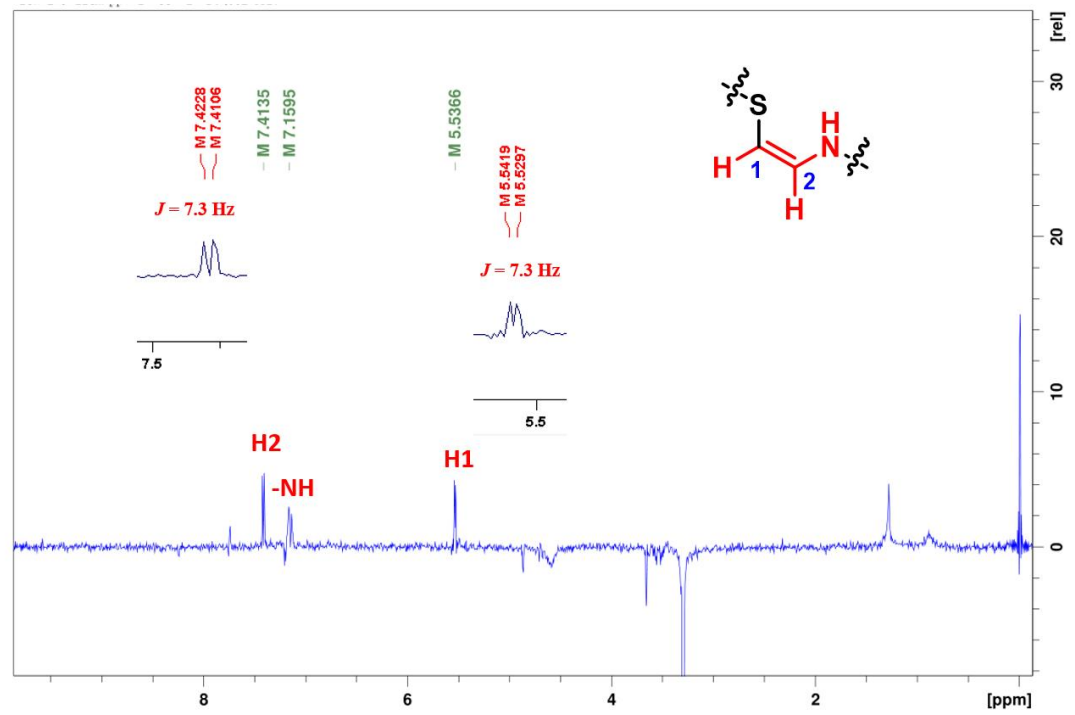

Supplementary Figure 9. Overall structural comparison of the monomers of $TvaF_{S-87}$, CypD, MrsD and the EpiD complex (shown by ribbon diagram). (**a**) $TvaF_{S-87}$ and CypD. (**b**) $TvaF_{S-87}$ EpiD. (**c**) CypD and EpiD. (**d**) $TvaF_{S-87}$ MrsD. (**e**) CypD and MrsD. (**f**) Two different $TvaF_{S-87}$ monomers (i.e., monomer 1 and monomer 2) found in $TvaF_{S-87}$ dodecamer. (**g**) The monomer of the EpiD H67N complex with a peptide substrate mimic (PDB ID: 1G5Q) and the $TvaF_{S-87}$ monomer 2.

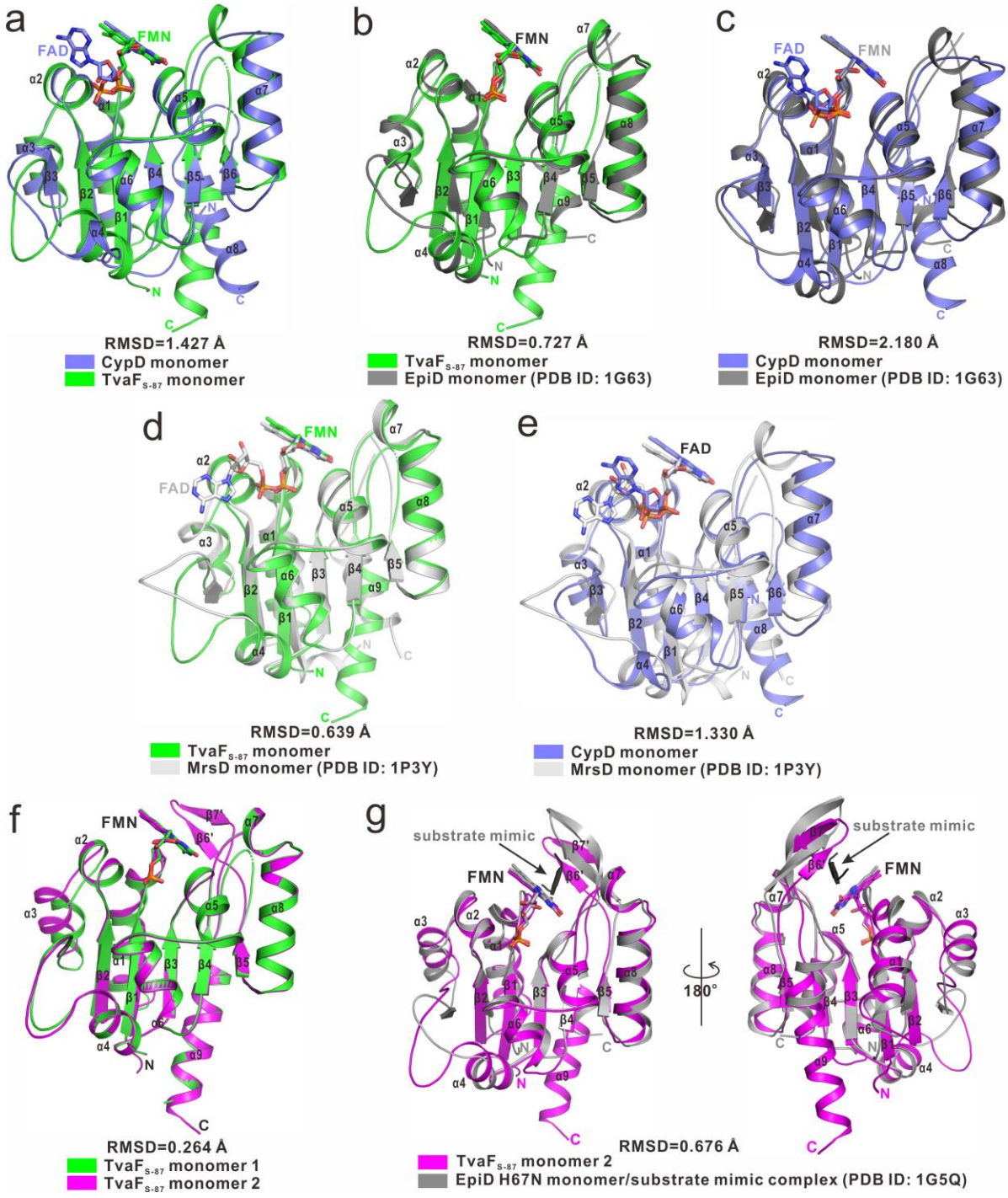

Supplementary Figure 10. FMN binding interface in the $TvaF_{S-87}$ structure. (**a**) The ribbon-stick model showing the FMN cofactors buried in the interfaces between two $TvaF_{S-87}$ monomers in a trimeric subunit. The three $TvaF_{S-87}$ monomers are shown in the ribbon model and colored in magenta, green, and orange, respectively, while the bound FMN cofactors are shown in the stick model. (**b**) The enlarged stereo view of the ribbon-stick-ball representation showing the detailed interactions between a FMN cofactor and two $TvaF_{S-87}$ monomers. The hydrogen bonds involved in the interaction are shown as dotted lines.

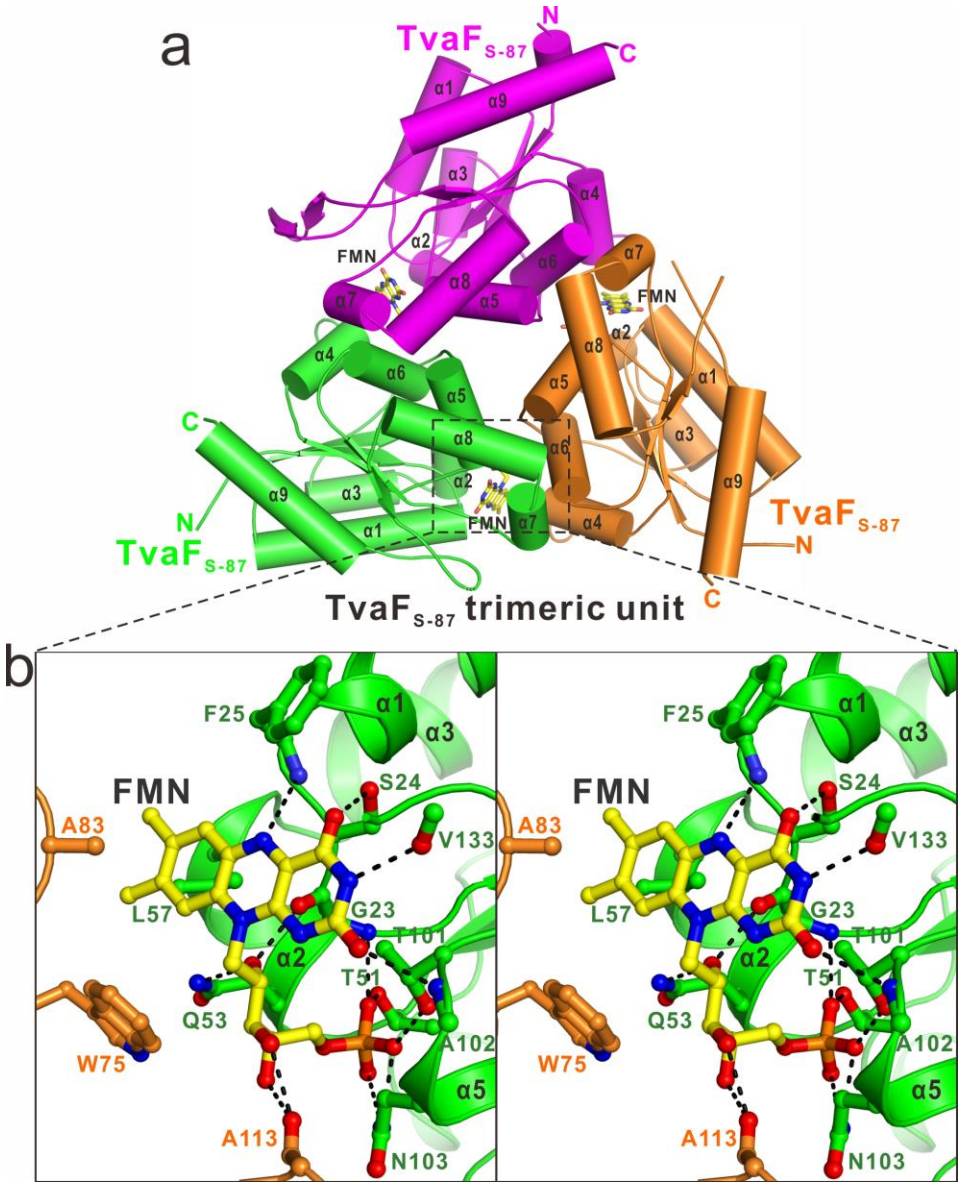

Supplementary Figure 11. FAD binding interface in the CypD structure. (**a**) The ribbon-stick model showing the FAD cofactors buried in the interfaces between two CypD monomers in a trimeric unit. The three CypD monmers are shown in the ribbon model and colored in cyan, slate blue, and hotpink, respectively, while the bound FAD cofactors are shown in the stick model. (**b**) The enlarged stereo view of the ribbon-stick-ball representation showing the detailed interactions between a FAD cofactor and two CypD monomers. The hydrogen bonds involved in the interaction are shown as dotted lines

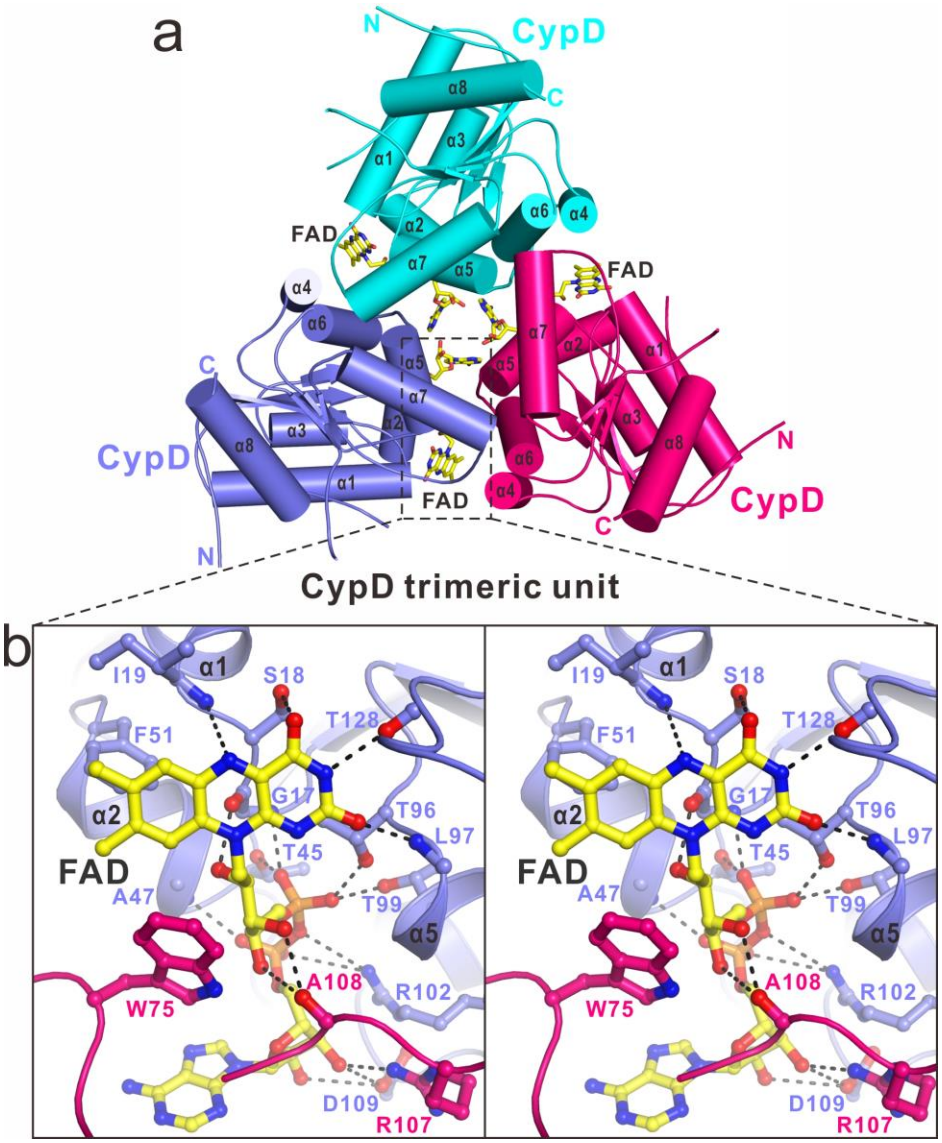

Supplementary Figure 12. Structure-based sequence alignment of CypD, EpiD and TvaF$_{S-87}$. The conserved residues are highlighted by colors using software Jalview2.8.1 (http://www.jalview.org/). The interface residues of TvaF$_{S-87}$ and CypD that are critical for the interactions with their bound cofactors are highlighted with red stars (polar interactions) or black triangles (hydrophobic interactions), while the interface residues of TvaF $_{S-87}$ and CypD that are crucial for the interaction between two trimeric subunits are labeled with black stars (polar interactions) or red triangles (hydrophobic interactions). Furthermore, the CypD residues involved in the interaction with **ISLVS** (the pentapeptide sequence of **8**) are labeled with red (polar interactions) or black (hydrophobic interactions) gears.

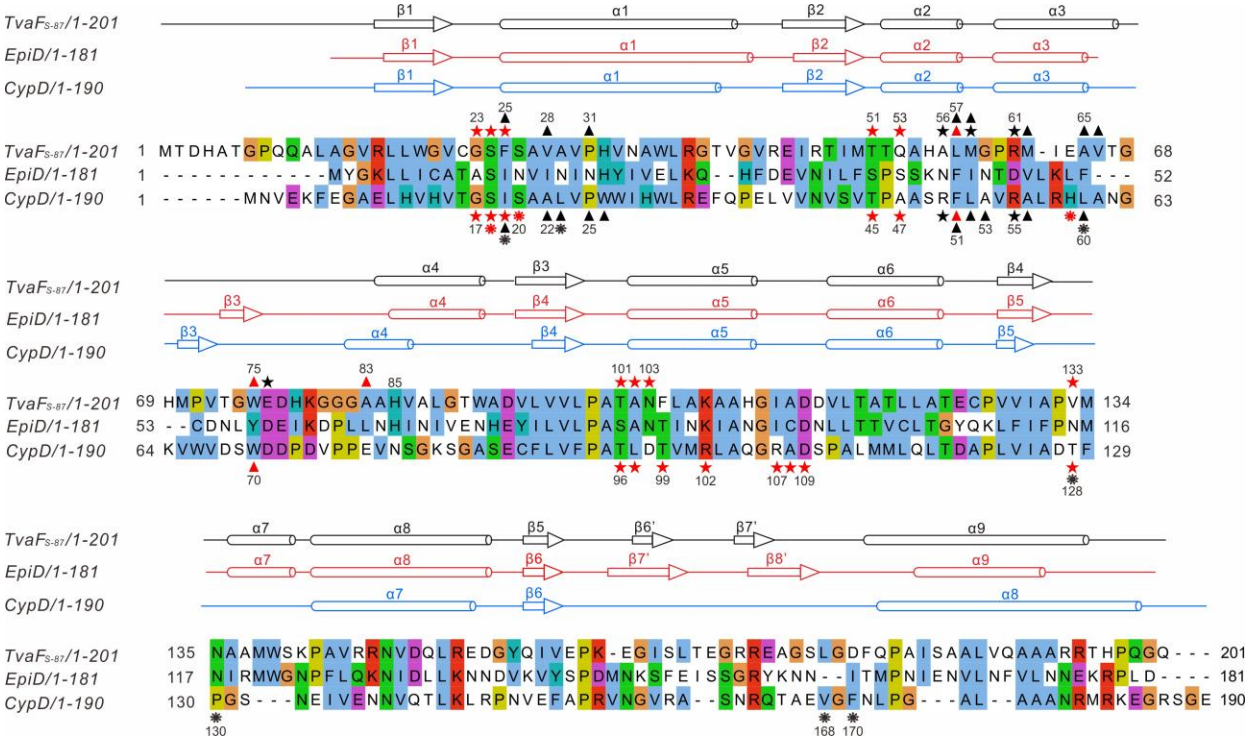

Supplementary Figure 13. Structural and biochemical analyses of the binding interface between two trimeric units of the TvaF$_{S-87}$ dodecamer. (**a**) The ribbon-stick model showing the structural packing between two trimeric units. The bound FMN cofactors are shown in the stick model, and the six monomers forming two trimeric subunits are shown in the ribbon model and labeled with different colors. (**b**) The enlarged stereo view of the ribbon-stick representation showing the binding interface between two trimeric units. The hydrogen bonds involved in the interaction are shown as dotted lines. (**c**) Overlay plot of the static light scattering data of wild type TvaF$_{S-87}$, and the TvaF$_{S-87}$-M62D and TvaF$_{S-87}$-V28D mutants. Clearly, the wide type TvaF$_{S-87}$ forms a stable dodecamer, while the two mutants exclusively form a stable trimer.

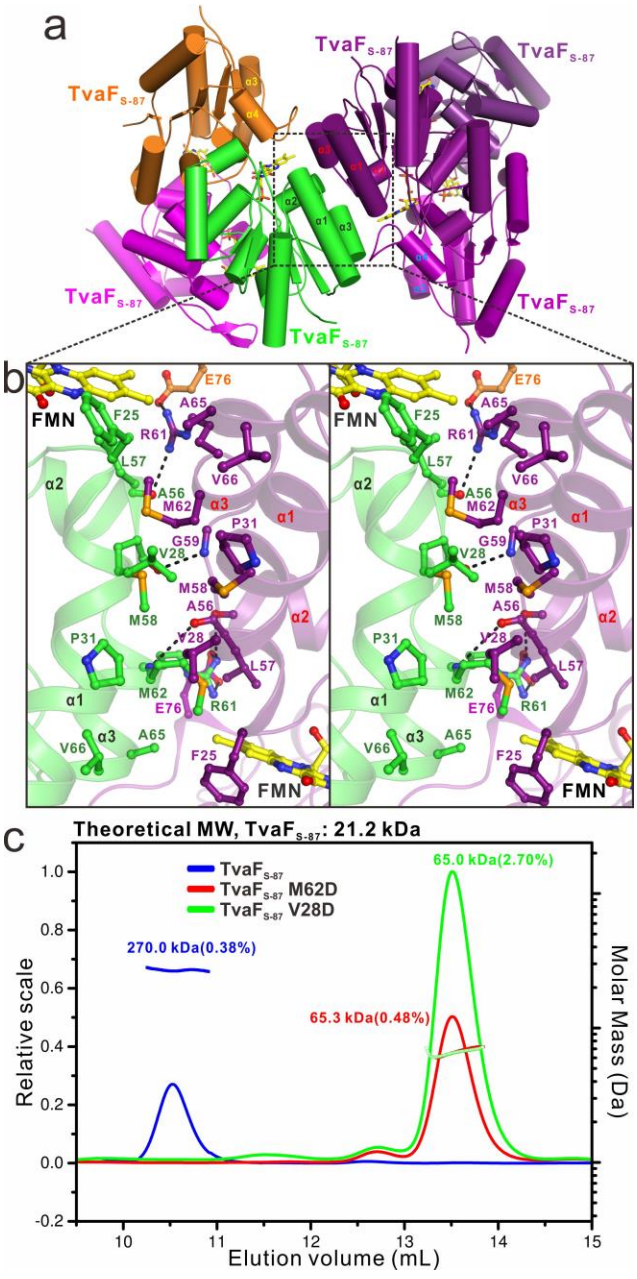

Supplementary Figure 14. Structural analysis of the binding interface between two trimeric subunits of the CypD dodecamer. (**a**) The ribbon-stick model showing the structural packing between two trimeric units. In this drawing, The bound FAD cofactors are shown in the stick model, and the six monomers forming two trimeric bunits are shown in the ribbon model and labeled with different colors. (**b**) The enlarged stereo view of the ribbon-stick representation showing the binding interface between two trimeric CypD units. The hydrogen bonds involved in the interaction are shown as dotted lines.

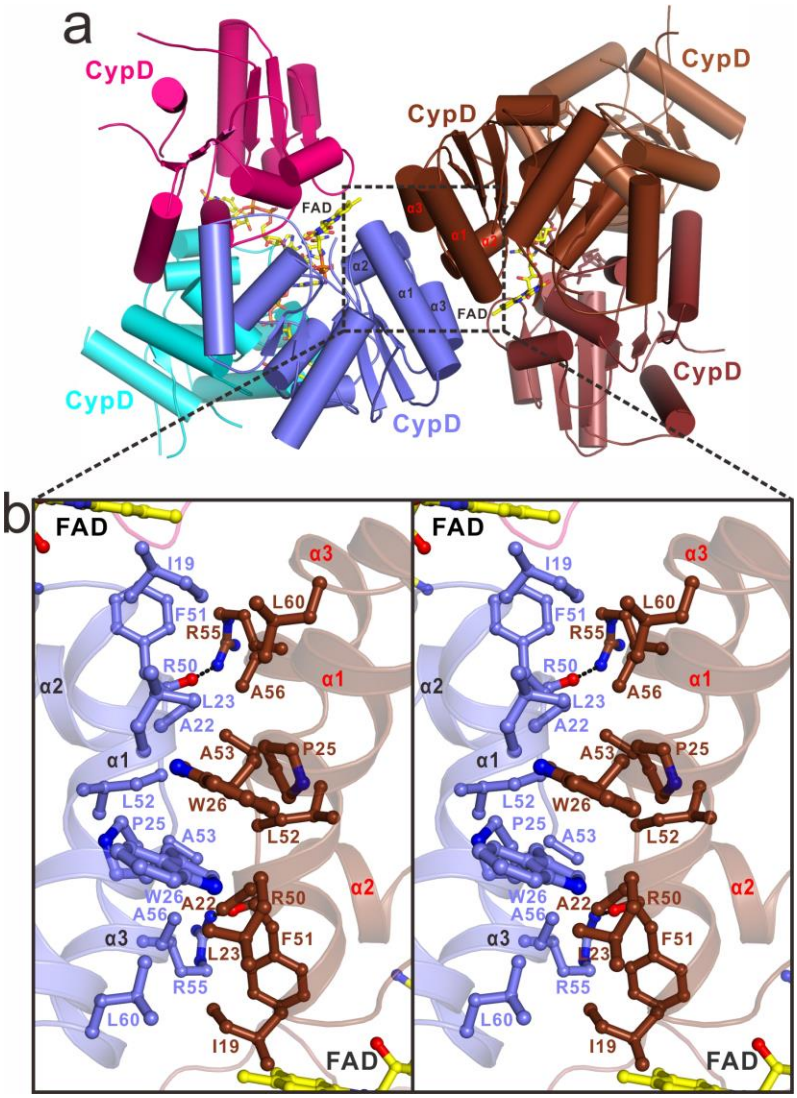

Supplementary Figure 15. Structural analysis of the CypD monomer in the CypD complex with the peptide substrate **8**. (**a**) Comparison of the CypD monomer in the complex (purple blue) and in its apo-form (slate blue), respectively. (**b**) The F_O-F_C map of the pentapeptide **IS$_{19}$LVS$_{22}$** sequence of **8** in the complex structure. The electron density map is calculated by omitting this sequence from the final PDB file of the complex and contoured at 2.0σ. The CypD is shown in the cartoon mode, while the bound **IS$_{19}$LVS$_{22}$** sequence and FAD are shown in the stick-ball mode.

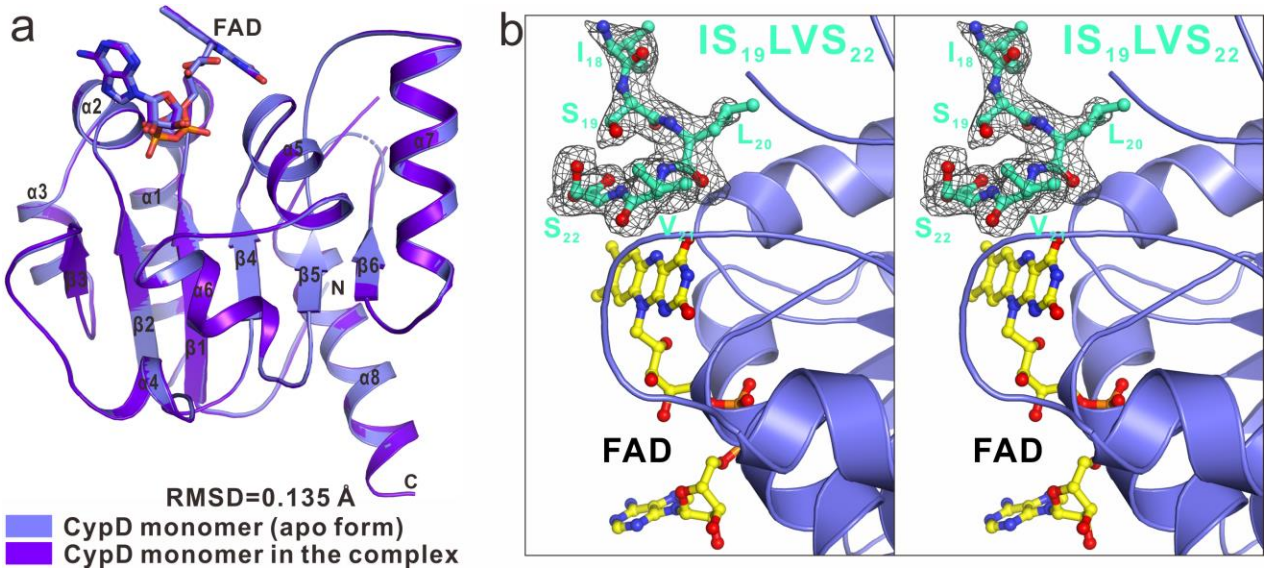

Supplementary Figure 16. Structural analysis of the substrate-binding pockets of CypD dodecamer. (**a**) The combined surface representation and the stick-ball model showing the substrate-binding pockets of CypD. (**b**) The combined surface charge potential representation and the stick-ball model showing that the solvent-exposed and highly charged pocket formed between two trimeric units is close to a bound FAD cofactor.

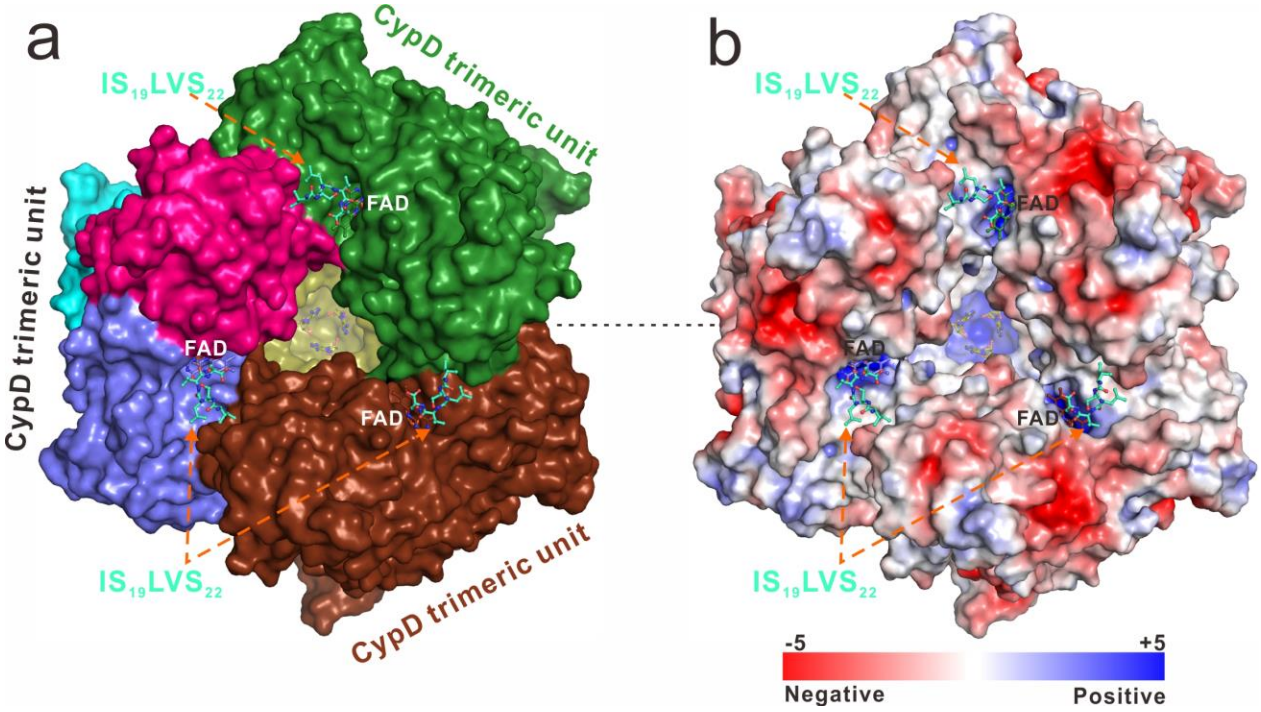

Supplementary Figure 17. Structural comparison of the CypD complex and the EpiD H67N mutant complex. (**a**) The superimposition of the CypD complex with the peptide substrate **8** (purple blue and green cyan) and the EpiD H67N mutant complex with a pentapeptide substrate mimic (grey and black). The ribbon-stick model reveals the overlapping of the two putative substrate binding pockets. (**b**) The combined surface representation and the stick-ball model showing the overlaps of the two substrate peptides in the CypD/**8** complex and the EpiD H67N mutant complex.

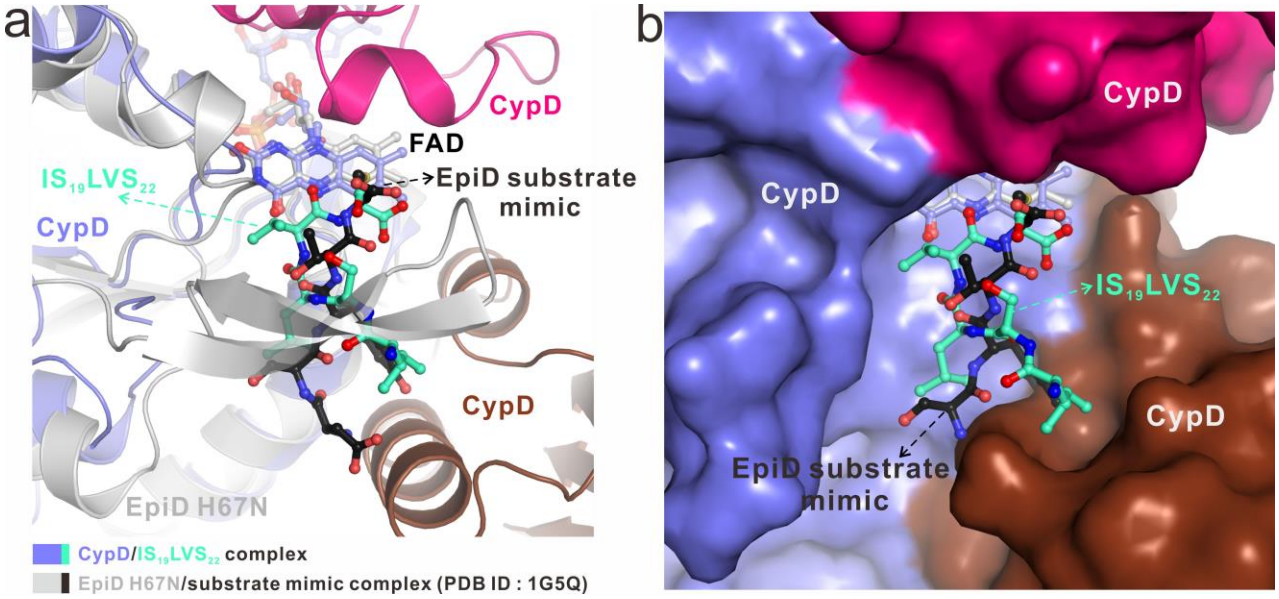

Supplementary Figure 18. *In vitro* assays of CypD activity using the substrates, **7** (i), **7-C19S** (ii) and **7-C19S-D$_3$** (containing the deuterium-labeled L-[2,3,3-D$_3$]Ser residue, iii). Conversions were conducted at 30°C for 4 hr in 60 μL of the reaction mixture that contained 100 μM synthetic peptide and 30 μM N-terminally TRX-tagged CypD along with 50 mM Tris-HCl (pH 8.5), 10 mM TCEP, 5 μM FAD and 1 μM 3C. The reaction mixture for **7-C19S-D$_3$** conversion was concentrated ten times for HR -MS analysis.

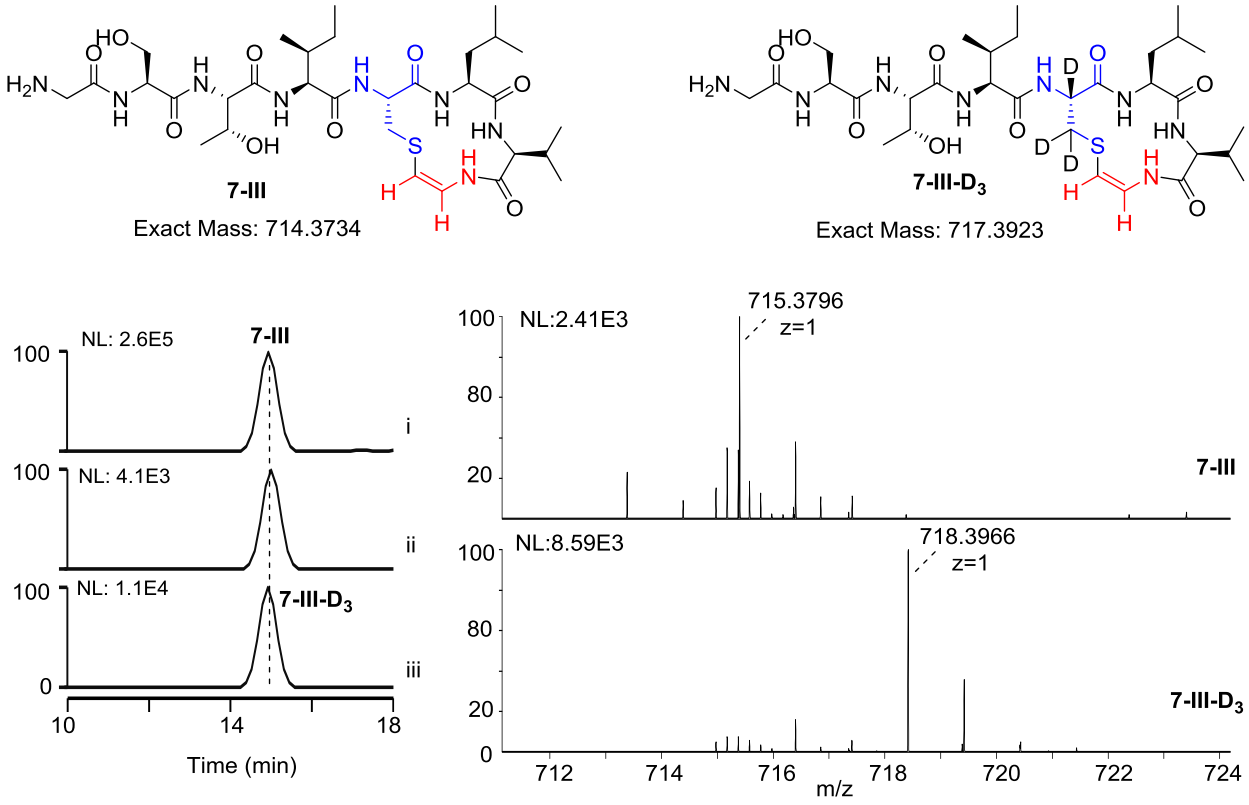

Supplementary Figure 19. Characterization of Dha-containing peptides in the CypD-catalyzed conversion of **7-Dha** by chemical derivation. (**a**) Examination of **7-Dha** and its derivatives by HPLC-MS. i, standard **7-Dha**; ii, treatment of **7-Dha** with DTT at 30°C for 2 hr; iii, transformation of **7-Dha** into **7-III** and **7-IV** at 30°C for 2 hr; and iv, treatment of the reaction mixture of iii with DTT. (**b**) HR-MS and HR-MS/MS data for the derivative **7-Dha-DTT**.

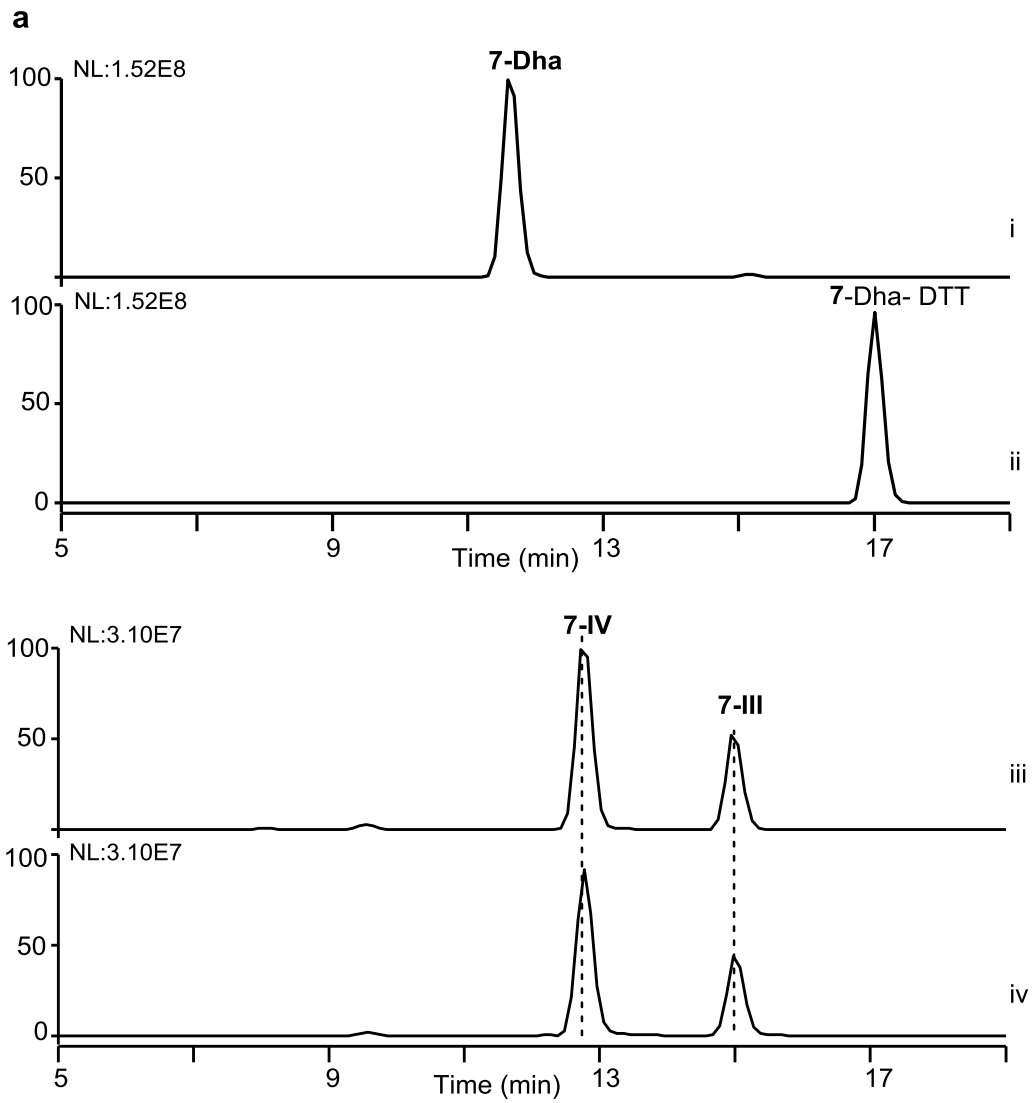

b

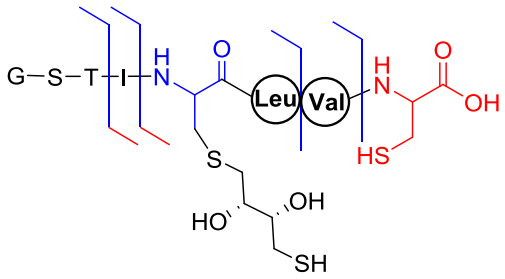

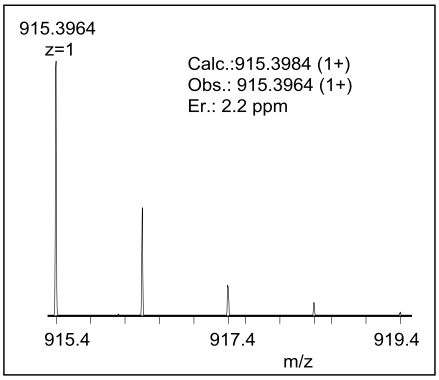

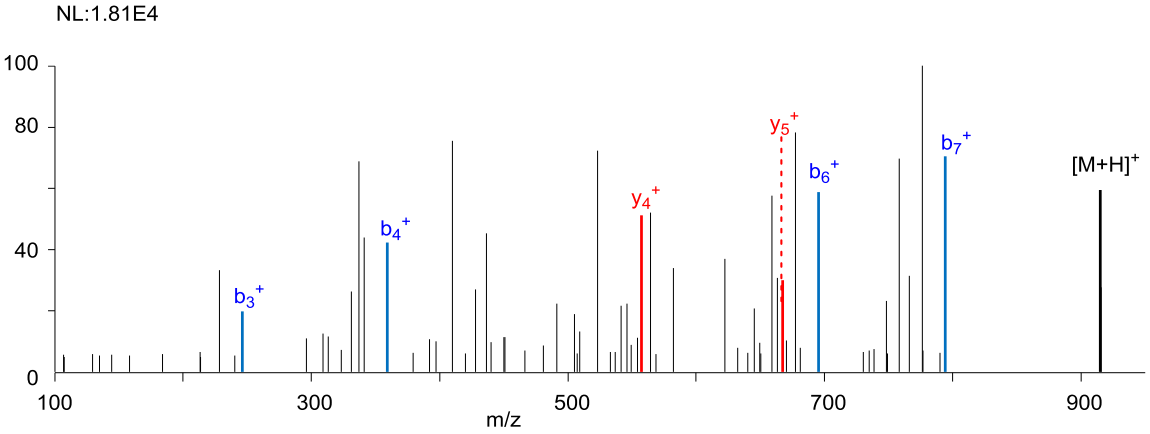

	Calcd.	Obs.	Er.(ppm)
$\mathbf{b_3}^+$	246.1090	246.1079	4.5
$\mathbf{b_4}^+$	359.1931	359.1927	1.1
$\mathbf{b_6}^+$	695.3093	695.3108	2.2
$\mathbf{b_7}^+$	794.3787	794.3792	0.6
$\mathbf{y_4}^+$	557.2137	557.2122	2.7
$\mathbf{y_5}^+$	670.2978	670.2968	1.5

Supplementary Figure 20. Comparison of the enzymatic activities of CypD with its variants based on examination of the production of **7-I**, **7-II** and **7-III**. The activity has been quantified by the intensities in HR-MS analysis, in which the activity of wild type CypD to produce **7-1** and **7-II** was normalized to 100%. Assays were performed in triplicates, and the standard deviations are indicated by the error bars. Conversions were conducted at 30°C for 4 hr in 60 μL of the reaction mixture that contained 100 μM **7** and 30 μM N-terminally TRX-tagged CypD, along with 50 mM Tris-HCl (pH 8.5), 10 mM TCEP, 5 μM FAD, 1 μM 3C.

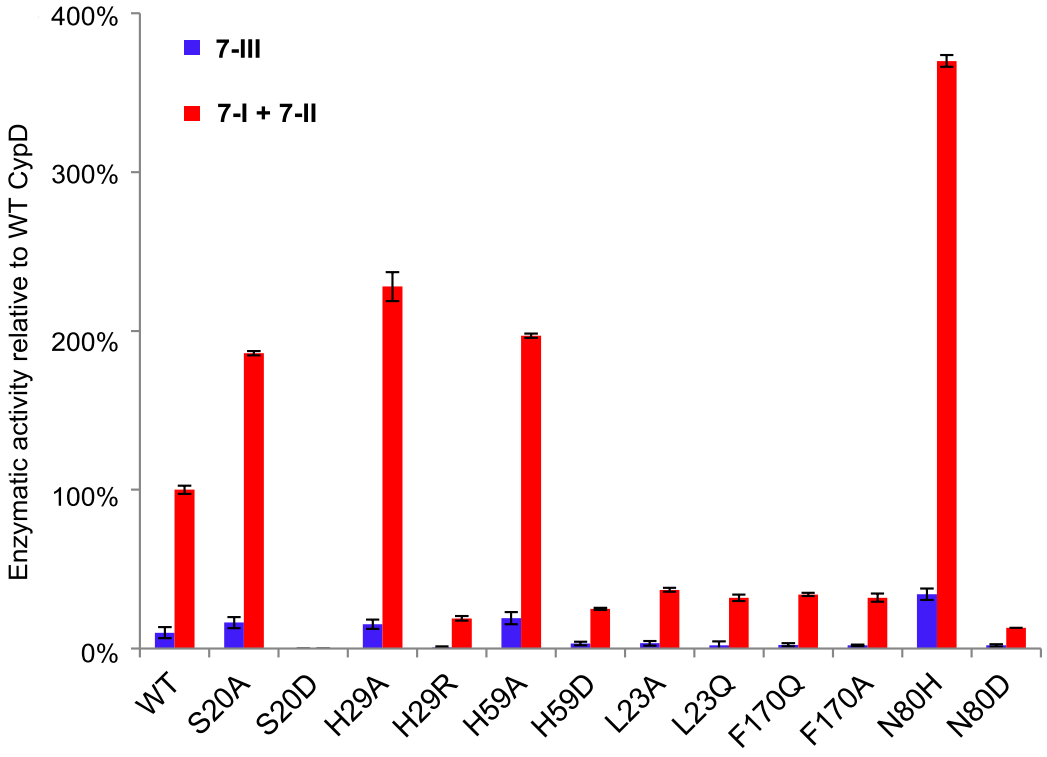

Supplementary Tables

Supplementary Table 1. Related bacterial strains and plasmids used in this study.

Strains/Plasmids	**Characteristic(s)**	**Sources/References**
***Streptomyces* sp.**		
NRRL S-87	Wild type strain, TVA-YJ-2-producing strain for PCR	NRRL
Escherichia coli		
DH5α	Host for general cloning	Transgen
BL21 (DE3)	Host for protein expression	Transgen
JZ101	BL21 (DE3) derivative, containing pZL 1001 for producing TRX-tagged $TvaF_{S-87}$	This study
JZ102	BL21 (DE3) derivative, containing pZL 1003for producing TRX-tagged CypD	This study
JZ103	BL21 (DE3) derivative, containing pZL 1002 for producing 3C	This study
JZ104	BL21 (DE3) derivative, containing pZL 1004 for producing TRX-tagged $TvaF_{S-87}$- V28D	This study
JZ105	BL21 (DE3) derivative, containing pZL1005 for producing TRX-tagged $TvaF_{S-87}$-M62D	This study
JZ106	BL21 (DE3) derivative, containing pZL 1006 for producing TRX-tagged $TvaF_{S-87}$- H85A	This study
JZ107	BL21 (DE3) derivative, containing pZL 1007 for producing TRX-tagged CypD-S20A	This study
JZ108	BL21 (DE3) derivative, containing pZL 1008 for producing TRX-tagged CypD-S20D	This study
JZ109	BL21 (DE3) derivative, containing pZL 1009 for producing TRX-tagged CypD-L23A	This study
JZ110	BL21 (DE3) derivative, containing pZL 1010 for producing TRX-tagged CypD-L23Q	This study
JZ111	BL21 (DE3) derivative, containing pZL 1011 for producing TRX-tagged CypD-F170A	This study
JZ112	BL21 (DE3) derivative, containing pZL 1012 for producing TRX-tagged CypD-F170Q	This study

JZ113	BL21 (DE3) derivative, containing pZL 1013 for producing TRX-tagged CypD-H59A	This study
JZ114	BL21 (DE3) derivative, containing pZL 1014 for producing TRX-tagged CypD-H59D	This study
JZ115	BL21 (DE3) derivative, containing pZL 1015 for producing TRX-tagged CypD-H29R	This study
JZ116	BL21 (DE3) derivative, containing pZL 1016 for producing TRX-tagged CypD-H29A	This study
JZ117	BL21 (DE3) derivative, containing pZL 1017 for producing TRX-tagged CypD-N80H	This study
JZ118	BL21 (DE3) derivative, containing pZL 1018 for producing TRX-tagged CypD- N80D	This study
Plasmids	*E. coli* subcloning vector	
pET28a(+)	Protein expression vector used in *E.coli*, encoding N-terminal His-tag, kanamycin resistance	Novagen
pRSFDeut-1	Protein expression vector used in *E.coli*, encoding N-terminal His-tag, kanamycin resistance	Novagen
pZL1001	pRSFDeut-1 derivative, containing *trx* and a 606 bp PCR product that encodes $tvaF_{S\text{-}87}$	This study
pZL1002	pET28a(+) derivative, containing a 552 bp synthesized gene that encodes *3c*	This study
pZL1003	pRSFDeut-1 derivative, containing *trx* and a 573 bp synthesized gene that encodes *cypD*	This study
pZL1004	pZL1001 derivative for V28D mutated $tvaF_{S\text{-}87}$	This study
pZL1005	pZL1001 derivative for M62D mutated $tvaF_{S\text{-}87}$	This study
pZL1006	pZL1001 derivative for H85A mutated $tvaF_{S\text{-}87}$	This study
pZL1007	pZL1003 derivative for S20A mutated *cypD*	This study
pZL1008	pZL1003 derivative for S20D mutated *cypD*	This study
pZL1009	pZL1003 derivative for L23A mutated *cypD*	This study
pZL1010	pZL1003 derivative for L23Q mutated *cypD*	This study
pZL1011	pZL1003 derivative for F170A mutated *cypD*	This study
pZL1012	pZL1003 derivative for F170Q mutated *cypD*	This study
pZL1013	pZL1003 derivative for H59D mutated *cypD*	This study
pZL1014	pZL1003 derivative for H59A mutated *cypD*	This study
pZL1015	pZL1003 derivative for H29R mutated *cypD*	This study

pZL1016	pZL1003 derivative for H29A mutated *cypD*	This study
pZL1017	pZL1003 derivative for N80H mutated *cypD*	This study
pZL1018	pZL1003 derivative for N80D mutated *cypD*	This study

Supplementary Table 2. Primers used in this study.

Primers	**Sequence (restriction sites are underlined)**
tvaF$_{S\text{-}87}$ -for	AAAAAGGATCCATGACCGACCACGCCACCG
tvaF$_{S\text{-}87}$ -rev	AAAAAGAATTCTCACTGTCCTTGTGGGTG
tvaF$_{S\text{-}87}$-V28D-for	TCCGCTGACGCGGTCCCCCACGTGAAC
tvaF$_{S\text{-}87}$-V28D-rev	GACCGGTCCAGCGGAGAAGGAGCCGCA
tvaF$_{S\text{-}87}$-M62D-for	CCGCGCGACATCGAGGCTGTCACCGGC
tvaF$_{S\text{-}87}$-M62D-rev	CTCGATGTCGCGCGGCCCCATGAGGGC
tvaF$_{S\text{-}87}$-H85A-for	GCCGCCGCAGTCGCCCTCGGCACCTGG
tvaF$_{S\text{-}87}$-H85A-rev	GGCGACTGCGGCGGCGCCTCCGCCCTTG
cypD-S20A-for	AGCATCGCAGCGGCGCTGGTTCCGTGG
cypD-S20A-rev	CGCCGCTGCGATGCTGCCGGTAACGTG
cypD-S20D-for	AGCATCGACGCGGCGCTGGTTCCGTGG
cypD-S20D-rev	CGCCGCGTCGATGCTGCCGGTAACGTG
cypD-L23A-for	GCGGCGGCAGTTCCGTGGTGGATTCAC
cypD-L23A-rev	CGGAACTGCCGCCGCGCTGATGCTGCC
cypD-L23Q-for	GCGGCGCAAGTTCCGTGGTGGATTCAC
cypD-L23Q-rev	CGGAACTTGCGCCGCGCTGATGCTGCC
cypD-F170A-for	GTGGGTGCAAACCTGCCGGGTGCGCTG
cypD-F170A-rev	CAGGTTTGCACCCACTTCCGCGGTTTG
cypD-F170Q-for	GTGGGTCAAAACCTGCCGGGTGCGCTG
cypD-F170Q-rev	CAGGTTTTGACCCACTTCCGCGGTTTG
cypD-H59D-for	CTGCGTGACCTGGCGAACGGCAAAGTG
cypD-H59D-rev	CGCCAGGTCACGCAGCGCACGCACCGC
cypD-H59A-for	CTGCGTGCACTGGCGAACGGCAAAGTG
cypD-H59A-rev	CGCCAGTGCACGCAGCGCACGCACCGC
cypD-H29R-for	TGGATTAGATGGCTGCGTGAGTTCCAG
cypD-H29R-rev	CAGCCATCTAATCCACCACGGAACCAG
cypD-H29A-for	TGGATTGCATGGCTGCGTGAGTTCCAG
cypD-H29A-rev	CAGCCATGCAATCCACCACGGAACCAG
cypD-N80H-for	GAAGTTCACAGCGGTAAAAGCGGCGCG
cypD-N80H-rev	ACCGCTGTGAACTTCCGGCGGCACATC
cypD-N80D-for	GAAGTTGACAGCGGTAAAAGCGGCGCG

*CypD*N80D-rev	ACCGCTGTCAACTTCCGGCGGCACATC

Supplementary Table 3. Gene sequences of *tvaF*$_{S-87}$, *cypD* and *3c*.

Name	Sequence
tvaF$_{S-87}$	ATGACCGACCACGCCACCGGCCCGCAGCAGGCACTGGCGGGGGTTCGGT TGTTGTGGGGCGTGTGCGGCTCCTTCTCCGCTGTTGCGGTCCCCCACGTG AACGCATGGCTGCGTGGCACCGTCGGGGTCCGGGAGATCCGCACCATCA TGACCACGCAGGCACACGCCCTCATGGGGCCGCGCATGATCGAGGCTGT CACCGGCCATATGCCGGTGACCGGCTGGGAGGACCACAAGGGCGGAGG CGCCGCCCACGTCGCCCTCGGCACCTGGGCGGACGTGCTGGTGGTCTTGC CGGCCACCGCCAATTTCCTGGCCAAGGCAGCACACGGCATCGCGGACGA CGTCCTGACAGCCACACTGCTCGCCACCGAGTGCCCCGTGGTGATCGCCC CCGTCATGAACGCGGCCATGTGGTCCAAACCCGCCGTACGCCGCAACGT CGATCAGCTCCGCGAAGACGGCTACCAGATCGTCGAGCCGAAGGAGGGC ATCTCCCTCACCGAGGGCCGACGGGAAGCCGGTTCACTCGGCGACTTCC AGCCGGCAATCTCCGCCGCTCTGGTCCAGGCAGCTGCACGACGCACCCA CCCACAAGGACAGTGA
cypD	ATGAACGTGGAGAAGTTCGAGGGTGCGGAGCTGCACGTGCACGTTACCG GCAGCATCAGCGCGGCGCTGGTTCCGTGGTGGATTCACTGGCTGCGTGA GTTCCAGCCGGAGCTGGTTGTGAACGTGAGCGTTACCCCGGCGGCGAGC CGTTTTCTGGCGGTGCGTGCGCTGCGTCACCTGGCGAACGGCAAAGTGTG GGTTGACAGCTGGGACGATCCGGATGTGCCGCCGGAAGTTAACAGCGGT AAAAGCGGCGCGAGCGAGTGCTTCCTGGTGTTTCCGGCGACCCTGGACA CCGTTATGCGTCTGGCGCAGGGTCGTGCGGATAGCCCGGCGCTGATGAT GCTGCAACTGACCGACGCGCCGCTGGTTATCGCGGATACCTTTCCGGGCA GCAACGAAATTGTGGAGAACAACGTTCAGACCCTGAAACTGCGTCCGAA CGTGGAGTTCGCGCCGCGTGTGAACGGTGTTCGTGCGAGCAACCGTCAA ACCGCGGAAGTGGGTTTTAACCTGCCGGGTGCGCTGGCGGCGGCGAACC GTATGCGTAAAGAAGGTCGTAGCGGCGAGTAA
3c	ATGGCTAGCATGACTGGTGGACAGCAAATGGGTCGCGGATCCGGACCTA ACACTGAGTTTGCTCTGTCTCTGCTGCGTAAAAACATCATGACTATCACC ACTAGTAAAGGCGAGTTCACTGGTCTGGGTATTCACGATCGTGTTTGTGT TATTCCTACTCATGCTCAGCCGGGTGACGATGTTCTGGTAAACGGTCAAA AAATTCGTGTTAAGGATAAATACAAACTGGTTGACCCGGAAAACATCAA TCTAGAACTGACCGTACTGACTCTGGATCGTAATGAAAAGTTCCGTGACA TCCGTGGTTTTATTTCTGAAGACCTGGAAGGTGTCGACGCAACCCTGGTT GTACATAGCAATAACTTTACTAACACTATTCTGGAGGTTGGTCCGGTAAC TATGGCTGGTCTGATCAACCTGTCTAGCACTCCGACCAACCGCATGATTC GTTACGACTACGCAACTAAAACTGGTCAGTGTGGTGGTGTTCTGTGCGCA ACCGGTAAGATCTTTGGCATCCATGTAGGCGGTAACGGTCGTCAGGGTTT CTCTGCACAACTGAAGAAGCAATACTTTGTAGAGAAGCAGTAA

Supplementary Table 4. HR-MS and HR-MS/MS Data collection of all compounds analyzed in this study. _ _, not observed; and N.D., not detected.

Peptidyl mimics (PM)	Calcd.	Obs.	Er. ppm
1 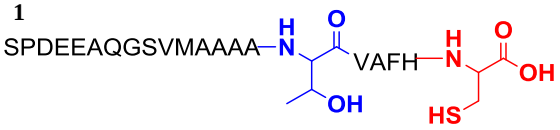	1046.4596 $[M+2H]^{2+}$	1046.4606 $[M+2H]^{2+}$	1.0
1-I 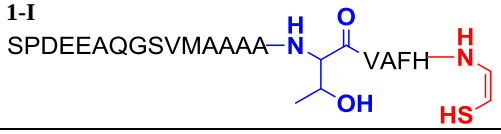	1023.4569 $[M+2H]^{2+}$	1023.4562 $[M+2H^{+}]^{2+}$	0.7
1-III 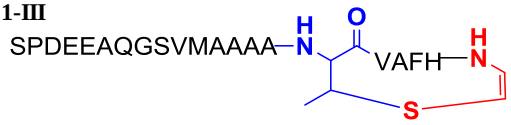	1014.4516 $[M+2H]^{2+}$	1014.4581 $[M+2H]^{2+}$	6.4
1-II 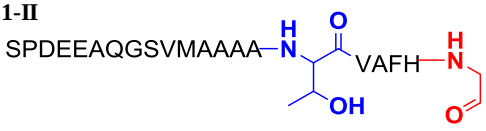	1015.4684 $[M+2H]^{2+}$	1015.4662 $[M+2H]^{2+}$	2.2
1-T8A 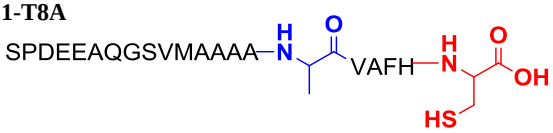	1031.4544 $[M+2H]^{2+}$	1031.4557 $[M+2H]^{2+}$	1.3
1-T8A-I 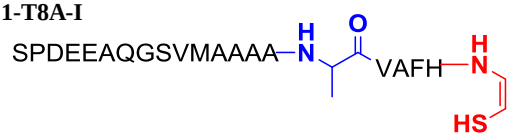	1008.4517 $[M+2H]^{2+}$	1008.4541 $[M+2H]^{2+}$	2.4
1-T8A-II 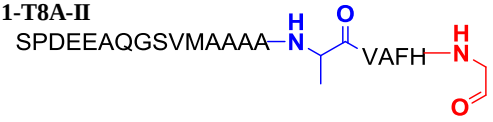	1000.4631 $[M+2H]^{2+}$	1000.4646 $[M+2H]^{2+}$	1.5
1-T8S 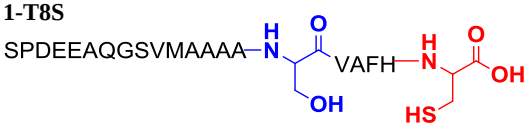	1039.4519 $[M+2H]^{2+}$	1039.4493 $[M+2H]^{2+}$	2.5
1-T8S-I 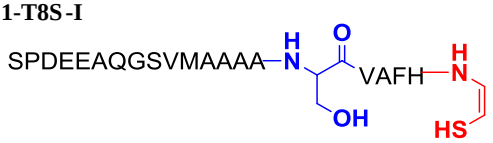	1016.4491 $[M+2H]^{2+}$	1016.4470 $[M+2H]^{2+}$	2.1

1-T8S-III 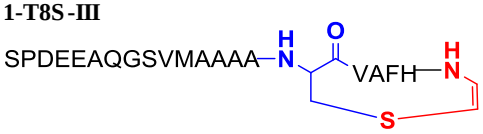	1007.4438 $[M+2H]^{2+}$	1007.4490 $[M+2H]^{2+}$	5.2
1-T8S-II 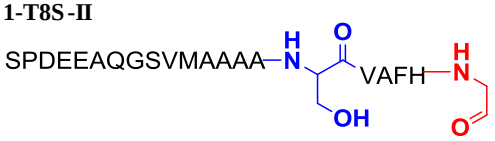	1008.4605 $[M+2H]^{2+}$	1008.4579 $[M+2H]^{2+}$	2.6
1-T8C 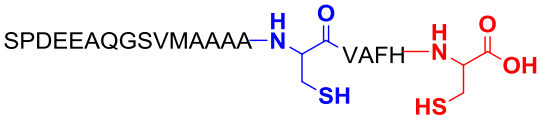	1047.4404 $[M+2H]^{2+}$	1047.4406 $[M+2H]^{2+}$	0.2
1-T8C-I 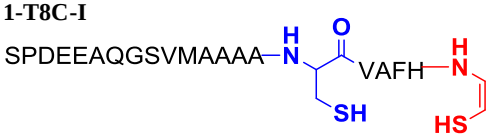	1024.4377 $[M+2H]^{2+}$	1024.4386 $[M+2H]^{2+}$	0.9
1-T8C-III 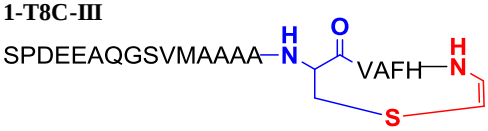	1007.4438 $[M+2H]^{2+}$	– –	– –
1-T8C-II 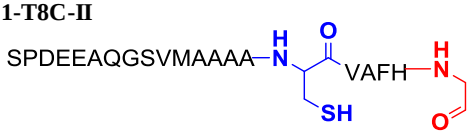	1016.4492 $[M+2H]^{2+}$	1016.4494 $[M+2H]^{2+}$	0.2
1-C13A 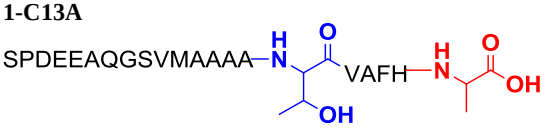	1030.4737 $[M+2H]^{2+}$	1030.4764 $[M+2H]^{2+}$	2.7
1-C13A-I 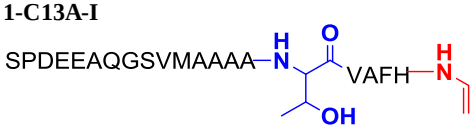	1007.4709 $[M+2H]^{2+}$	– –	– –
1-C13S 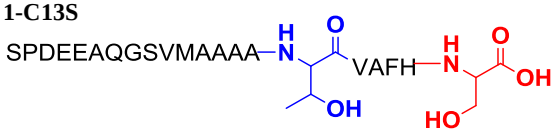	1038.4711 $[M+2H]^{2+}$	1038.4697 $[M+2H]^{2+}$	1.4
1-C13S-I 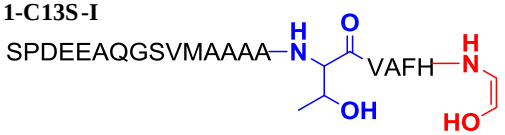	1015.4684 $[M+2H]^{2+}$	– –	– –

1-C13T 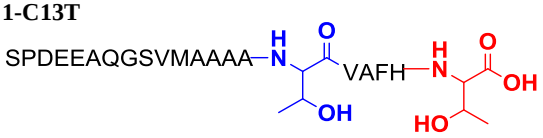	1045.4790 $[M+2H]^{2+}$	1045.4780 $[M+2H]^{2+}$	1.0
1-C13T-I 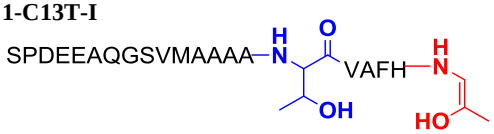	1022.4762 $[M+2H]^{2+}$	– –	– –
1-NEM 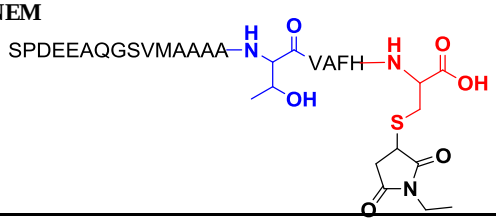	1108.9835 $[M+2H]^{2+}$	1108.9807 $[M+2H]^{2+}$	2.5
1-I-NEM 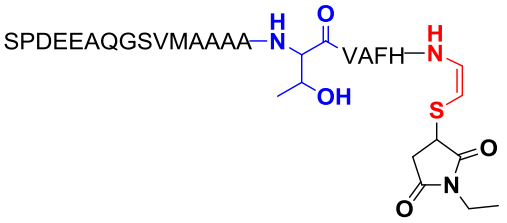	1085.9807 $[M+2H]^{2+}$	1085.9799 $[M+2H]^{2+}$	0.7
1-II-HOPI 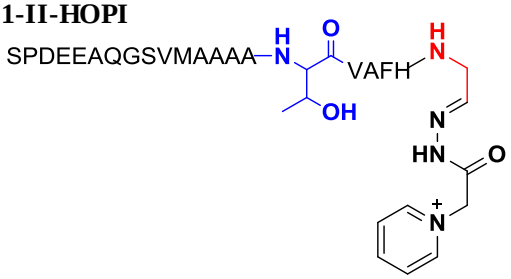	1082.0001 $[M+2H]^{2+}$	1081.9943 $[M+2H]^{2+}$	5.3
2 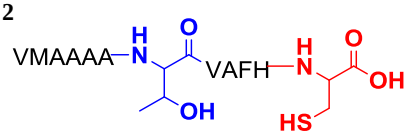	596.2866 $[M+2H]^{2+}$	596.2846 $[M+2H]^{2+}$	3.4
2-I 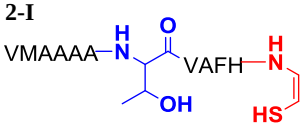	573.2839 $[M+2H]^{2+}$	573.2809 $[M+2H]^{2+}$	5.2
2-III 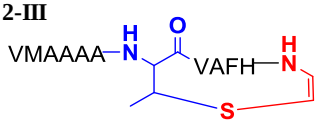	564.2786 $[M+2H]^{2+}$	564.2836 $[M+2H]^{2+}$	8.9

2-II 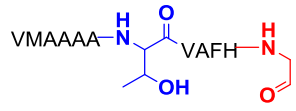	565.2953 $[M+2H]^{2+}$	565.2923 $[M+2H]^{2+}$	5.7
3 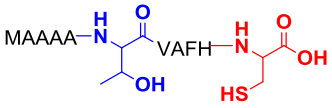	546.7524 $[M+2H]^{2+}$	546.7499 $[M+2H]^{2+}$	4.6
3-I 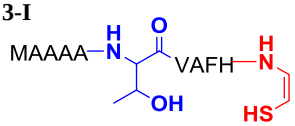	523.7497 $[M+2H]^{2+}$	523.7488 $[M+2H]^{2+}$	1.7
3-III 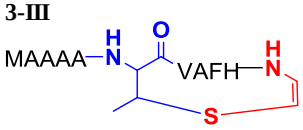	514.7444 $[M+2H]^{2+}$	514.7419 $[M+2H]^{2+}$	4.9
3-II 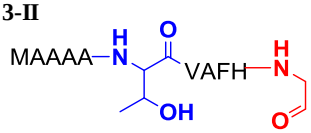	515.7611 $[M+2H]^{2+}$	515.7584 $[M+2H]^{2+}$	5.2
4 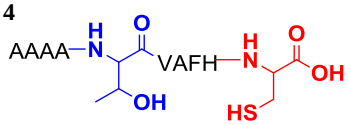	961.4566 $[M+H]^{+}$	961.4536 $[M+H]^{+}$	3.1
4-I 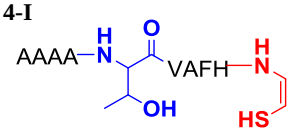	915.4511 $[M+H]^{+}$	915.4510 $[M+H]^{+}$	0.1
4-III 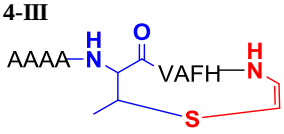	897.4405 $[M+H]^{+}$	– –	– –
4-II 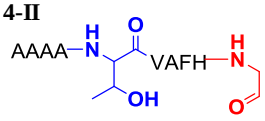	899.4739 $[M+H]^{+}$	N.D.	N.D.
5 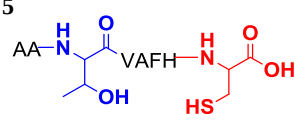	819.3823 $[M+H]^{+}$	819.3790 $[M+H]^{+}$	4.0

5-I 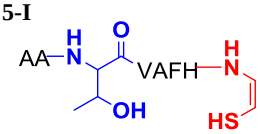	773.3769 $[M+H]^+$	773.3810 $[M+H]^+$	5.3
5-III 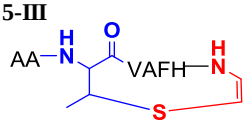	755.3663 $[M+H]^+$	– –	– –
5-II 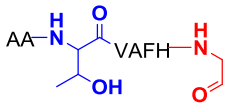	757.3997 $[M+H]^+$	N.D.	N.D.
6 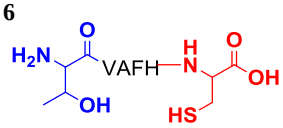	677.3081 $[M+H]^+$	677.3058 $[M+H]^+$	3.4
6-I 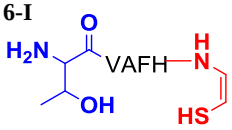	631.3026 $[M+H]^+$	631.3067 $[M+H]^+$	6.5
6-III 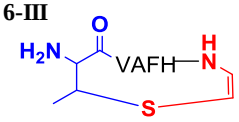	613.2921 $[M+H]^+$	– –	– –
6-II 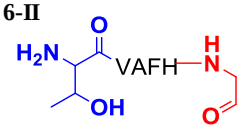	615.3255 $[M+H]^+$	N.D.	N.D.
7 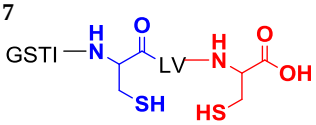	795.3739 $[M+H]^+$	795.3726 $[M+H]^+$	1.6
7-I 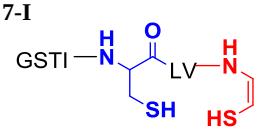	749.3684 $[M+H]^+$	749.3668 $[M+H]^+$	2.1
7-III/IV 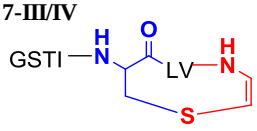	715.3808 $[M+H]^+$	715.3805 $[M+H]^+$	0.4
7-II 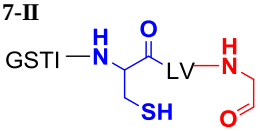	733.3913 $[M+H]^+$	733.3898 $[M+H]^+$	2.1

7-NEM 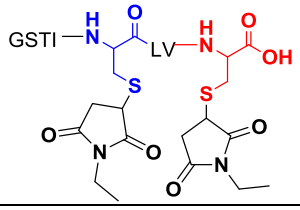	1045.4693 $[M+H]^+$	1045.4646 $[M+H]^+$	4.5
7-I-NEM 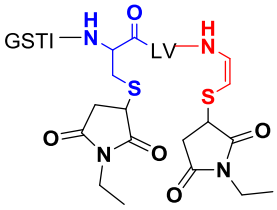	999.4638 $[M+H]^+$	999.4646 $[M+H]^+$	0.8
7-C19S 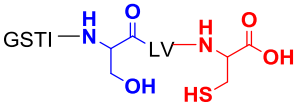	779.3968 $[M+H]^+$	779.3934 $[M+H]^+$	4.4
7-C19S-I 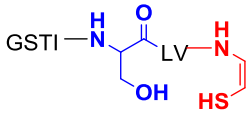	733.3913 $[M+H]^+$	733.3911 $[M+H]^+$	0.3
7-C19S-III 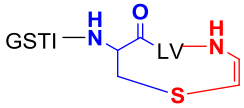	715.3808 $[M+H]^+$	715.3802 $[M+H]^+$	0.8
7-C19S-II 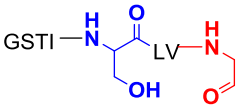	717.4141 $[M+H]^+$	717.4122 $[M+H]^+$	2.7
7-C19T 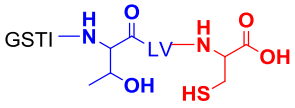	793.4124 $[M+H]^+$	793.4112 $[M+H]^+$	1.5
7-C19T-I 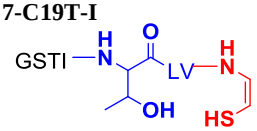	747.4069 $[M+H]^+$	747.4070 $[M+H]^+$	0.1
7-C19T-III 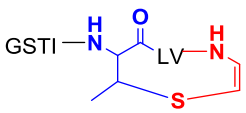	729.3965 $[M+H]^+$	– –	– –

7-C19T-II 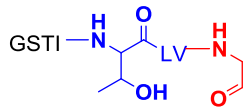	731.4298 $[M+H]^+$	731.4286 $[M+H]^+$	1.6
7-C19A 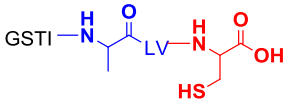	763.4019 $[M+H]^+$	763.4012 $[M+H]^+$	0.9
7-C19A-I 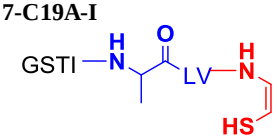	717.3964 $[M+H]^+$	717.3962 $[M+H]^+$	0.3
7-C19A-II 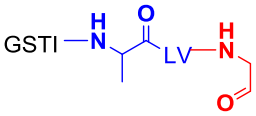	701.4192 $[M+H]^+$	701.4181 $[M+H]^+$	1.6
7-C22A	763.4019 $[M+H]^+$	763.4013 $[M+H]^+$	0.8
7- C22A-I 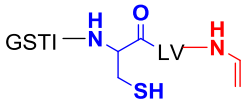	717.3964 $[M+H]^+$	– –	– –
7-C22S 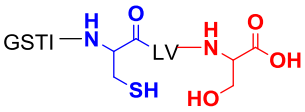	779.3968 $[M+H]^+$	779.3947 $[M+H]^+$	2.7
7- C22S-I 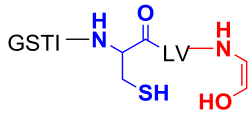	733.3913 $[M+H]^+$	– –	– –
7-C22T 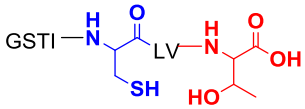	793.4124 $[M+H]^+$	793.4112 $[M+H]^+$	1.5
7- C22T-I 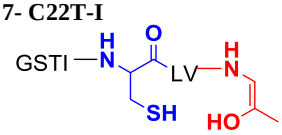	747.4069 $[M+H]^+$	– –	– –

7-C19S-Ac 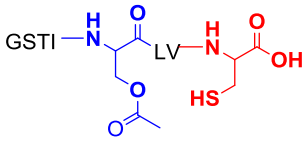	821.4073 $[M+H]^+$	821.4020 $[M+H]^+$	6.5
7-C19S-Ac-I 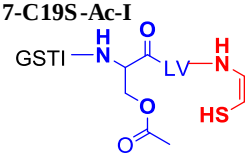	775.4019 $[M+H]^+$	775.3988 $[M+H]^+$	4.0
7-C19S-Ac-II 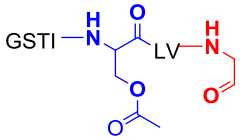	759.4247 $[M+H]^+$	759.4232 $[M+H]^+$	2.0
7-C19S-P 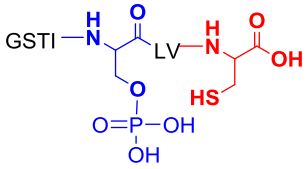	859.3631 $[M+H]^+$	859.3580 $[M+H]^+$	5.9
7-C19S-P-I 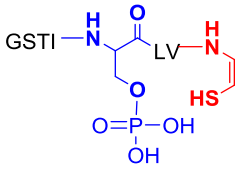	813.3576 $[M+H]^+$	– –	– –
7-C19S-P-II 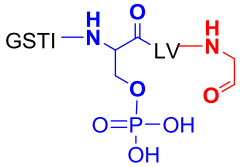	797.3805 $[M+H]^+$	– –	– –
7-C19S-Glu 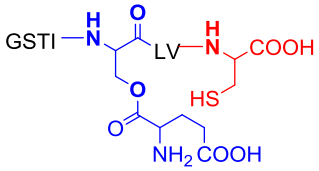	454.7233 $[M+2H]^{2+}$	454.7211 $[M+2H]^{2+}$	4.9
7-C19S-Glu-I 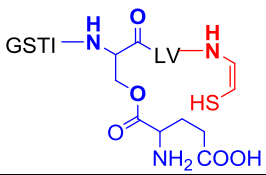	431.7206 $[M+2H]^{2+}$	– –	– –

7-C19S-Glu-II 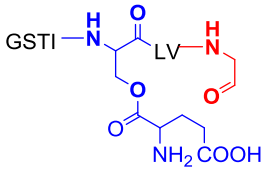	423.7320 $[M+2H]^{2+}$	– –	– –
7-Dha19 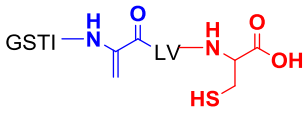	761.3862 $[M+H]^{+}$	761.3836 $[M+H]^{+}$	3.4
7-Dha19-I 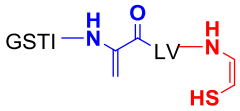	715.3808 $[M+H]^{+}$	– –	– –
7-Dha19-II 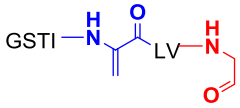	699.4036 $[M+H]^{+}$	– –	– –
7- d-C19 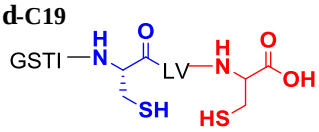	795.3739 $[M+H]^{+}$	795.3711 $[M+H]^{+}$	3.5
7-C19S-D_3 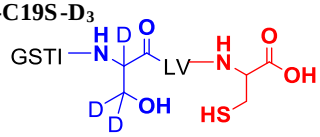	782.4156 $[M+H]^{+}$	782.4136 $[M+H]^{+}$	2.6
7-C19S-D_3-I 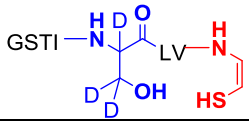	736.4101 $[M+H]^{+}$	736.4086 $[M+H]^{+}$	2.0
7-C19S-D_3-II 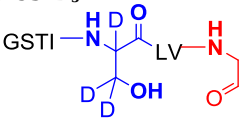	720.4330 $[M+H]^{+}$	720.4305 $[M+H]^{+}$	3.5

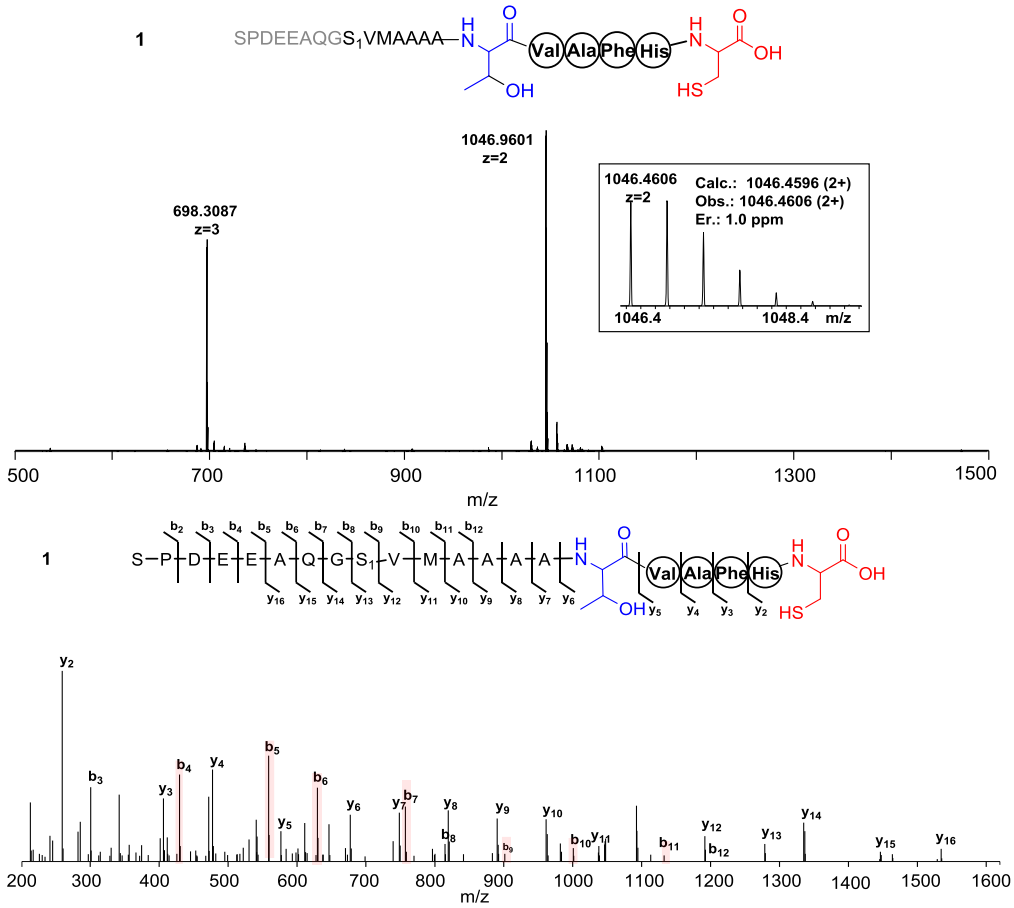

Ions	Calcd.	Obs.	Er. (ppm)	Ions	Calcd.	Obs.	Er. (ppm)
b_2	185.0926	185.0921	2.7	y_2	259.0864	259.0860	1.5
b_3	300.1196	300.1190	2.0	y_3	406.1548	406.1544	1.0
b_4	429.1621	429.1617	0.9	y_4	477.1920	477.1917	0.6
b_5	558.2047	558.2045	0.4	y_5	576.2604	576.2601	0.5
b_6	629.2418	629.2414	0.6	y_6	677.3081	677.3079	0.3
b_7	757.3004	757.3000	0.5	y_7	748.3452	748.3447	0.7
b_8	814.3219	814.3214	0.6	y_8	819.3823	819.3820	0.4
b_9	901.3539	901.3528	1.2	y_9	890.4194	890.4192	0.2
b_{10}	1000.4223	1000.4218	0.5	y_{10}	961.4565	961.4564	0.1
b_{11}	1131.4628	1131.4623	0.4	y_{11}	1092.4970	1092.4971	0.1
b_{12}	1202.4999	1202.4978	1.7	y_{12}	1191.5654	1191.5647	0.3
				y_{13}	1278.5974	1278.5996	1.7
				y_{14}	1335.6189	1335.6188	0.1
				y_{15}	1463.6775	1463.6702	5.0
				y_{16}	1534.7146	1534.7172	1.7

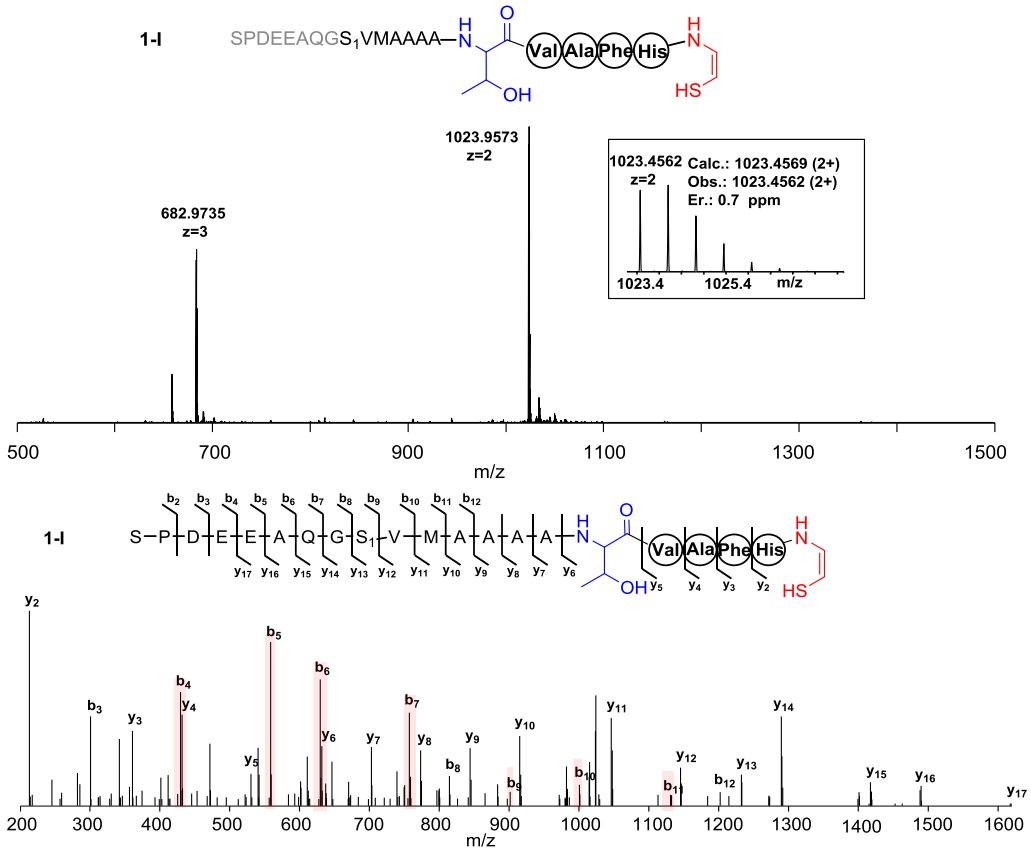

Ions	Calcd.	Obs.	Er. (ppm)	Ions	Calcd.	Obs.	Er. (ppm)
b_2	185.0926	185.0921	2.7	y_2	213.0810	213.0807	1.4
b_3	300.1196	300.1189	2.3	y_3	360.1494	360.1489	1.4
b_4	429.1621	429.1618	0.7	y_4	431.1865	431.1861	0.9
b_5	558.2047	558.2045	0.4	y_5	530.2549	530.2548	0.2
b_6	629.2418	629.2413	0.8	y_6	631.3026	631.3021	0.8
b_7	757.3004	757.3003	0.1	y_7	702.3397	702.3392	0.7
b_8	814.3219	814.3215	0.5	y_8	773.3768	773.3760	1.0
b_9	901.3539	901.3558	2.1	y_9	844.4139	844.4139	0.0
b_{10}	1000.4223	1000.4229	0.6	y_{10}	915.4510	915.4505	0.5
b_{11}	1131.4628	1131.4623	0.4	y_{11}	1046.4915	1046.4917	0.2
b_{12}	1202.4999	1202.5009	0.8	y_{12}	1145.5599	1145.5603	0.3
				y_{13}	1232.5920	1232.5917	0.2
				y_{14}	1289.6134	1289.6141	0.5
				y_{15}	1417.6720	1417.6727	0.5
				y_{16}	1488.7091	1488.7134	2.9
				y_{17}	1617.7517	1617.7543	1.6

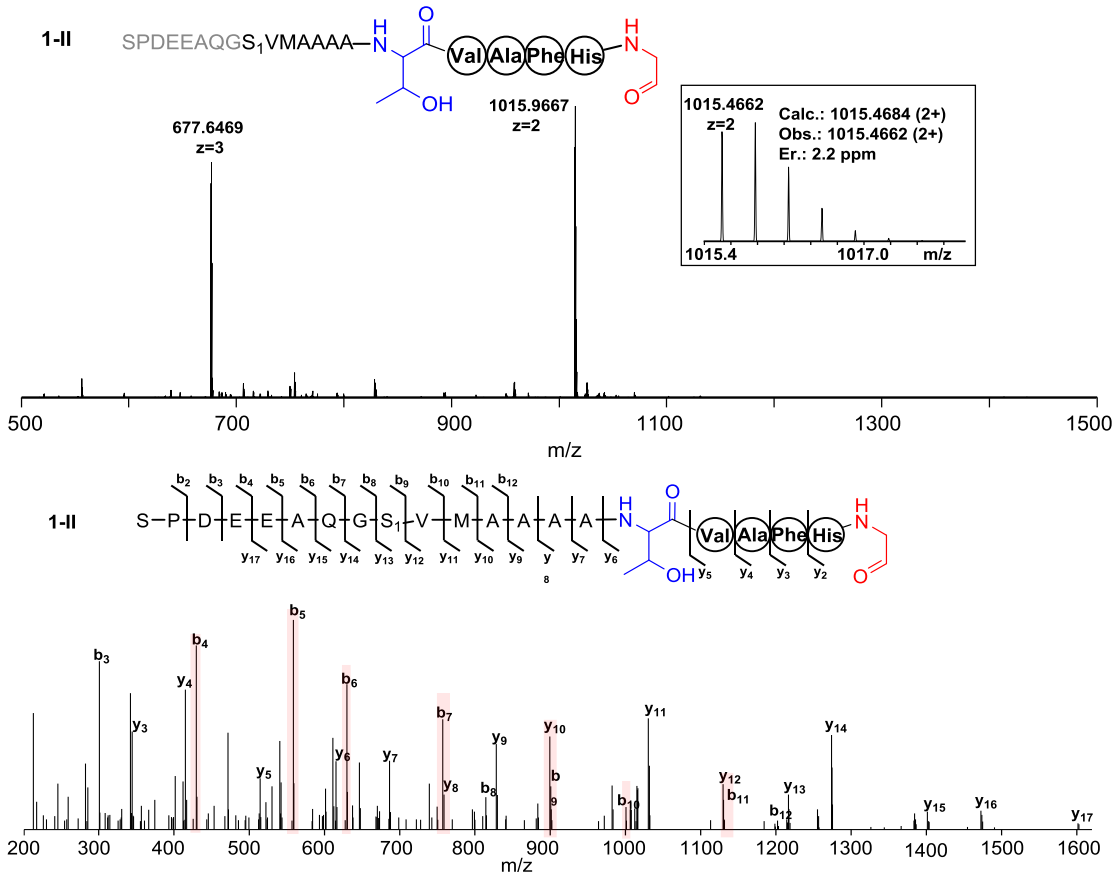

Ions	Calcd.	Obs.	Er. (ppm)	Ions	Calcd.	Obs.	Er. (ppm)
b_2	185.0926	185.0921	2.7	y_2	197.1038	197.1034	2.0
b_3	300.1196	300.1190	2.0	y_3	344.1722	344.1717	1.5
b_4	429.1621	429.1617	0.9	y_4	415.2093	415.2089	1.0
b_5	558.2047	558.2043	0.7	y_5	514.2777	514.2776	0.2
b_6	629.2418	629.2415	0.5	y_6	615.3254	615.3251	0.5
b_7	757.3004	757.3001	0.4	y_7	686.3625	686.3622	0.4
b_8	814.3219	814.3215	0.5	y_8	757.3996	757.3990	0.8
b_9	901.3539	901.3535	0.4	y_9	828.4368	828.4363	0.6
b_{10}	1000.4223	1000.4216	0.7	y_{10}	899.4739	899.4739	0.0
b_{11}	1131.4628	1131.4618	0.9	y_{11}	1030.5144	1030.5140	0.4
b_{12}	1202.4999	1202.5031	2.7	y_{12}	1129.5828	1129.5831	0.3
				y_{13}	1216.6148	1216.6149	0.1
				y_{14}	1273.6363	1273.6371	0.6
				y_{15}	1401.6948	1401.6958	0.7
				y_{16}	1472.7320	1472.7324	0.3
				y_{17}	1601.7746	1601.7646	6.2

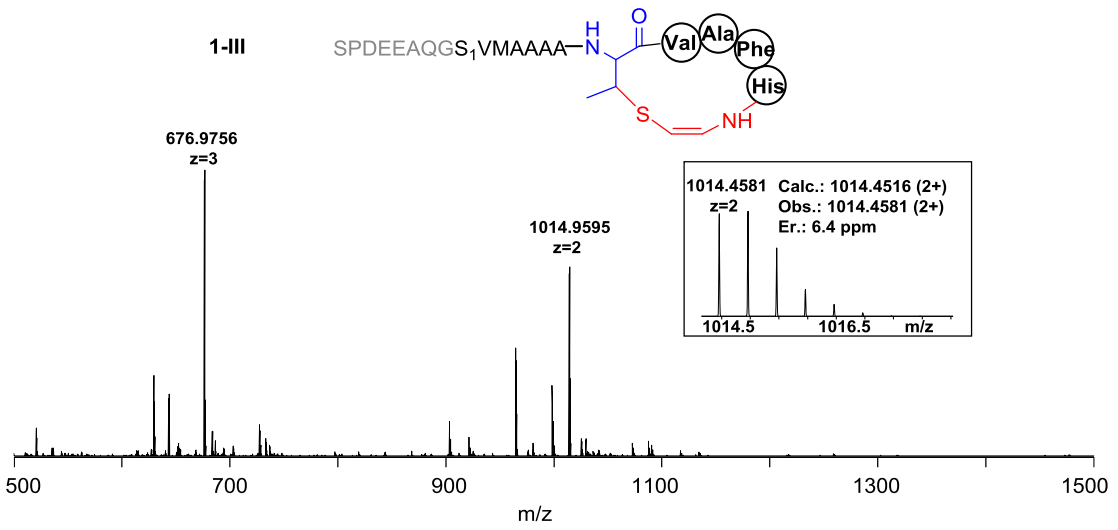

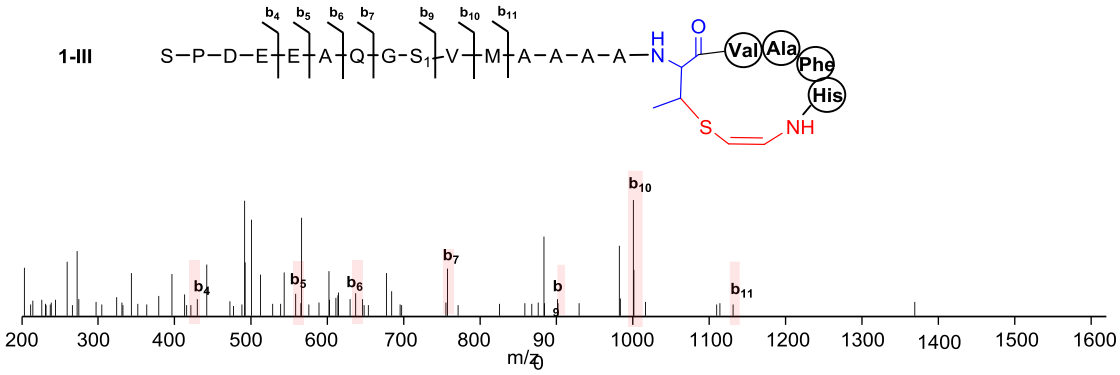

Ions	Calcd.	Obs.	Er. (ppm)
b_4	429.1621	429.1612	2.1
b_5	558.2047	558.2034	2.3
b_6	629.2418	629.2401	2.7
b_7	757.3004	757.2979	3.3
b_9	901.3539	901.3539	0.0
b_{10}	1000.4223	1000.4206	1.7
b_{11}	1131.4628	1131.4624	0.4

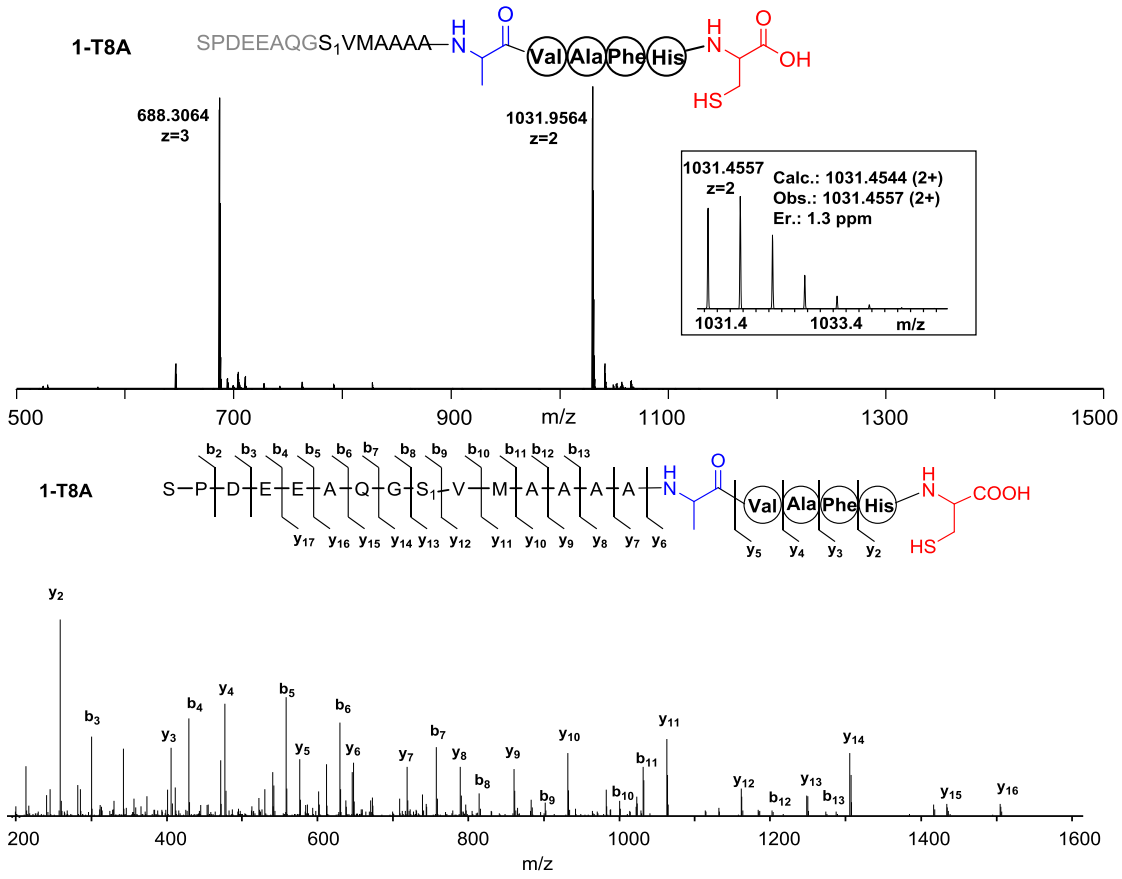

Ions	Calcd.	Obs.	Er. (ppm)	Ions	Calcd.	Obs.	Er. (ppm)
b_2	185.0926	185.0925	0.5	y_2	259.0864	259.0865	0.4
b_3	300.1196	300.1196	0.0	y_3	406.1548	406.1553	1.2
b_4	429.1621	429.1627	1.4	y_4	477.1920	477.1927	1.5
b_5	558.2047	558.2057	1.8	y_5	576.2604	576.2614	1.7
b_6	629.2418	629.2428	1.6	y_6	647.2975	647.2982	1.1
b_7	757.3004	757.3016	1.6	y_7	718.3346	718.3358	1.7
b_8	814.3219	814.3230	1.4	y_8	789.3717	789.3732	1.9
b_9	901.3539	901.3554	1.7	y_9	860.4088	860.4099	1.3
b_{10}	1000.4223	1000.4249	2.6	y_{10}	931.4459	931.4471	1.3
b_{11}	1131.4628	1131.4663	3.1	y_{11}	1062.4864	1062.4883	1.8
b_{12}	1202.4999	1202.4990	0.7	y_{12}	1161.5548	1161.5579	2.7
b_{13}	1273.5371	1273.5366	0.4	y_{13}	1248.5869	1248.5912	3.4
				y_{14}	1305.6083	1305.6116	2.5
				y_{15}	1433.6669	1433.6674	0.3
				y_{16}	1504.7040	1504.7078	2.5
				y_{17}	1633.7466	1633.7512	2.8

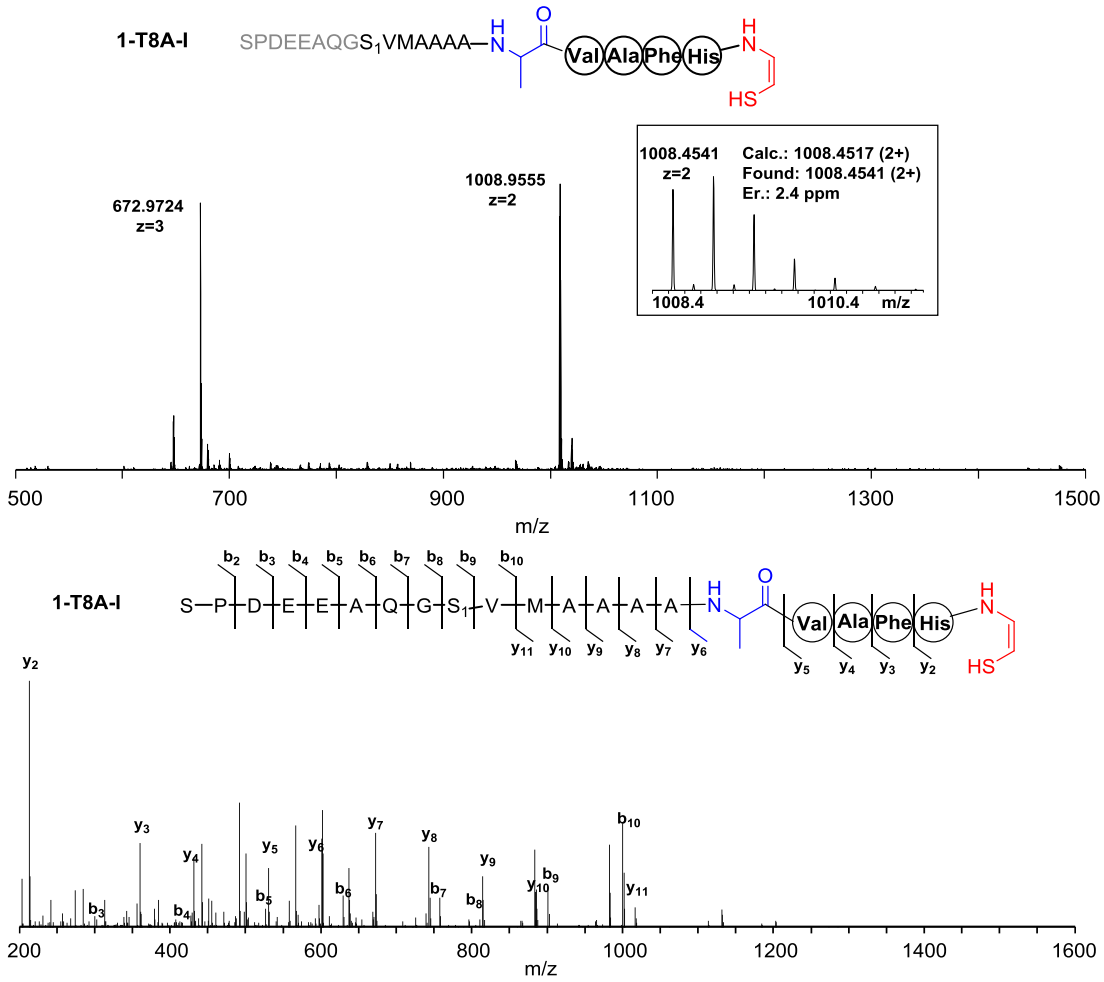

Ions	Calcd.	Obs.	Er. (ppm)	Ions	Calcd.	Obs.	Er. (ppm)
b_2	185.0926	185.0924	1.1	y_2	213.0810	213.0809	0.5
b_3	300.1196	300.1194	0.7	y_3	360.1494	360.1495	0.3
b_4	429.1621	429.1620	0.2	y_4	431.1865	431.1869	0.9
b_5	558.2047	558.2054	1.3	y_5	530.2549	530.2557	1.5
b_6	629.2418	629.2429	1.7	y_6	601.2920	601.2928	1.3
b_7	757.3004	757.3011	0.9	y_7	672.3291	672.3300	1.3
b_8	814.3219	814.3228	1.1	y_8	743.3662	743.3671	1.2
b_9	901.3539	901.3548	1.0	y_9	814.4034	814.4041	0.9
b_{10}	1000.4223	1000.4239	1.6	y_{10}	885.4405	885.4415	1.1
				y_{11}	1016.4810	1016.4821	1.1

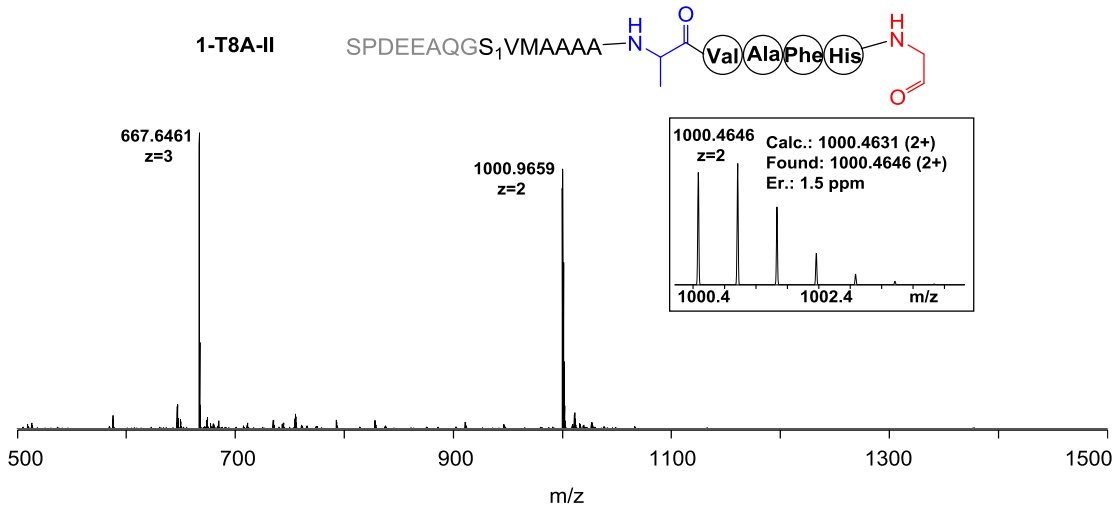
1-T8A-II
SPDEEAQGS1VMAAAA
Val
Ala
Phe
His
667.6461
z=3
1000.9659
z=2
1000.4646
z=2
Calc.: 1000.4631 (2+)
Found: 1000.4646 (2+)
Er.: 1.5 ppm
1000.4
1002.4
m/z
500
700
900
1100
1300
1500
m/z

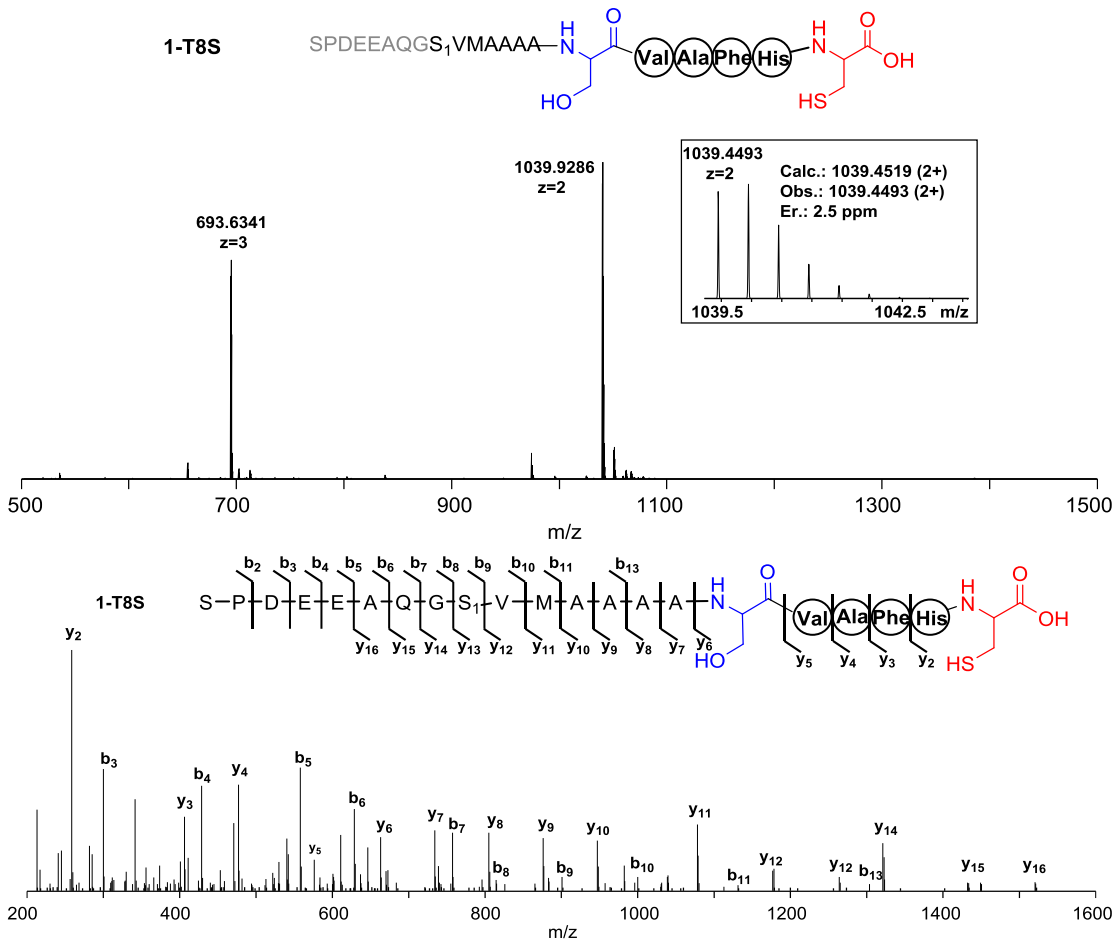

Ions	Calcd.	Obs.	Er. (ppm)	Ions	Calcd.	Obs.	Er. (ppm)
b_2	185.0926	185.0918	4.3	y_2	259.0864	259.0855	3.5
b_3	300.1196	300.1185	3.7	y_3	406.1548	406.1536	3.0
b_4	429.1621	429.1608	3.0	y_4	477.1920	477.1907	2.7
b_5	558.2047	558.2032	2.7	y_5	576.2604	576.2590	2.4
b_6	629.2418	629.2401	2.7	y_6	663.2924	663.2906	2.7
b_7	757.3004	757.2986	2.4	y_7	734.3295	734.3281	1.9
b_8	814.3219	814.3184	4.3	y_8	805.3666	805.3644	2.7
b_9	901.3539	901.3513	2.9	y_9	876.4037	876.4011	3.0
b_{10}	1000.4223	1000.4188	3.5	y_{10}	947.4409	947.4387	2.3
b_{11}	1131.4628	1131.4606	1.9	y_{11}	1078.4813	1078.4789	2.2
b_{13}	1273.5371	1273.5305	5.2	y_{12}	1177.5498	1177.5486	1.0
				y_{13}	1264.5818	1264.5795	1.8
				y_{14}	1321.6033	1321.6012	1.6
				y_{15}	1449.6618	1449.6553	4.5
				y_{16}	1520.6989	1520.6921	4.5

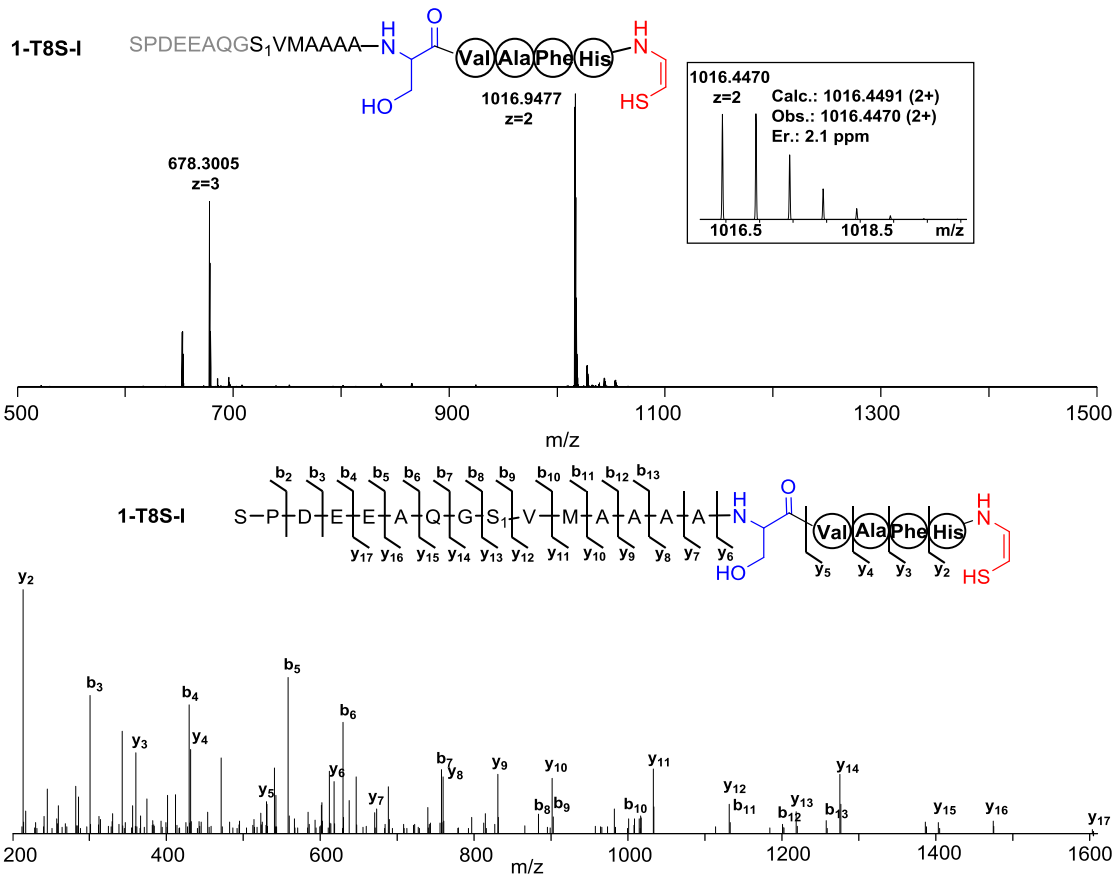

Ions	Calcd.	Obs.	Er. (ppm)	Ions	Calcd.	Obs.	Er. (ppm)
b_2	185.0926	185.0917	4.9	y_2	213.0810	213.0800	4.7
b_3	300.1196	300.1182	4.7	y_3	360.1494	360.1481	3.6
b_4	429.1621	429.1607	3.3	y_4	431.1865	431.1850	3.5
b_5	558.2047	558.2030	3.0	y_5	530.2549	530.2532	3.2
b_6	629.2418	629.2397	3.3	y_6	617.2869	617.2850	3.1
b_7	757.3004	757.2979	3.3	y_7	688.3240	688.3217	3.3
b_8	814.3219	814.3190	3.6	y_8	759.3612	759.3586	3.4
b_9	901.3539	901.3532	0.8	y_9	830.3983	830.3956	3.3
b_{10}	1000.4223	1000.4202	2.1	y_{10}	901.4354	901.4319	3.9
b_{11}	1131.4628	1131.4576	4.6	y_{11}	1032.4759	1032.4729	2.9
b_{12}	1202.4999	1202.4965	2.8	y_{12}	1131.5443	1131.5414	2.6
b_{13}	1273.5371	1273.5314	4.8	y_{13}	1218.5763	1218.5739	2.0
				y_{14}	1275.5978	1275.5944	2.7
				y_{15}	1403.6564	1403.6528	2.6
				y_{16}	1474.6935	1474.6876	4.0
				y_{17}	1603.7361	1603.7247	7.1

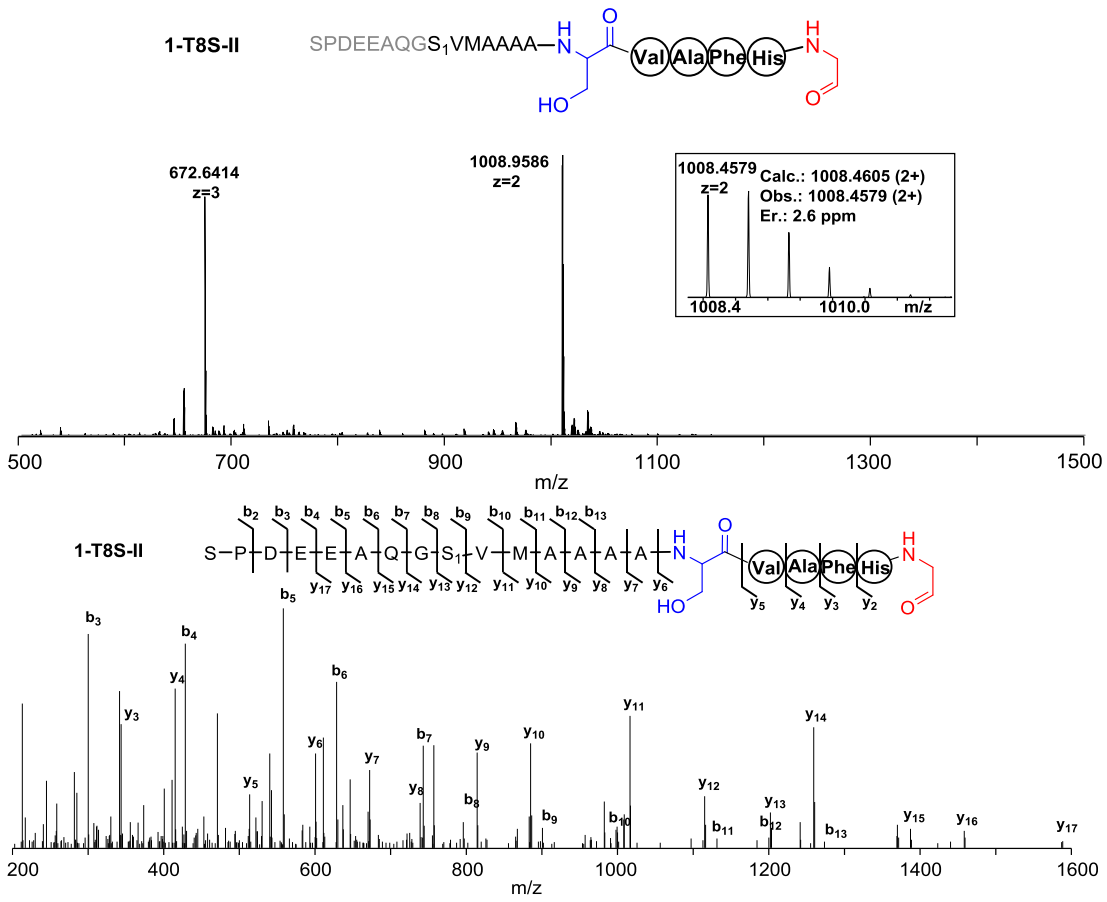

Ions	Calcd.	Obs.	Er. (ppm)	Ions	Calcd.	Obs.	Er. (ppm)
b_2	185.0926	185.0917	4.9	y_2	197.1038	197.1029	4.6
b_3	300.1196	300.1183	4.3	y_3	344.1722	344.1709	3.8
b_4	429.1621	429.1607	3.3	y_4	415.2093	415.2079	3.4
b_5	558.2047	558.2031	2.9	y_5	514.2777	514.2762	2.9
b_6	629.2418	629.2399	3.0	y_6	601.3098	601.3080	3.0
b_7	757.3004	757.2979	3.3	y_7	672.3469	672.3448	3.1
b_8	814.3219	814.3194	3.1	y_8	743.3840	743.3818	3.0
b_9	901.3539	901.3522	1.9	y_9	814.4211	814.4185	3.2
b_{10}	1000.4223	1000.4153	7.0	y_{10}	885.4582	885.4559	2.6
b_{11}	1131.4628	1131.4601	2.4	y_{11}	1016.4987	1016.4959	2.6
b_{12}	1202.4999	1202.4944	4.6	y_{12}	1115.5671	1115.5648	2.1
b_{13}	1273.5371	1273.5309	4.9	y_{13}	1202.5992	1202.5963	2.4
				y_{14}	1259.6206	1259.6176	2.4
				y_{15}	1387.6792	1387.6765	1.9
				y_{16}	1458.7163	1458.7126	2.5
				y_{17}	1587.7589	1587.7516	4.6

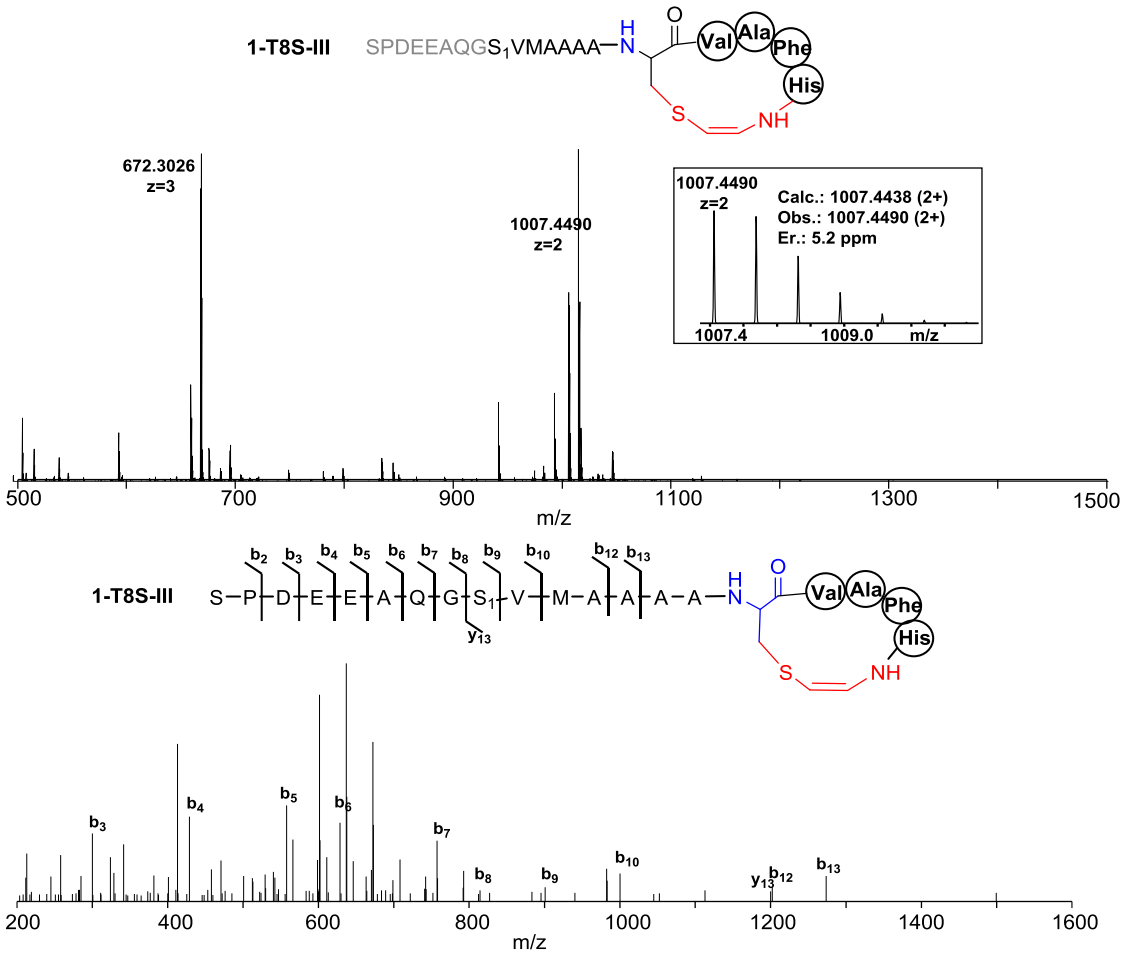

Ions	Calcd.	Obs.	Er. (ppm)
b_2	185.0926	185.0917	4.9
b_3	300.1196	300.1182	4.7
b_4	429.1621	429.1604	3.9
b_5	558.2047	558.2034	2.3
b_6	629.2418	629.2399	3.0
b_7	757.3004	757.2980	3.2
b_8	814.3219	814.3208	1.4
b_9	901.3539	901.3511	3.1
b_{10}	1000.4223	1000.4196	2.7
b_{12}	1202.4999	1202.4965	2.8
b_{13}	1273.5371	1273.5314	4.5
y_{13}	1200.5657	1200.5712	4.6

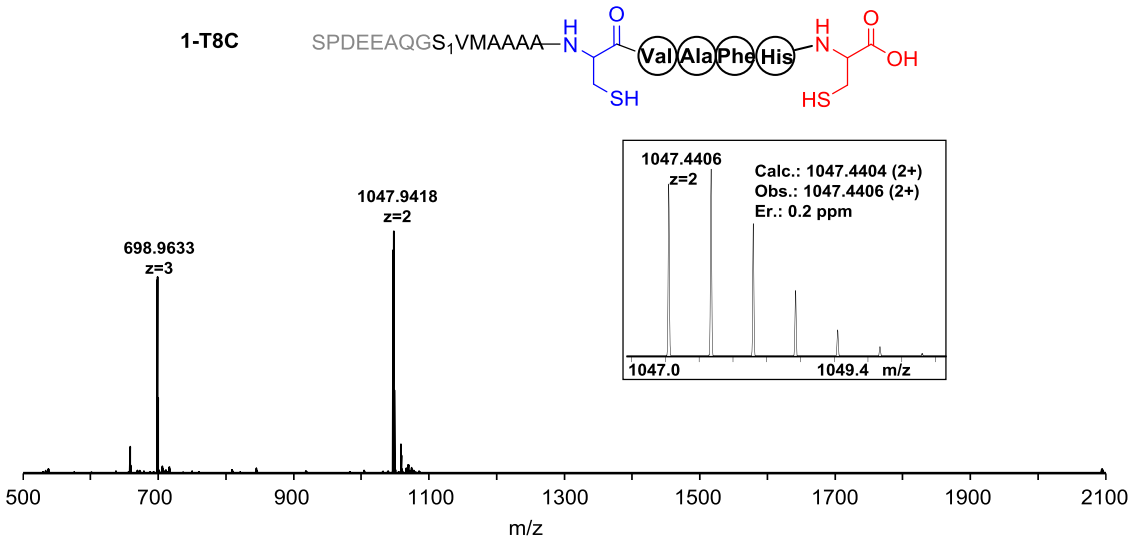
1-T8C
SPDEEAQGS1VMAAAA
Val Ala Phe His
SH
HS
OH
1047.4406
z=2
Calc.: 1047.4404 (2+)
Obs.: 1047.4406 (2+)
Er.: 0.2 ppm
1047.0
1049.4 m/z
1047.9418
z=2
698.9633
z=3
500 700 900 1100 1300 1500 1700 1900 2100
m/z

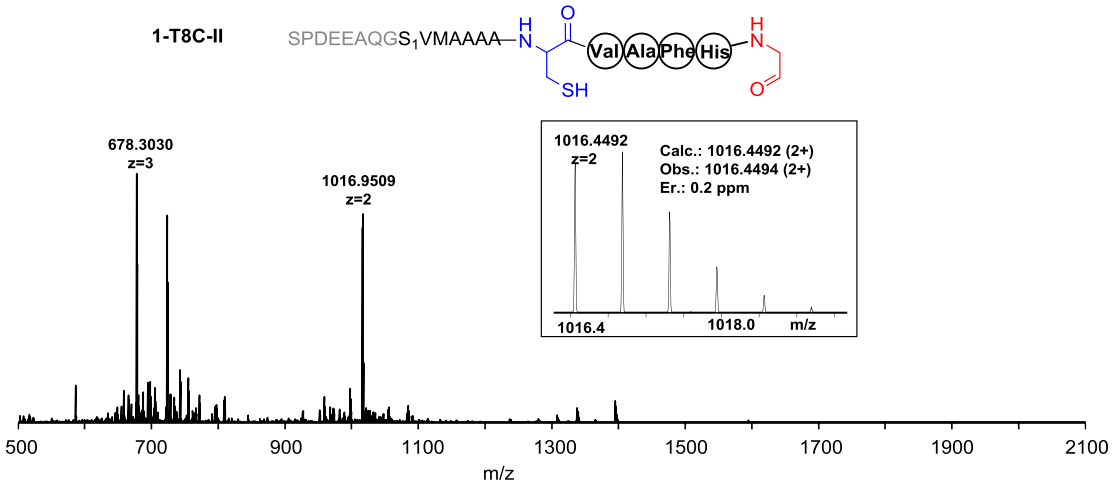
1-T8C-II
SPDEEAQGS1VMAAAA
Val Ala Phe His
SH
1016.4492
z=2
Calc.: 1016.4492 (2+)
Obs.: 1016.4494 (2+)
Er.: 0.2 ppm
1016.4
1018.0 m/z
678.3030
z=3
1016.9509
z=2
500 700 900 1100 1300 1500 1700 1900 2100
m/z

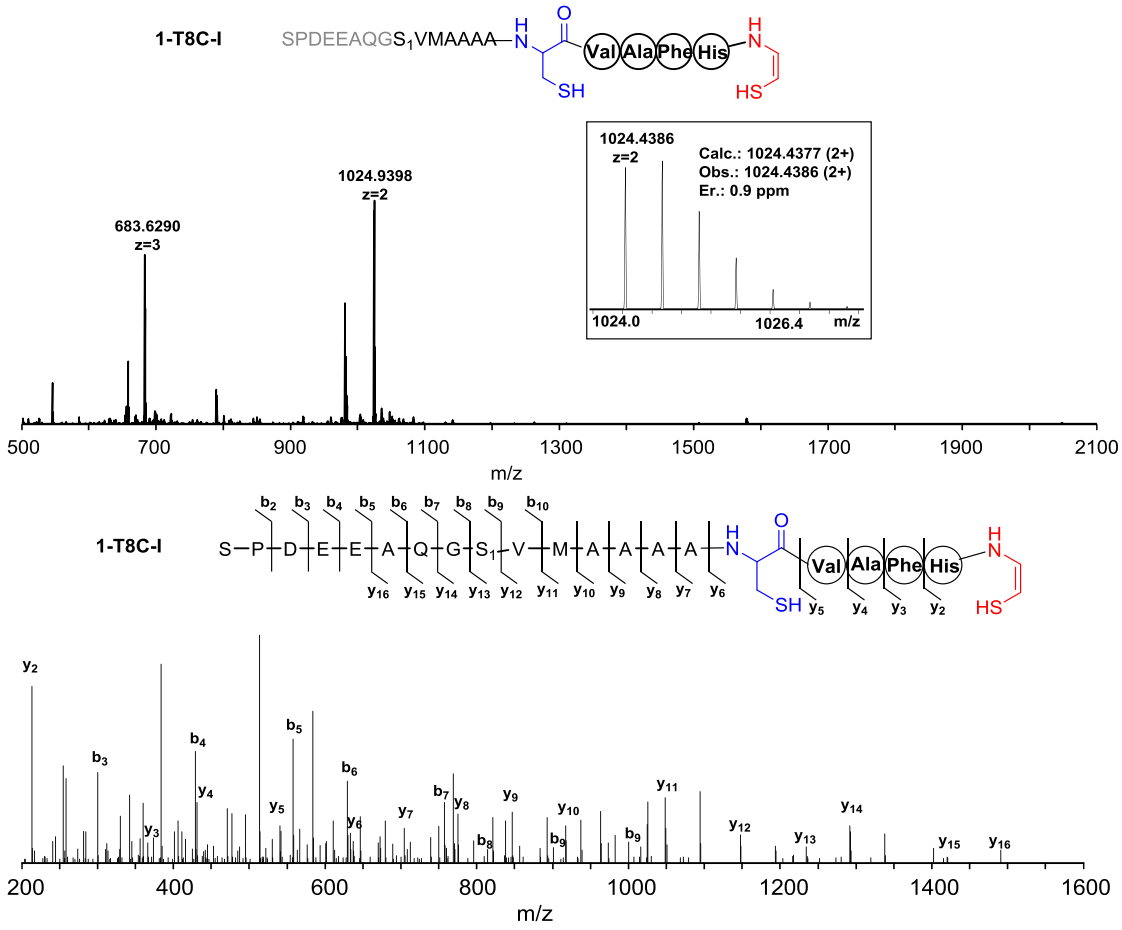

Ions	Calcd.	Obs.	Er. (ppm)	Ions	Calcd.	Obs.	Er. (ppm)
b_2	185.0926	185.0924	1.1	y_2	213.0810	213.0808	0.9
b_3	300.1196	300.1195	0.3	y_3	360.1494	360.1494	0.0
b_4	429.1621	429.1626	1.2	y_4	431.1865	431.1870	1.2
b_5	558.2047	558.2055	1.4	y_5	530.2549	530.2564	2.8
b_6	629.2418	629.2422	0.6	y_6	633.2641	633.2654	2.1
b_7	757.3004	757.3005	0.1	y_7	704.3012	704.3013	0.1
b_8	814.3219	814.3226	0.9	y_8	775.3383	775.3394	1.4
b_9	901.3539	901.3531	0.9	y_9	846.3754	846.3764	1.2
b_{10}	1000.4223	1000.4243	2.0	y_{10}	917.4125	917.4136	1.2
				y_{11}	1048.4530	1048.4552	2.1
				y_{12}	1147.5214	1147.5211	0.3
				y_{13}	1234.5535	1234.5518	1.4
				y_{14}	1291.5749	1291.5773	1.9
				y_{15}	1419.6335	1419.6300	2.5
				y_{16}	1490.6706	1490.6726	1.3

1-C13A

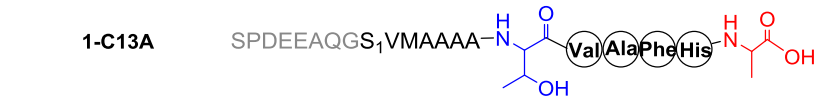

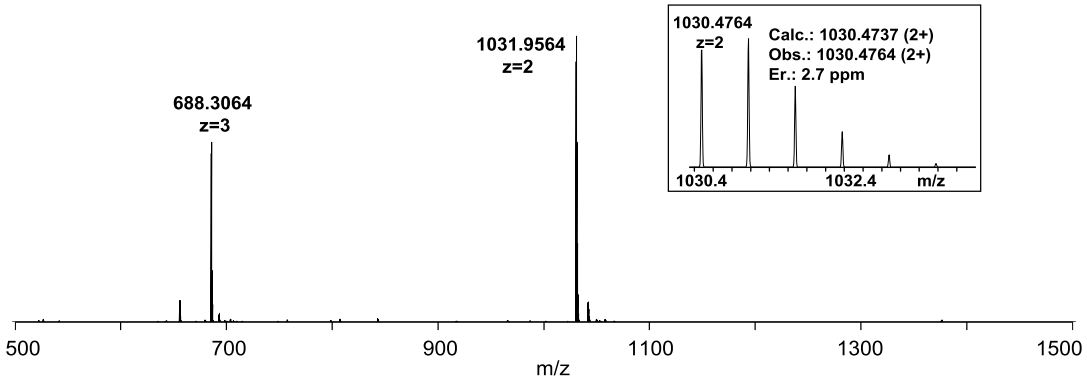

1-C13S

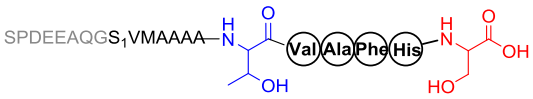

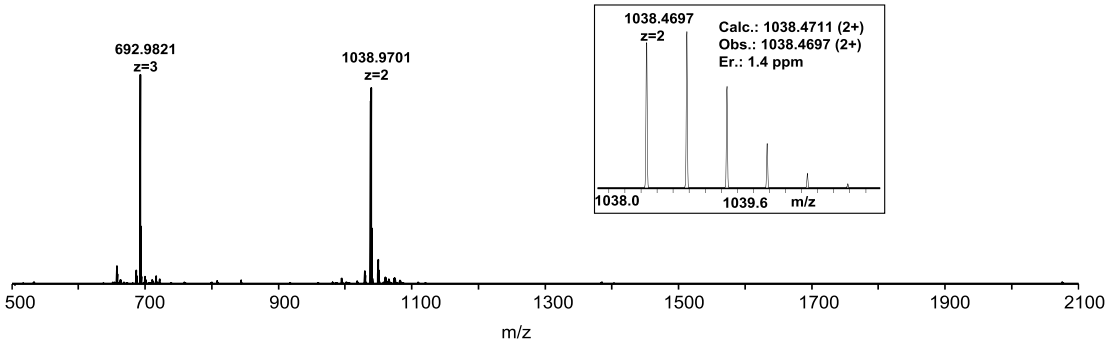

1-C13T

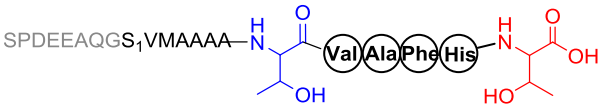

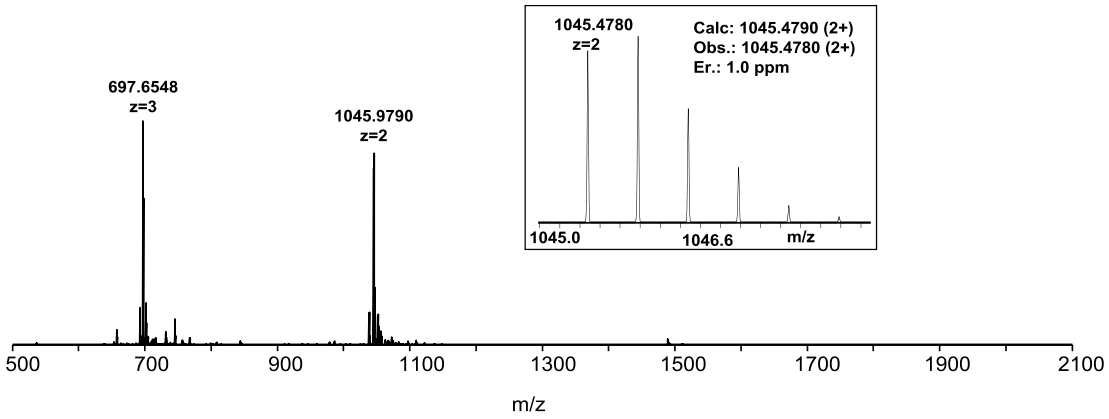

2

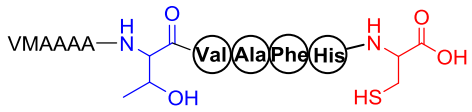
VMAAAA
Val
Ala
Phe
His
OH
HS

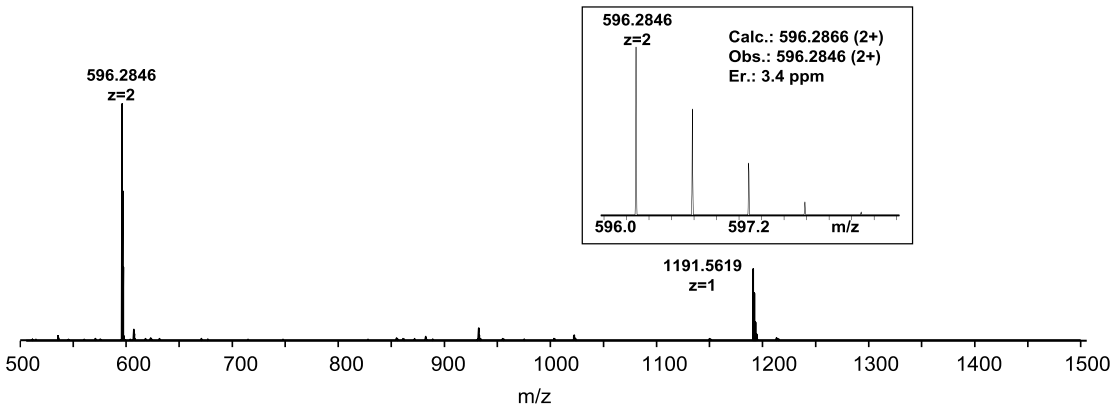
596.2846
z=2
1191.5619
z=1
500
600
700
800
900
1000
1100
1200
1300
1400
1500
m/z
596.2846
z=2
Calc.: 596.2866 (2+)
Obs.: 596.2846 (2+)
Er.: 3.4 ppm
596.0
597.2
m/z

2-I

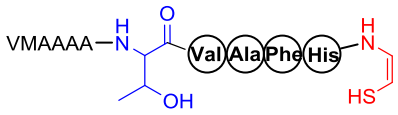
VMAAAA
Val
Ala
Phe
His
OH
HS

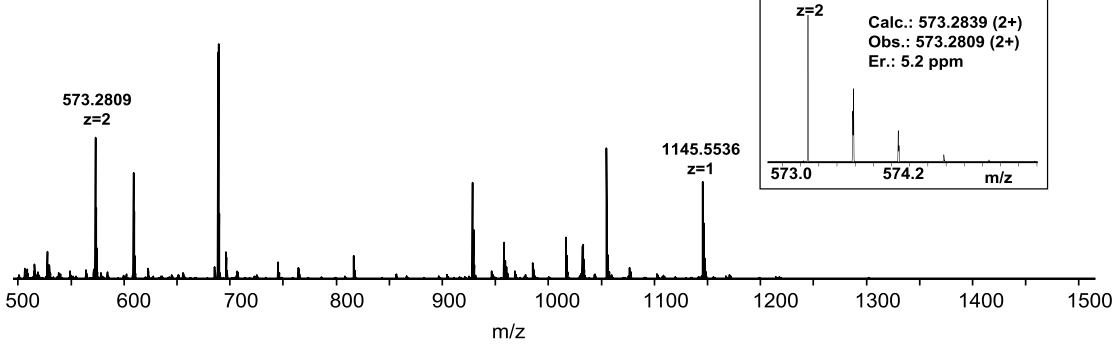
573.2809
z=2
1145.5536
z=1
500
600
700
800
900
1000
1100
1200
1300
1400
1500
m/z
573.2809
z=2
Calc.: 573.2839 (2+)
Obs.: 573.2809 (2+)
Er.: 5.2 ppm
573.0
574.2
m/z

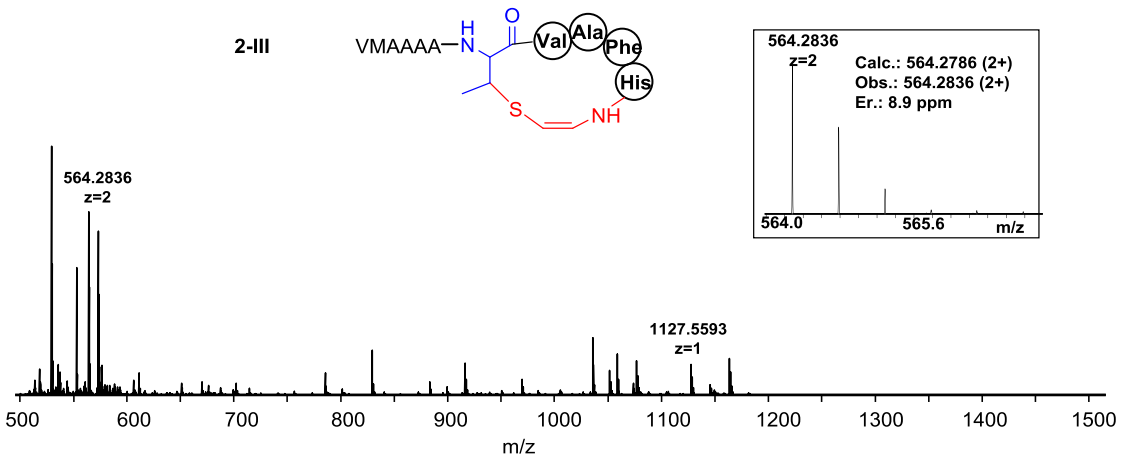
2-III
VMAAAA
Val
Ala
Phe
His
NH
564.2836
z=2
1127.5593
z=1
564.2836
z=2
Calc.: 564.2786 (2+)
Obs.: 564.2836 (2+)
Er.: 8.9 ppm
564.0
565.6
m/z
500
600
700
800
900
1000
1100
1200
1300
1400
1500
m/z

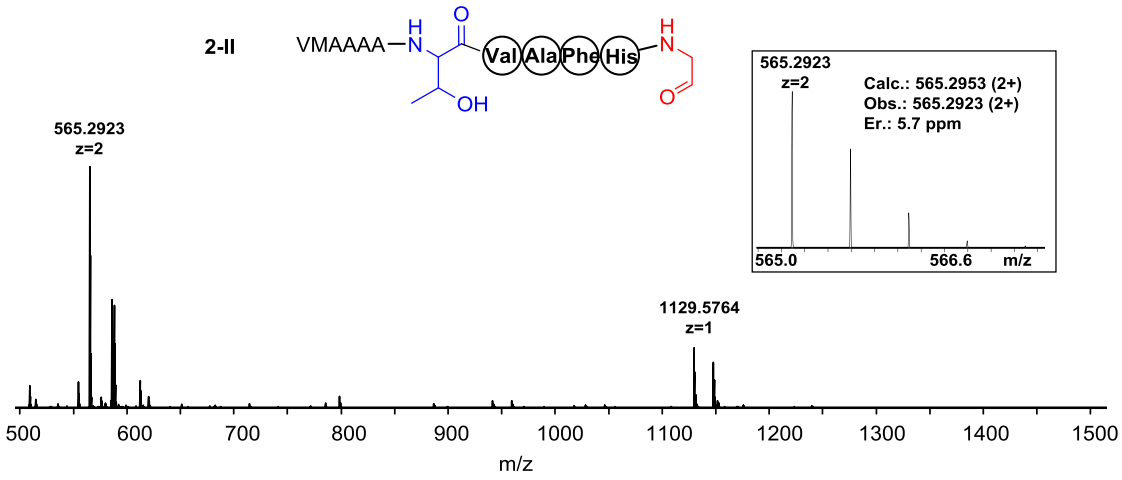
2-II
VMAAAA
Val
Ala
Phe
His
OH
565.2923
z=2
1129.5764
z=1
565.2923
z=2
Calc.: 565.2953 (2+)
Obs.: 565.2923 (2+)
Er.: 5.7 ppm
565.0
566.6
m/z
500
600
700
800
900
1000
1100
1200
1300
1400
1500
m/z

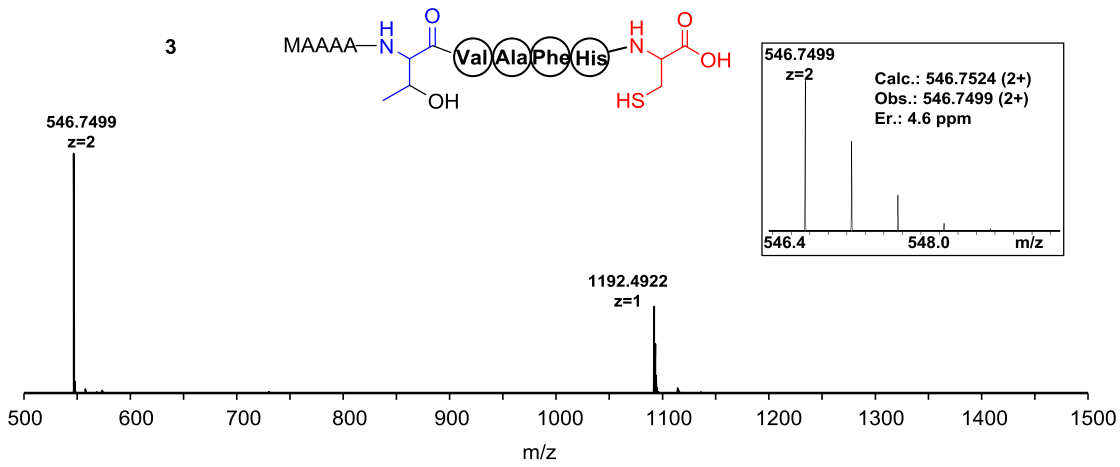
3
MAAAA
Val Ala Phe His
OH
HS
546.7499
z=2
1192.4922
z=1
500 600 700 800 900 1000 1100 1200 1300 1400 1500
m/z
546.7499
z=2
Calc.: 546.7524 (2+)
Obs.: 546.7499 (2+)
Er.: 4.6 ppm
546.4
548.0
m/z

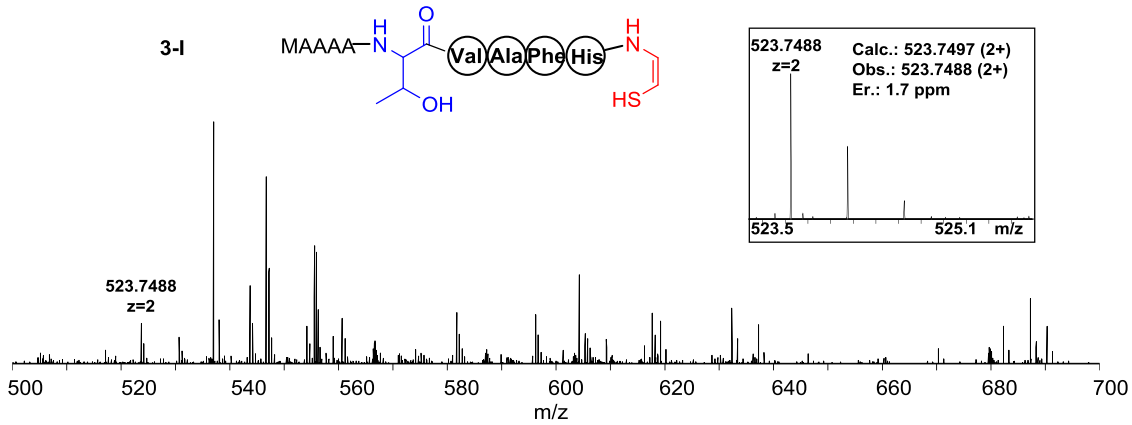
3-I
MAAAA
Val Ala Phe His
OH
HS
523.7488
z=2
500 520 540 560 580 600 620 640 660 680 700
m/z
523.7488
z=2
Calc.: 523.7497 (2+)
Obs.: 523.7488 (2+)
Er.: 1.7 ppm
523.5
525.1
m/z

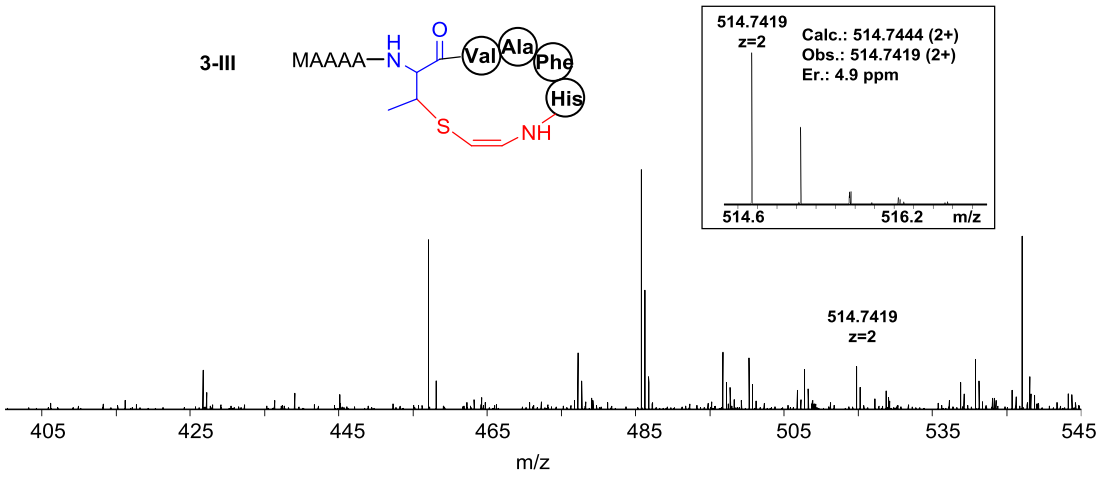
3-III
MAAAA
Val
Ala
Phe
His
514.7419
z=2
Calc.: 514.7444 (2+)
Obs.: 514.7419 (2+)
Er.: 4.9 ppm
514.6
516.2
m/z
514.7419
z=2
405
425
445
465
485
505
535
545
m/z

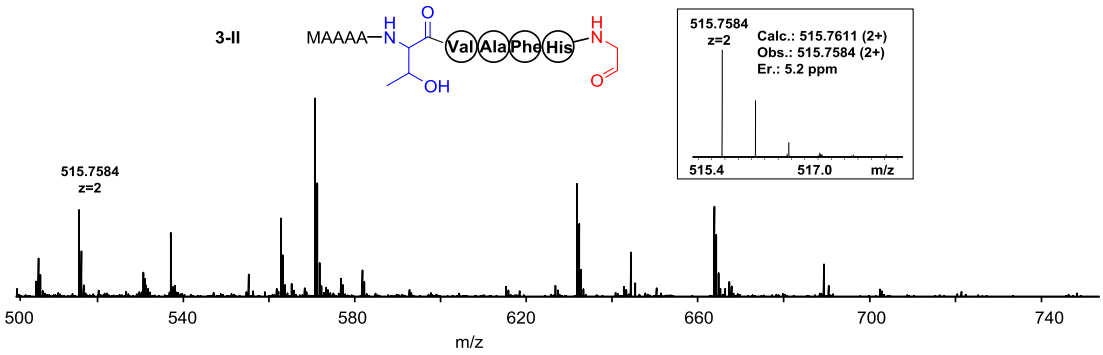
3-II
MAAAA
Val
Ala
Phe
His
OH
515.7584
z=2
Calc.: 515.7611 (2+)
Obs.: 515.7584 (2+)
Er.: 5.2 ppm
515.4
517.0
m/z
515.7584
z=2
500
540
580
620
660
700
740
m/z

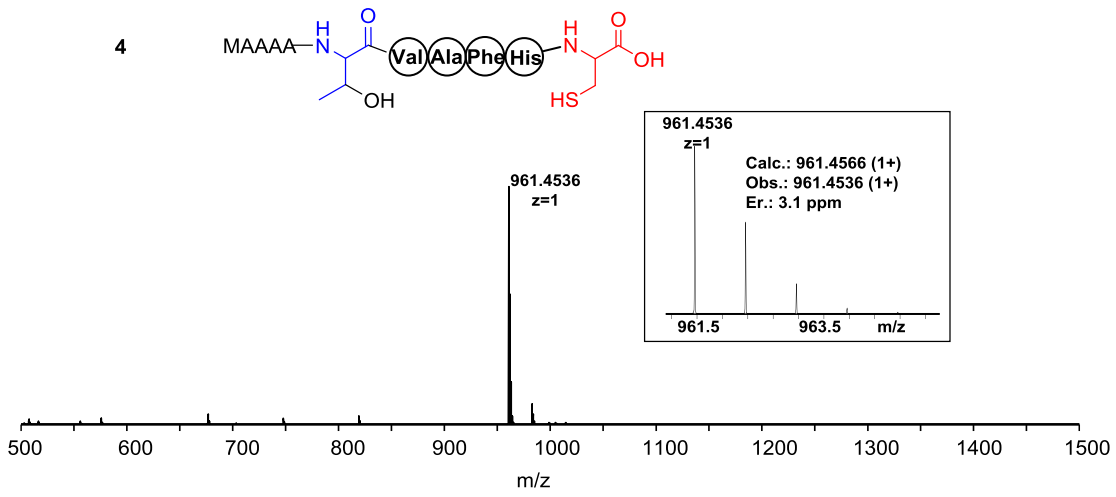
4
MAAAA
Val Ala Phe His
OH
HS
961.4536
z=1
961.4536
z=1
Calc.: 961.4566 (1+)
Obs.: 961.4536 (1+)
Er.: 3.1 ppm
961.5
963.5
m/z
500
600
700
800
900
1000
1100
1200
1300
1400
1500
m/z

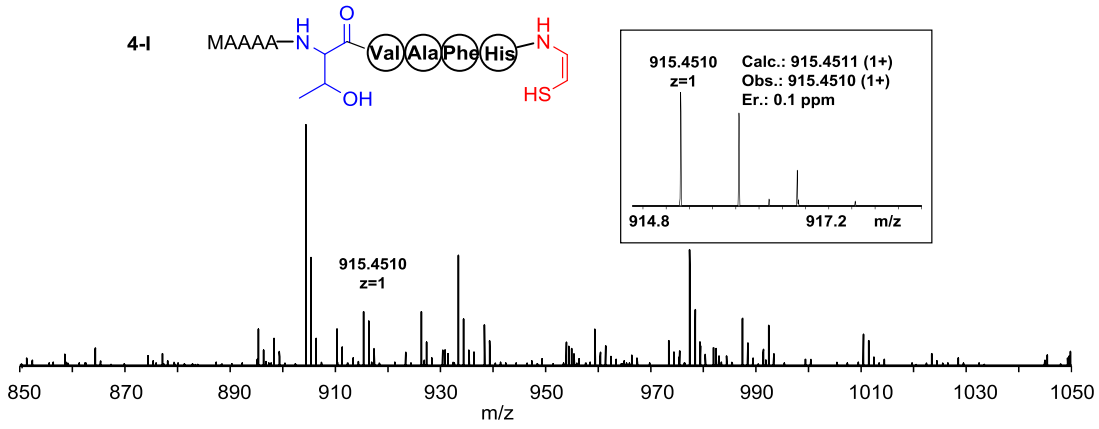
4-I
MAAAA
Val Ala Phe His
OH
HS
915.4510
z=1
915.4510
z=1
Calc.: 915.4511 (1+)
Obs.: 915.4510 (1+)
Er.: 0.1 ppm
914.8
917.2
m/z
850
870
890
910
930
950
970
990
1010
1030
1050
m/z

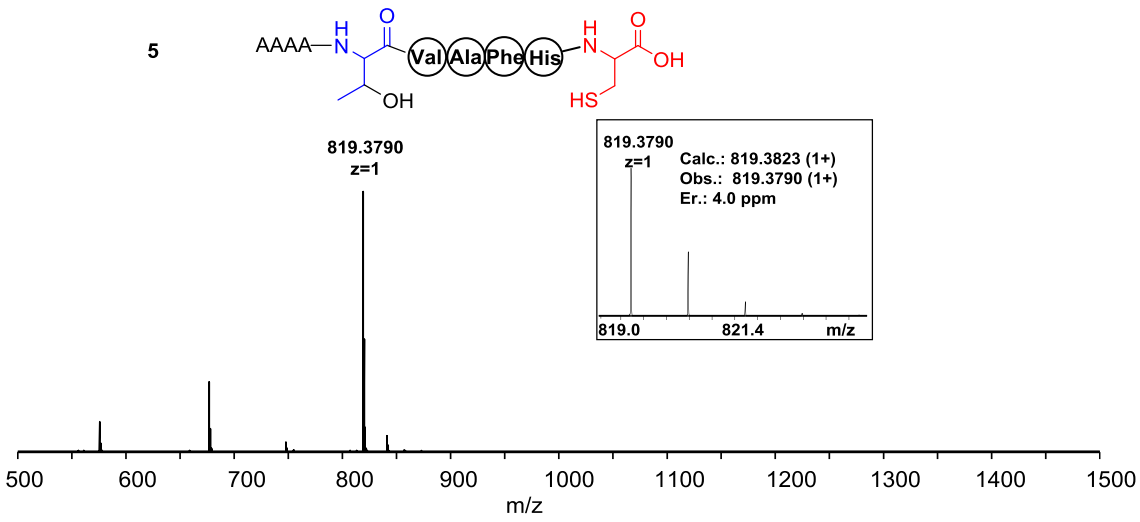
5
AAAA
Val
Ala
Phe
His
OH
HS
819.3790
z=1
819.3790
z=1
Calc.: 819.3823 (1+)
Obs.: 819.3790 (1+)
Er.: 4.0 ppm
819.0
821.4
m/z
500
600
700
800
900
1000
1100
1200
1300
1400
1500
m/z

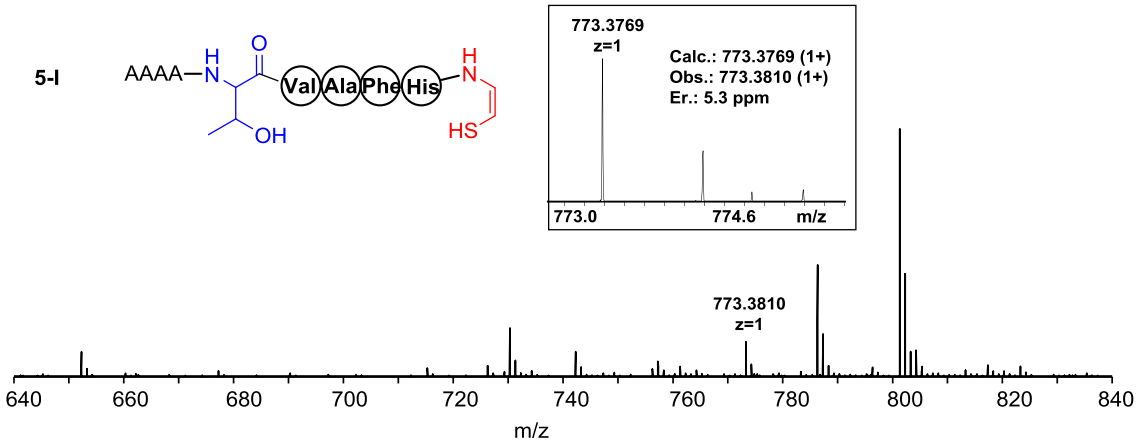
5-I
AAAA
Val
Ala
Phe
His
OH
HS
773.3769
z=1
Calc.: 773.3769 (1+)
Obs.: 773.3810 (1+)
Er.: 5.3 ppm
773.0
774.6
m/z
773.3810
z=1
640
660
680
700
720
740
760
780
800
820
840
m/z

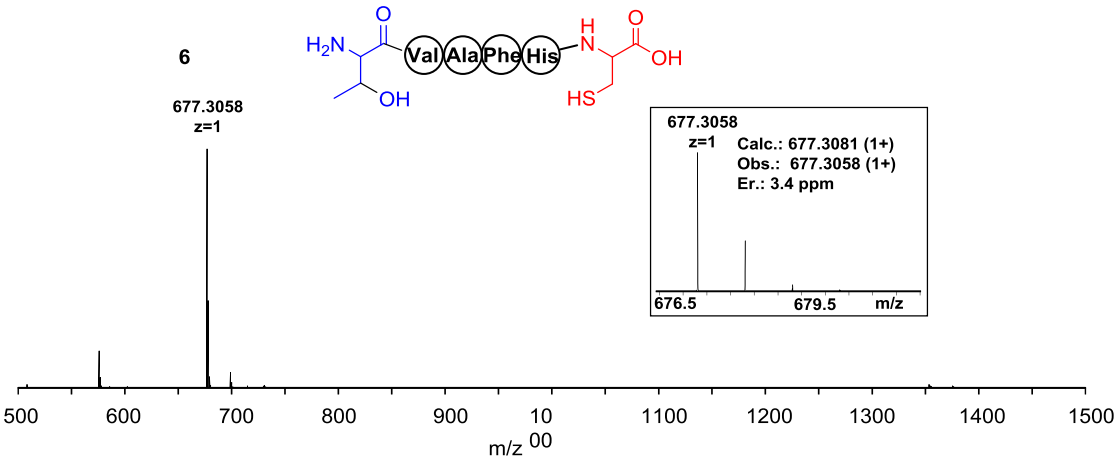
6
677.3058
z=1
Val Ala Phe His
677.3058
z=1
Calc.: 677.3081 (1+)
Obs.: 677.3058 (1+)
Er.: 3.4 ppm
676.5
679.5
m/z
500
600
700
800
900
1000
1100
1200
1300
1400
1500
m/z

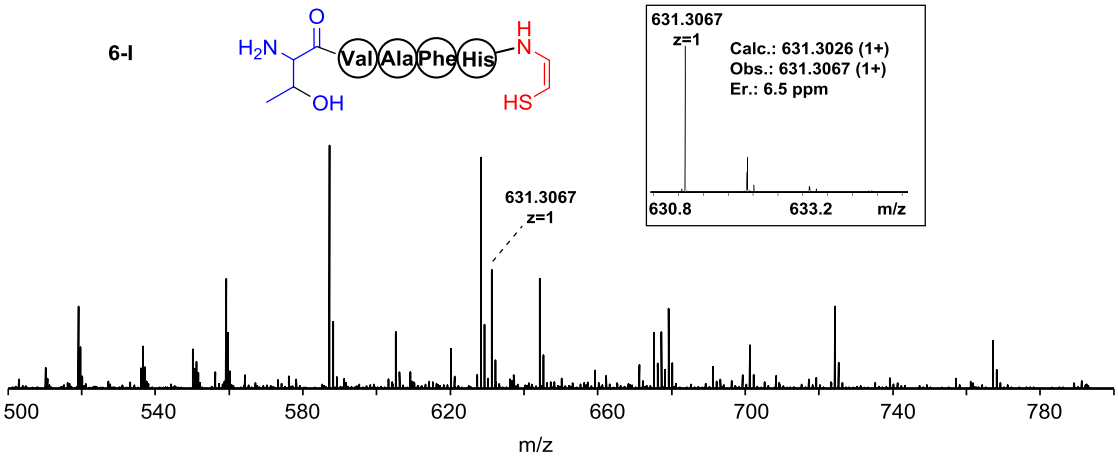
6-I
Val Ala Phe His
631.3067
z=1
631.3067
z=1
Calc.: 631.3026 (1+)
Obs.: 631.3067 (1+)
Er.: 6.5 ppm
630.8
633.2
m/z
500
540
580
620
660
700
740
780
m/z

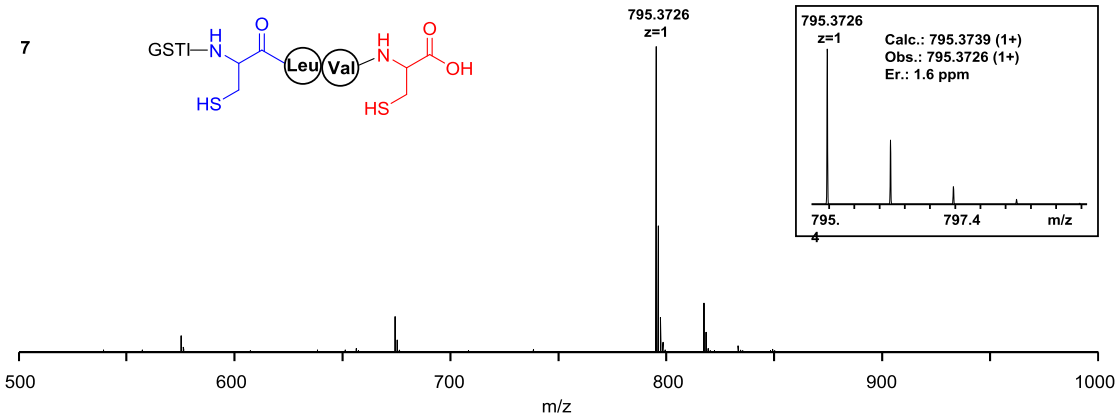

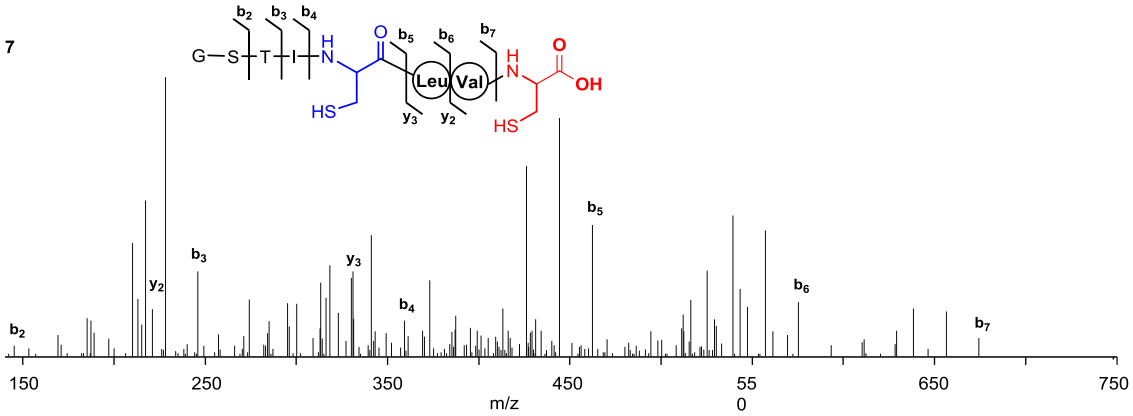

Ions	Calcd.	Obs.	Er. (ppm)
b_2	145.0613	145.0606	5.5
b_3	246.1090	246.1080	4.5
b_4	359.1931	359.1917	3.6
b_5	462.2022	462.2008	3.0
b_6	575.2863	575.2847	3.1
b_7	674.3547	674.3527	4.2
y_2	221.0959	221.0951	4.1
y_3	334.1800	334.1786	5.1

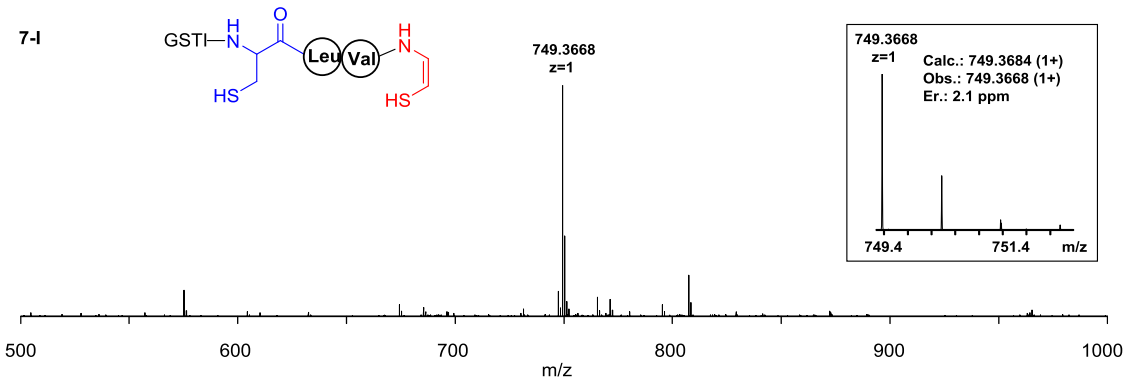

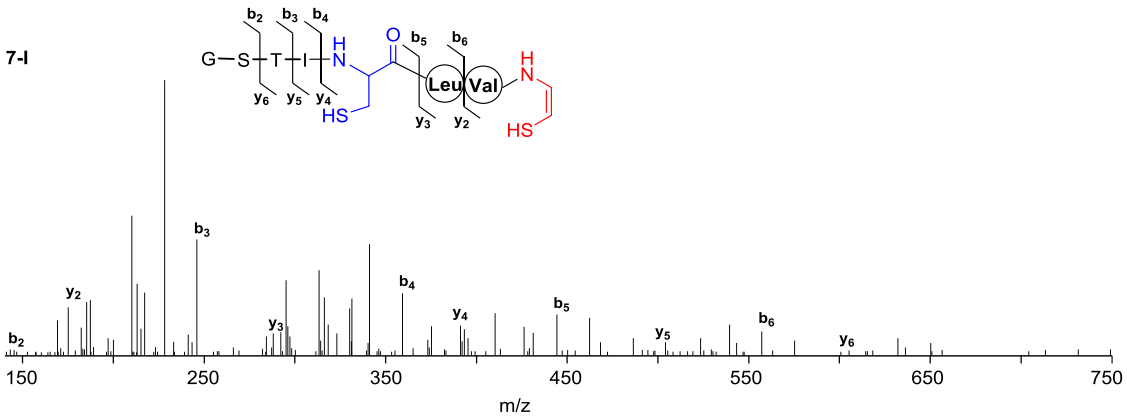

Ions	Calcd.	Obs.	Er. (ppm)
b_2	145.0613	145.0606	4.8
b_3	246.1090	246.1079	4.5
b_4	359.1931	359.1917	3.9
b_5	462.2022	462.2006	3.5
b_6	575.2863	575.2836	4.7
y_2	175.0905	175.0896	5.1
y_3	288.1745	288.1731	4.9
y_4	391.1837	391.1823	3.6
y_5	504.2678	504.2656	4.4
y_6	605.3154	605.3120	5.6

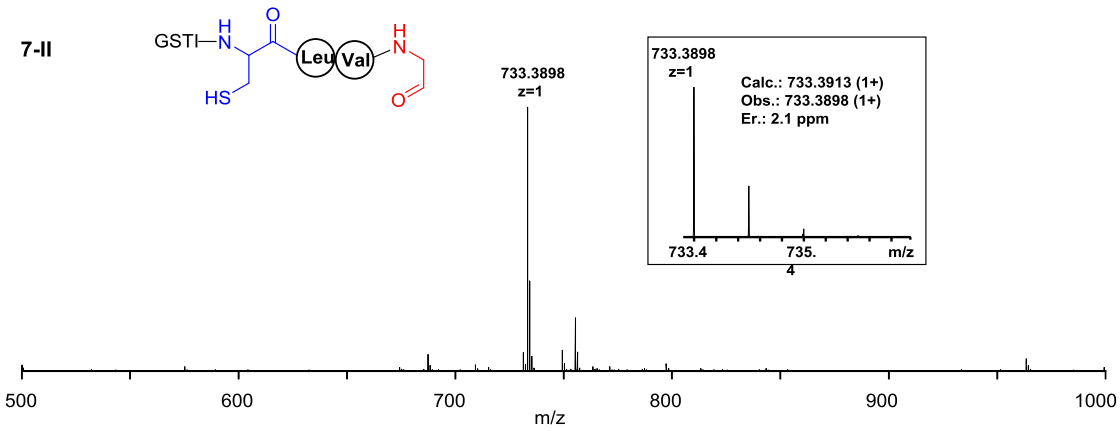

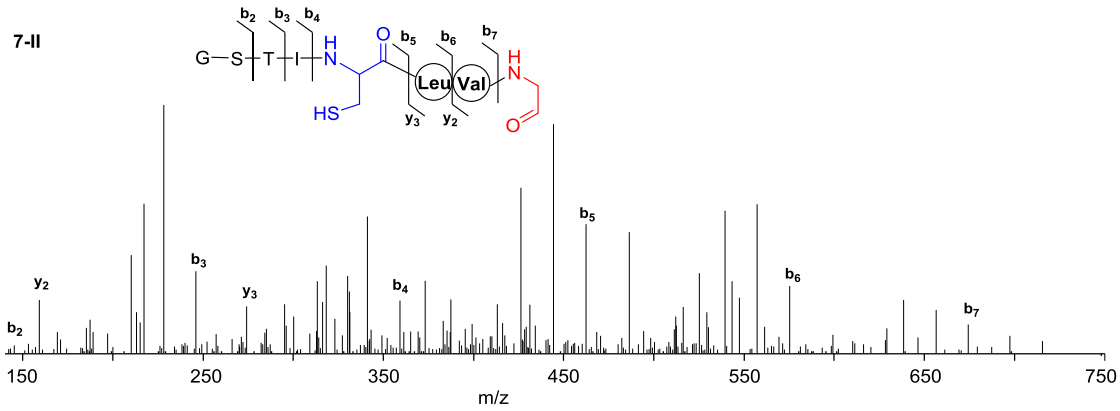

Ions	Calcd.	Obs.	Er. (ppm)
b_2	145.0613	145.0605	5.5
b_3	246.1090	246.1079	4.5
b_4	359.1931	359.1917	3.9
b_5	462.2022	462.2006	3.5
b_6	575.2863	575.2844	3.3
b_7	674.3547	674.3523	3.6
y_2	159.1133	159.1125	5.0
y_3	272.1974	272.1961	4.8

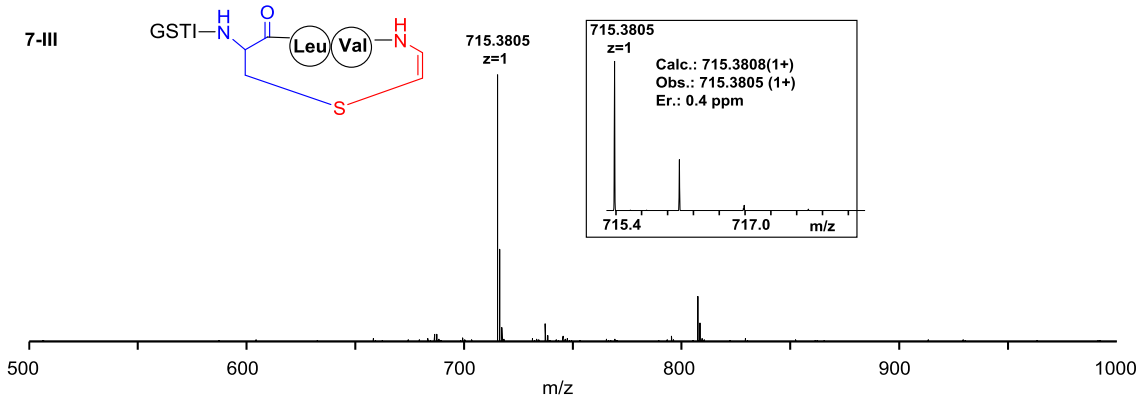

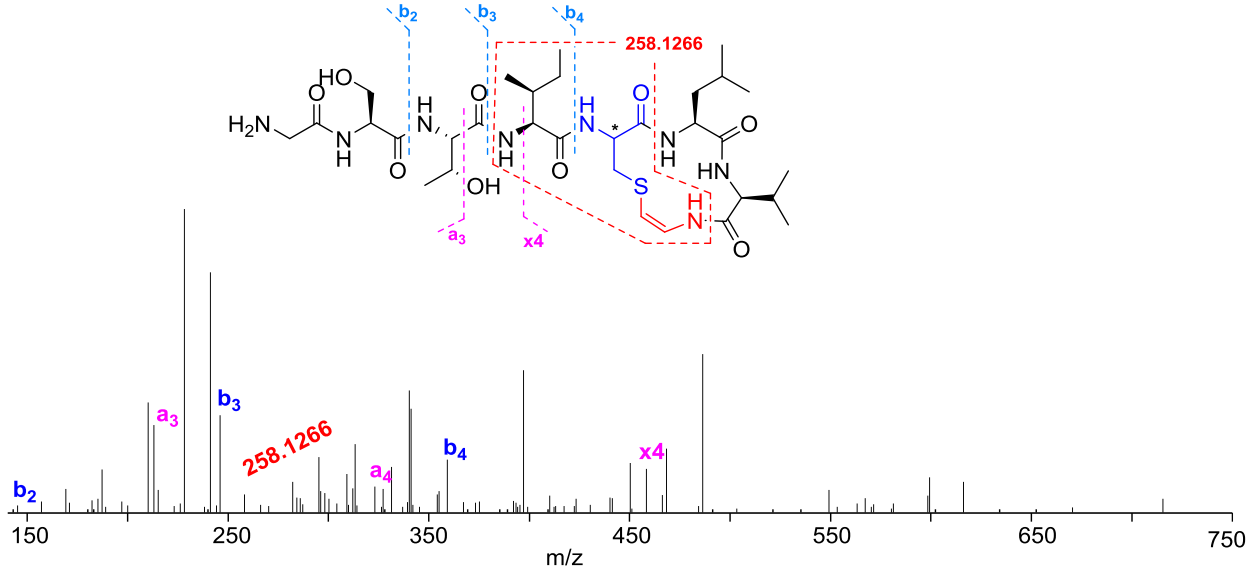

Ions	Calcd.	Obs.	Er. (ppm)
b_2	145.0613	145.0607	4.1
b_3	246.1090	246.1080	4.1
b_4	359.1931	359.1918	3.6
a_3	218.1135	218.1134	0.5
a_4	331.1976	331.1969	2.1
x_4	453.2530	453.2513	3.8
	258.1271	258.1266	1.9

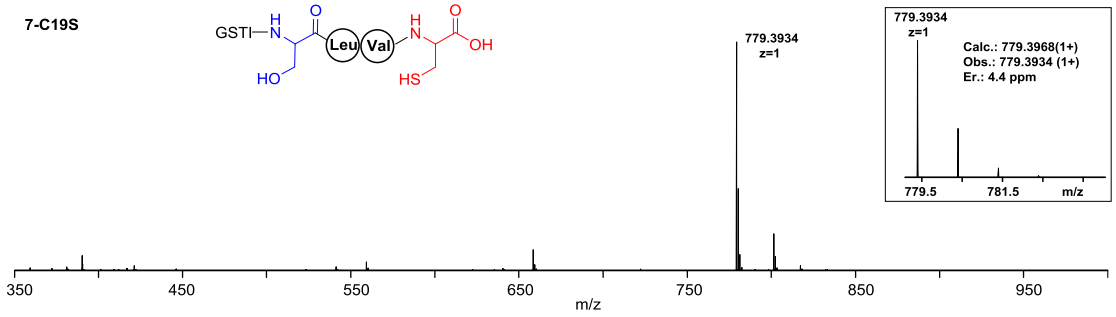

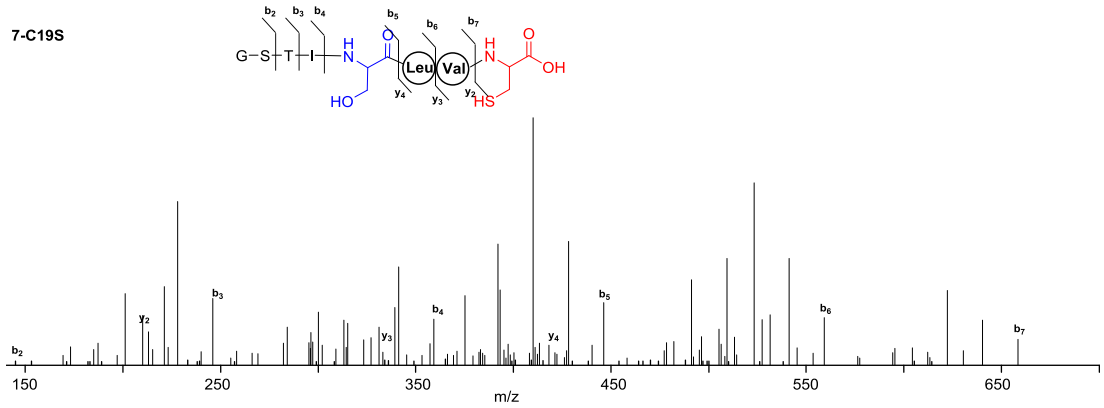

Ions	Calcd.	Obs.	Er. (ppm)
b_2	145.0613	145.0609	2.8
b_3	246.1090	246.1084	2.4
b_4	359.1931	359.1923	2.2
b_5	446.2251	446.2247	0.9
b_6	559.3092	559.3085	1.3
b_7	658.3776	658.3774	0.3
y_2	221.0959	221.0955	1.8
y_3	334.1800	334.1795	1.5
y_4	421.2120	421.2110	2.4

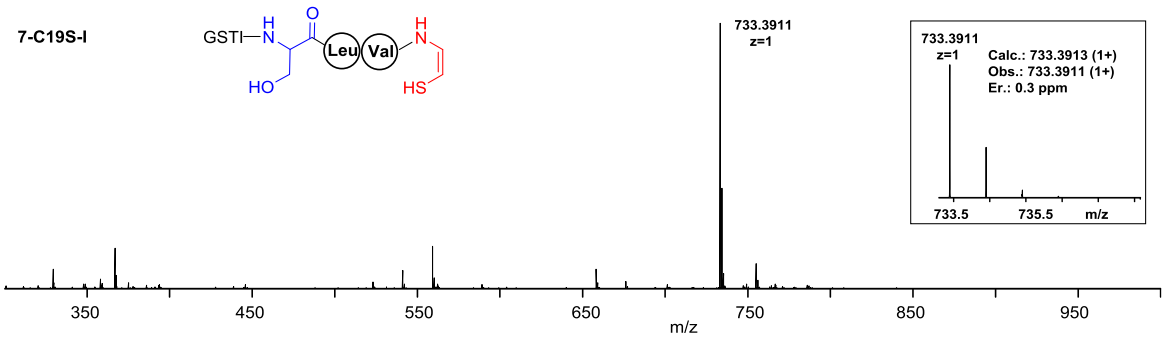

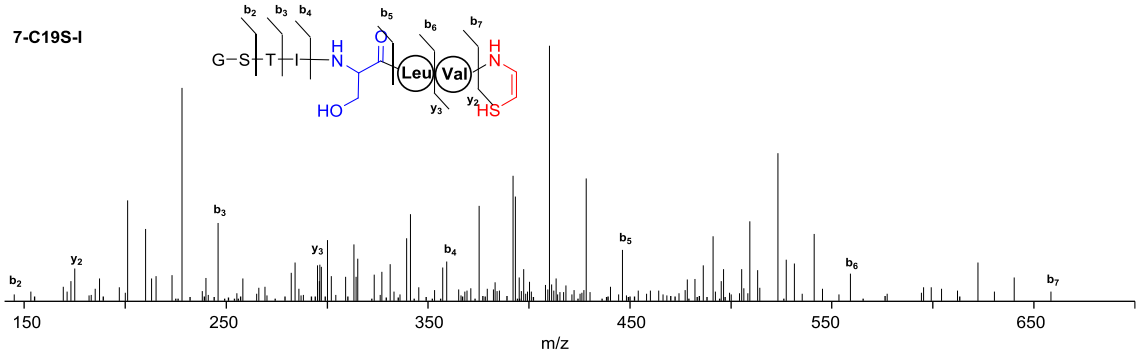

Ions	Calcd.	Obs.	Er. (ppm)
b_2	145.0613	145.0608	3.4
b_3	246.1090	246.1083	2.8
b_4	359.1931	359.1922	2.5
b_5	446.2251	446.2244	1.6
b_6	559.3092	559.3081	2.0
b_7	658.3776	658.3769	1.1
y_2	175.0905	175.0900	2.9
y_3	288.1745	288.1739	2.1

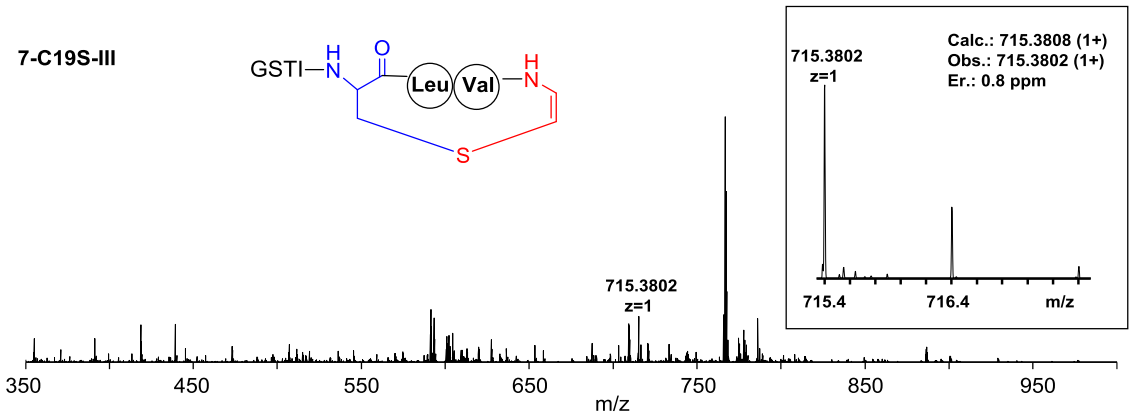
7-C19S-III
GSTI
Leu
Val
715.3802
z=1
Calc.: 715.3808 (1+)
Obs.: 715.3802 (1+)
Er.: 0.8 ppm
715.4
716.4
m/z
350
450
550
650
750
850
950
m/z

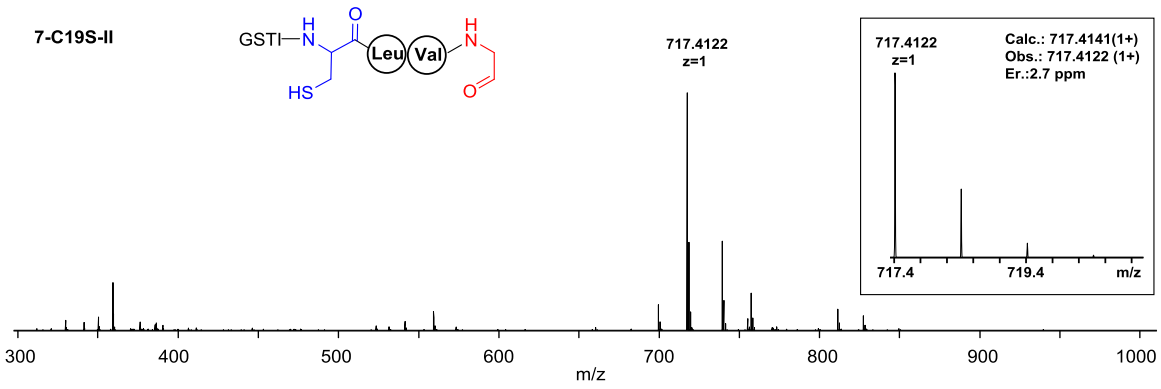
7-C19S-II
GSTI
Leu
Val
HS
717.4122
z=1
Calc.: 717.4141(1+)
Obs.: 717.4122 (1+)
Er.:2.7 ppm
717.4
719.4
m/z
300
400
500
600
700
800
900
1000
m/z

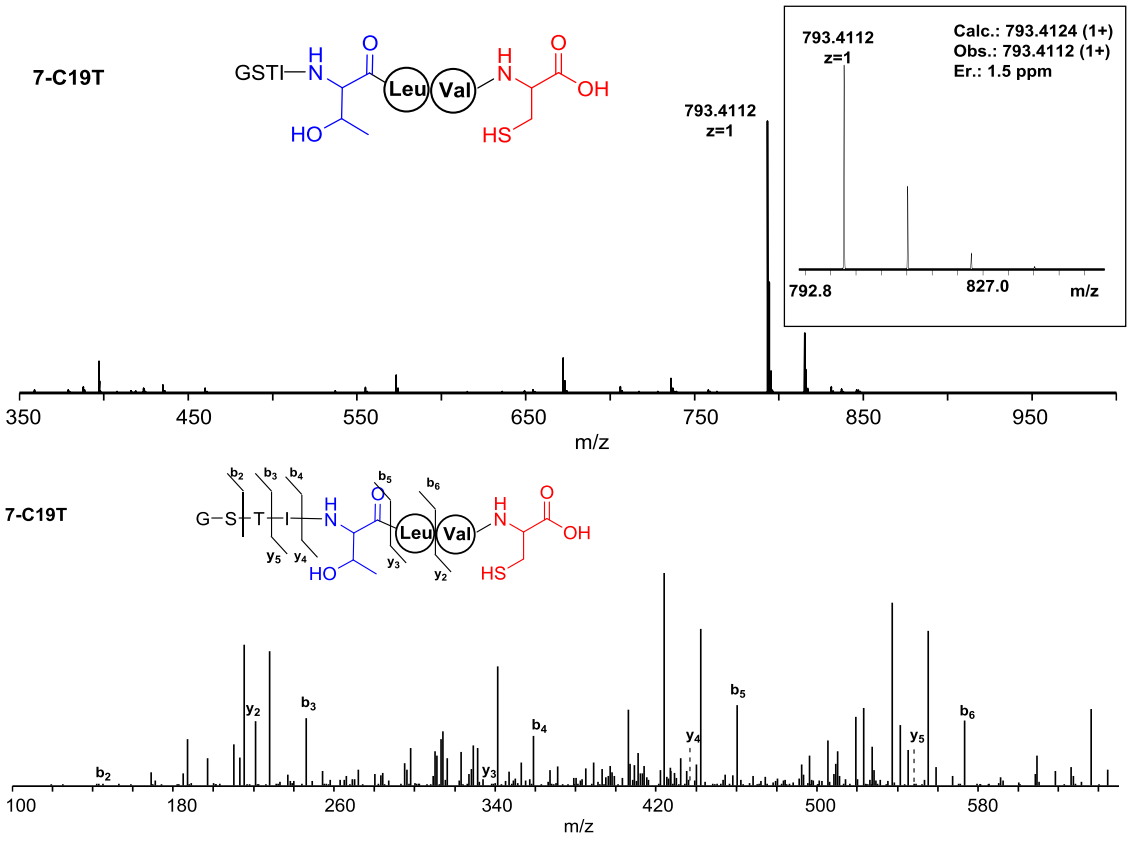

Ions	Calcd.	Obs.	Er. (ppm)
b_2	145.0613	145.0607	4.1
b_3	246.1090	246.1085	2.0
b_4	359.1931	359.1925	1.7
b_5	460.2407	460.2403	0.9
b_6	573.3248	573.3245	0.5
y_2	221.0959	221.0955	1.8
y_3	334.1800	334.1795	1.5
y_4	435.2277	435.2274	0.7
y_5	548.3119	548.3126	1.3

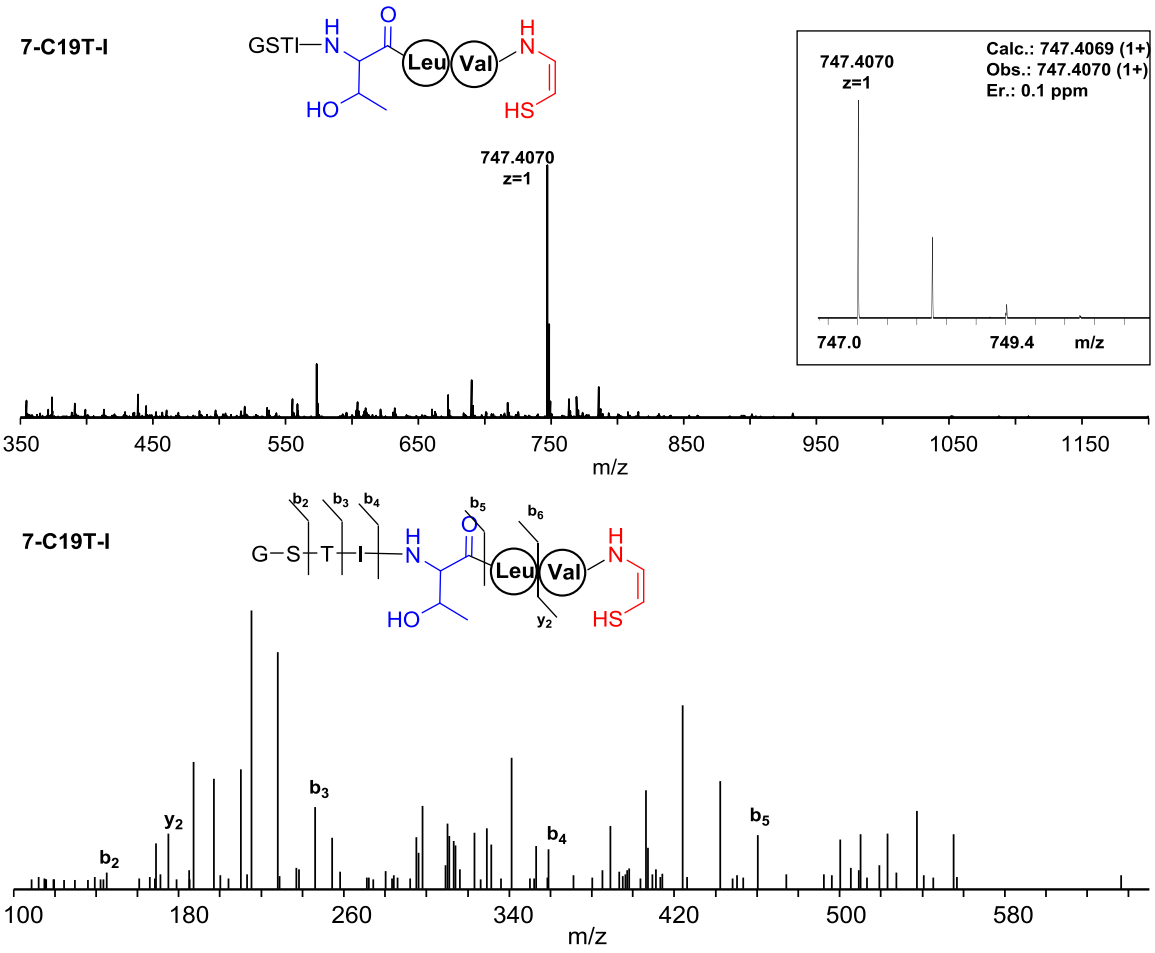

Ions	Calcd.	Obs.	Er. (ppm)
b_2	145.0613	145.0607	4.1
b_3	246.1090	246.1082	3.2
b_4	359.1931	359.1920	3.1
b_5	460.2407	460.2396	2.4
y_2	175.0905	175.0900	2.9

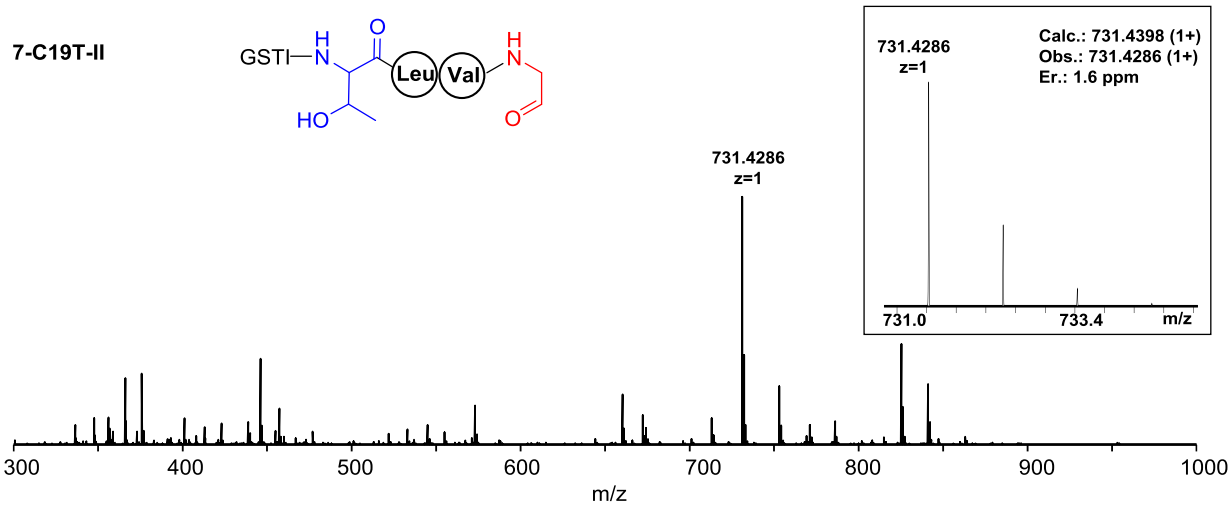
7-C19T-II
GSTI
H
N
O
Leu
Val
H
N
HO
O
731.4286
z=1
731.4286
z=1
Calc.: 731.4398 (1+)
Obs.: 731.4286 (1+)
Er.: 1.6 ppm
731.0
733.4
m/z
300
400
500
600
700
800
900
1000
m/z

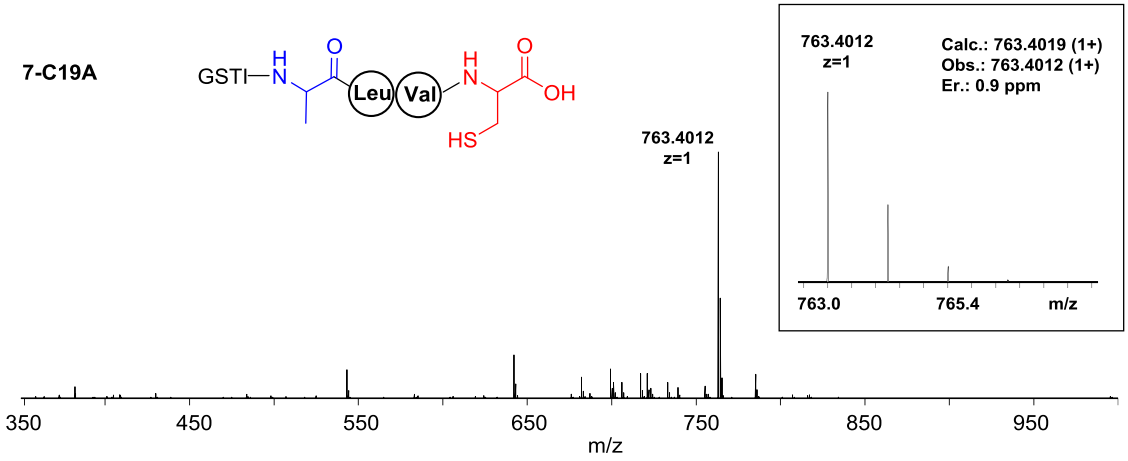

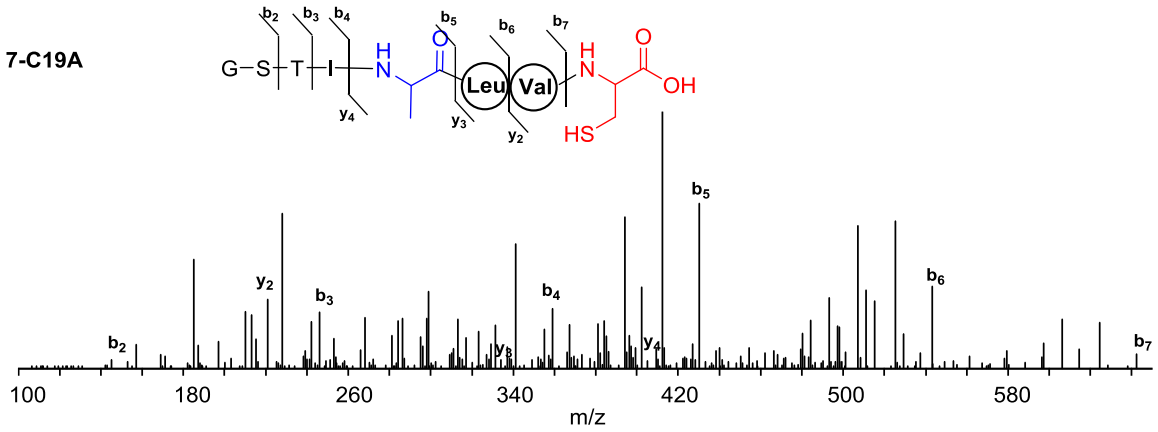

Ions	Calcd.	Obs.	Er. (ppm)
b_2	145.0613	145.0603	6.9
b_3	246.1090	246.1078	4.9
b_4	359.1931	359.1915	4.5
b_5	430.2302	430.2286	3.7
b_6	543.3142	543.3124	3.3
b_7	642.3827	642.3804	3.6
y_2	221.0959	221.0949	4.5
y_3	334.1800	334.1784	4.8
y_4	405.2171	405.2165	1.5

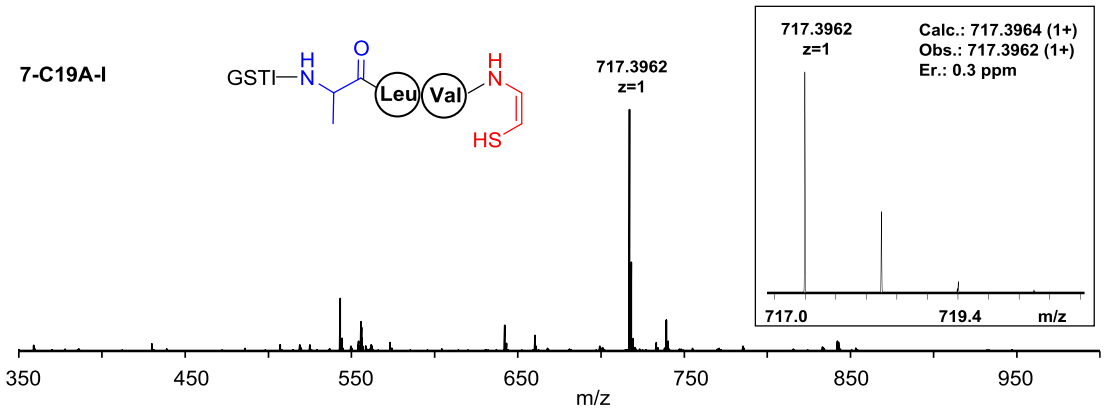

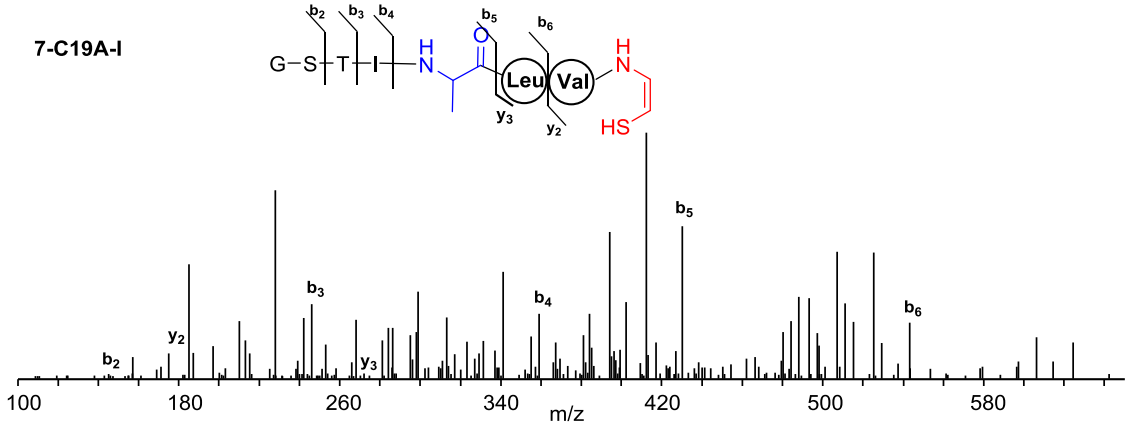

Ions	Calcd.	Obs.	Er. (ppm)
b_2	145.0613	145.0606	4.8
b_3	246.1090	246.1081	3.7
b_4	359.1931	359.1918	3.6
b_5	430.2302	430.2292	2.3
b_6	543.3142	543.3132	1.8
y_2	175.0905	175.0898	4.0
y_3	288.1745	288.1736	3.1

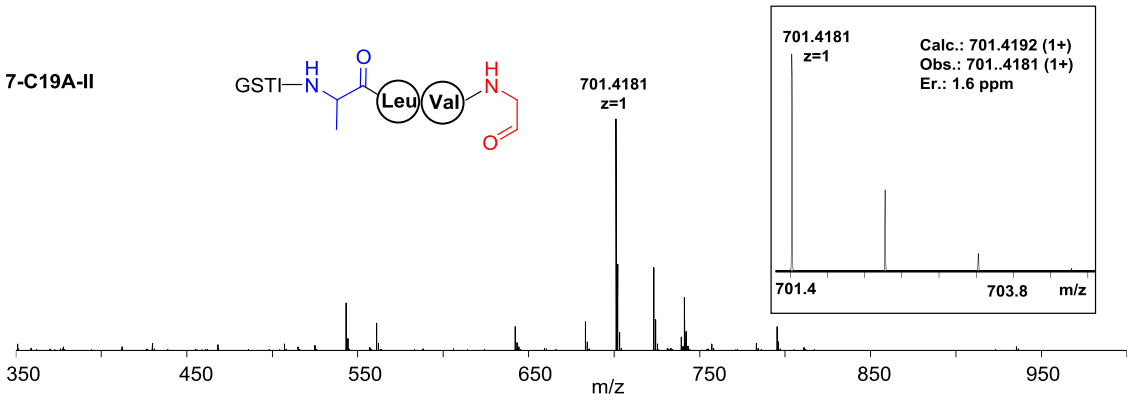
7-C19A-II
GSTI
Leu
Val
701.4181
z=1
701.4181
z=1
Calc.: 701.4192 (1+)
Obs.: 701..4181 (1+)
Er.: 1.6 ppm
701.4
703.8
m/z
350
450
550
650
750
850
950
m/z

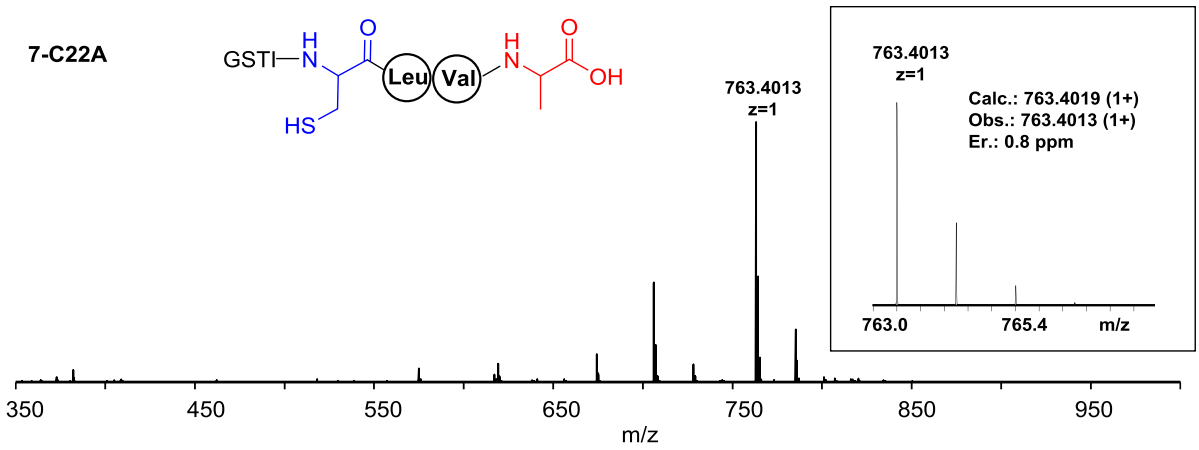
7-C22A
GSTI
Leu
Val
OH
HS
763.4013
z=1
763.4013
z=1
Calc.: 763.4019 (1+)
Obs.: 763.4013 (1+)
Er.: 0.8 ppm
763.0
765.4
m/z
350
450
550
650
750
850
950
m/z

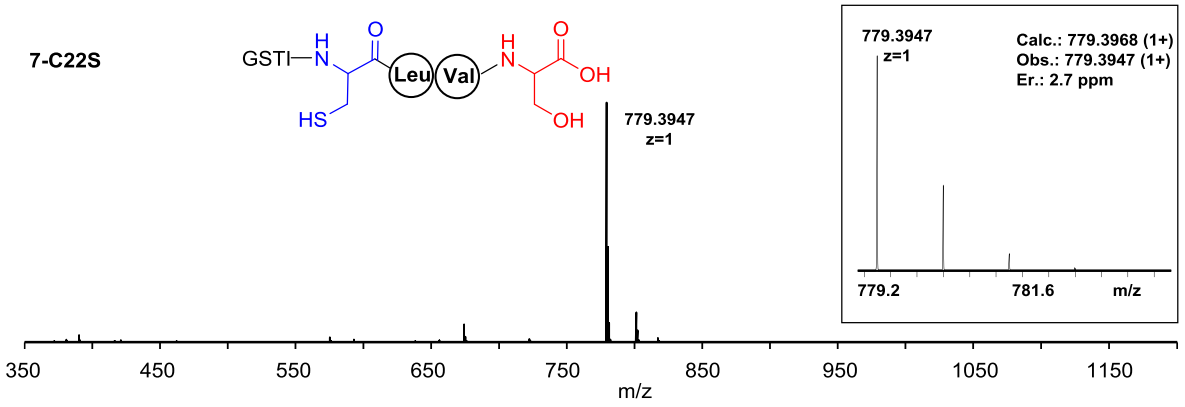
7-C22S
GSTI
Leu
Val
OH
OH
HS
779.3947
z=1
779.3947
z=1
Calc.: 779.3968 (1+)
Obs.: 779.3947 (1+)
Er.: 2.7 ppm
779.2
781.6
m/z
350
450
550
650
750
850
950
1050
1150
m/z

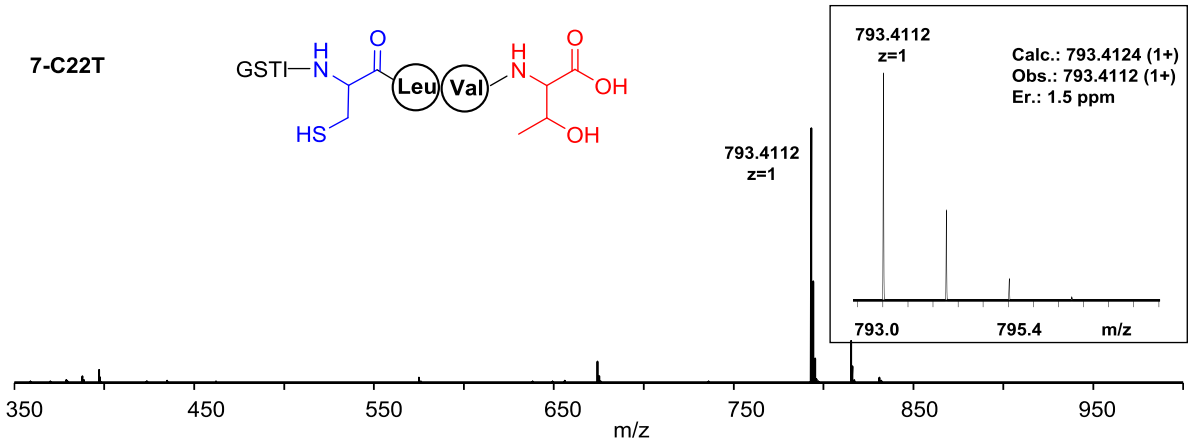
7-C22T
GSTI
Leu
Val
OH
OH
HS
793.4112
z=1
793.4112
z=1
Calc.: 793.4124 (1+)
Obs.: 793.4112 (1+)
Er.: 1.5 ppm
793.0
795.4
m/z
350
450
550
650
750
850
950
m/z

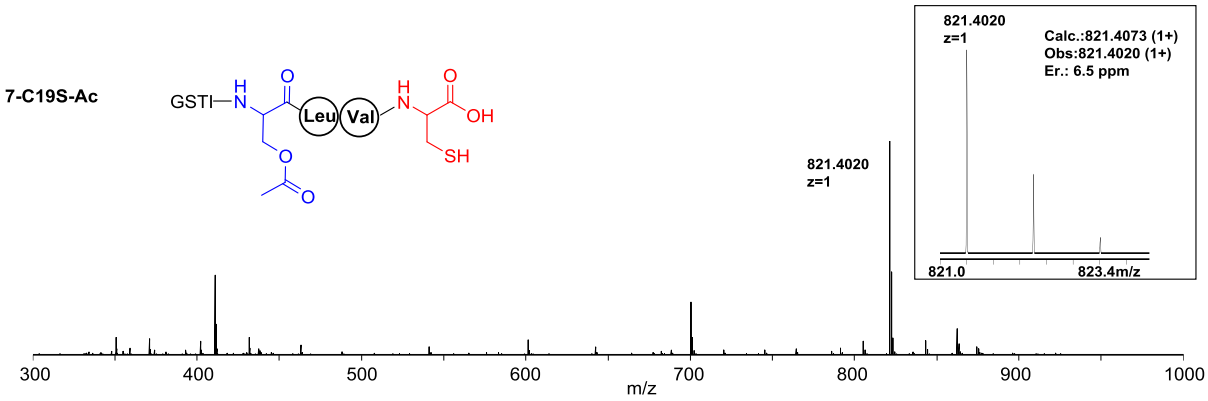
7-C19S-Ac
GSTI
Leu
Val
OH
SH
821.4020
z=1
821.4020
z=1
Calc.:821.4073 (1+)
Obs:821.4020 (1+)
Er.: 6.5 ppm
821.0
823.4m/z
300
400
500
600
700
800
900
1000
m/z

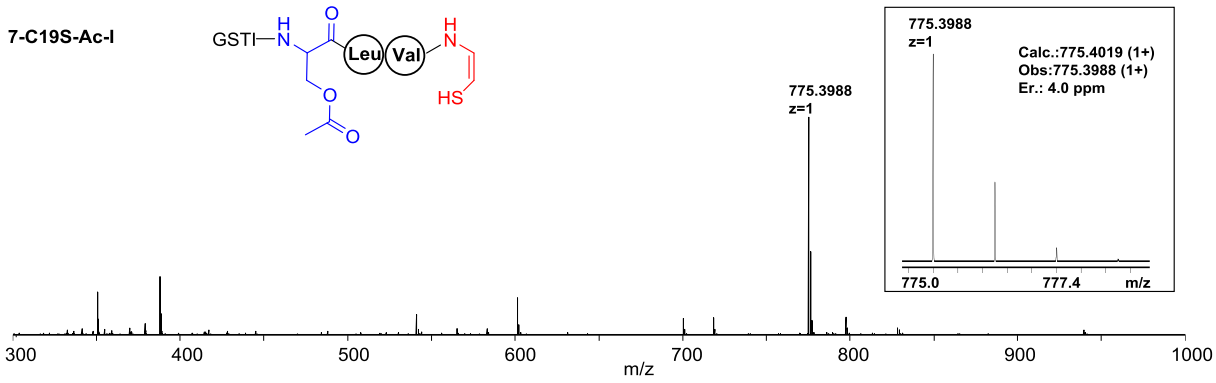
7-C19S-Ac-I
GSTI
Leu
Val
HS
775.3988
z=1
775.3988
z=1
Calc.:775.4019 (1+)
Obs:775.3988 (1+)
Er.: 4.0 ppm
775.0
777.4
m/z
300
400
500
600
700
800
900
1000
m/z

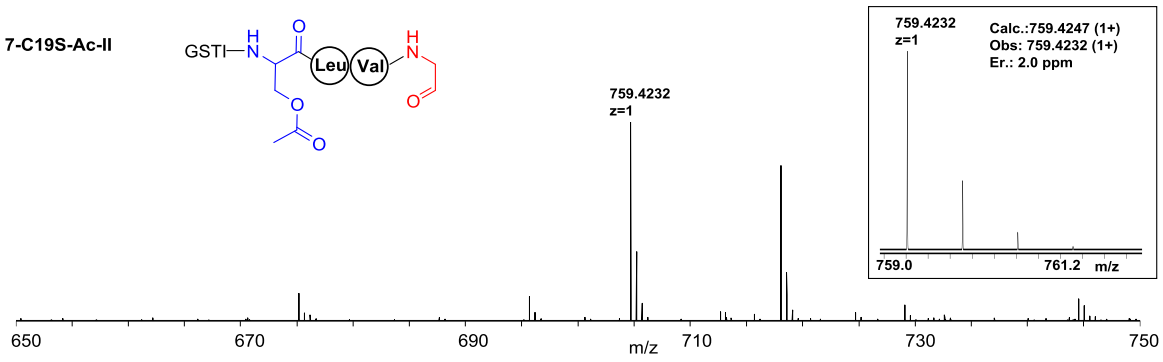
7-C19S-Ac-II
GSTI
Leu
Val
759.4232
z=1
759.4232
z=1
Calc.:759.4247 (1+)
Obs: 759.4232 (1+)
Er.: 2.0 ppm
759.0
761.2
m/z
650
670
690
710
730
750
m/z

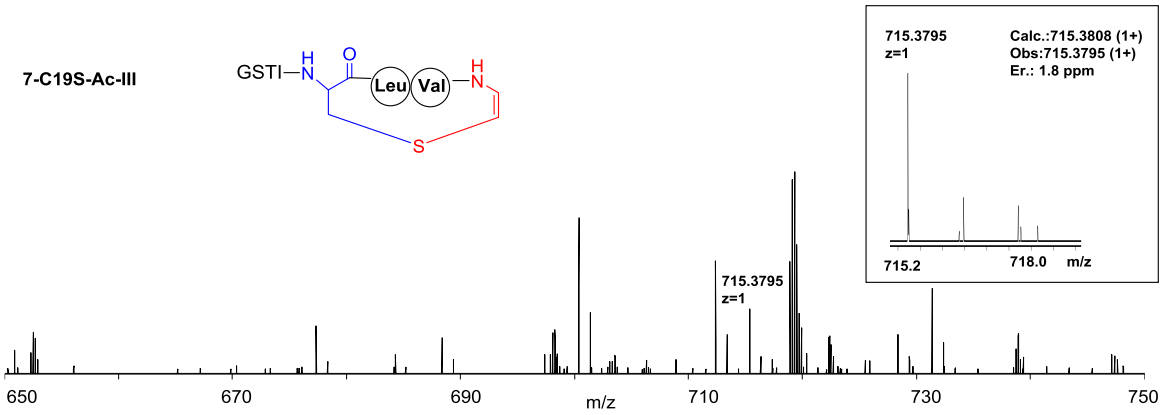
7-C19S-Ac-III
GSTI
Leu
Val
S
715.3795
z=1
715.3795
z=1
Calc.:715.3808 (1+)
Obs:715.3795 (1+)
Er.: 1.8 ppm
715.2
718.0
m/z
650
670
690
710
730
750
m/z

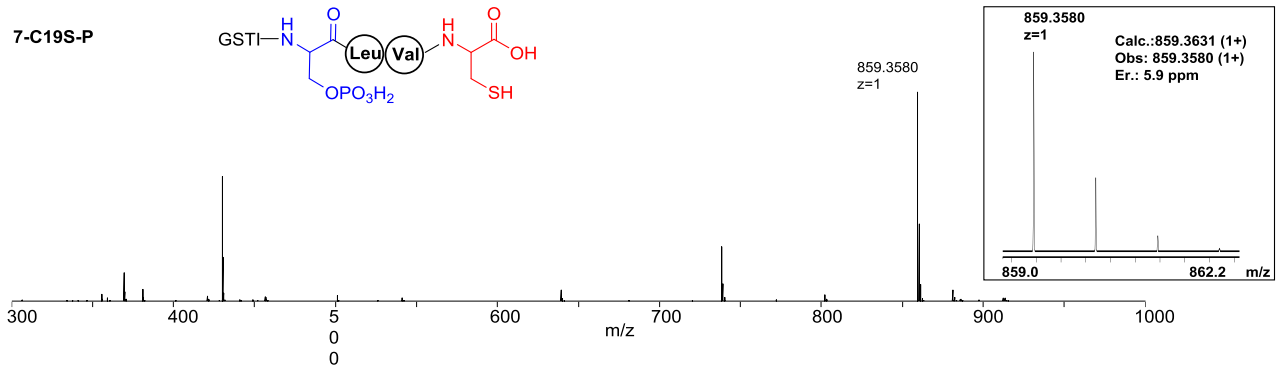
7-C19S-P
GSTI
Leu
Val
OH
SH
OPO3H2
859.3580
z=1
Calc.:859.3631 (1+)
Obs: 859.3580 (1+)
Er.: 5.9 ppm
859.0
862.2
m/z
300
400
500
600
700
800
900
1000
m/z

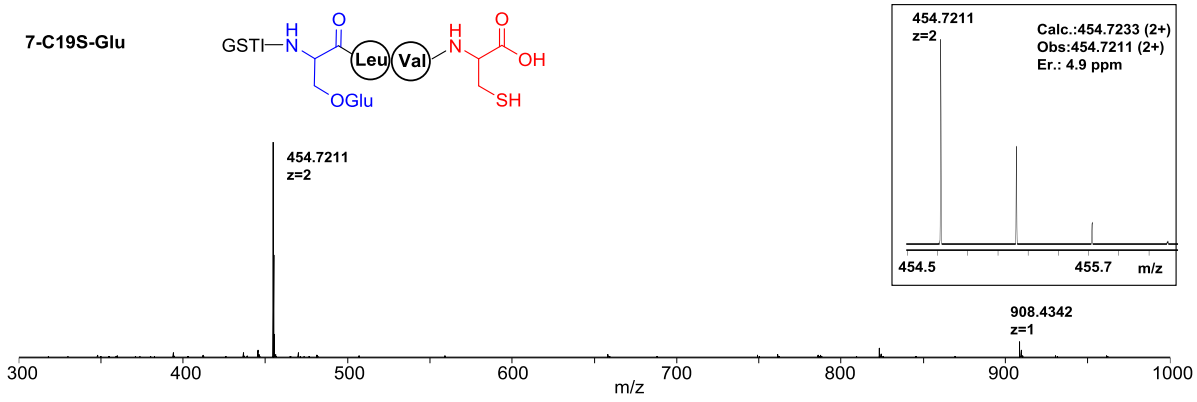
7-C19S-Glu
GSTI
Leu
Val
OH
SH
OGlu
454.7211
z=2
Calc.:454.7233 (2+)
Obs:454.7211 (2+)
Er.: 4.9 ppm
454.5
455.7
m/z
908.4342
z=1
300
400
500
600
700
800
900
1000
m/z

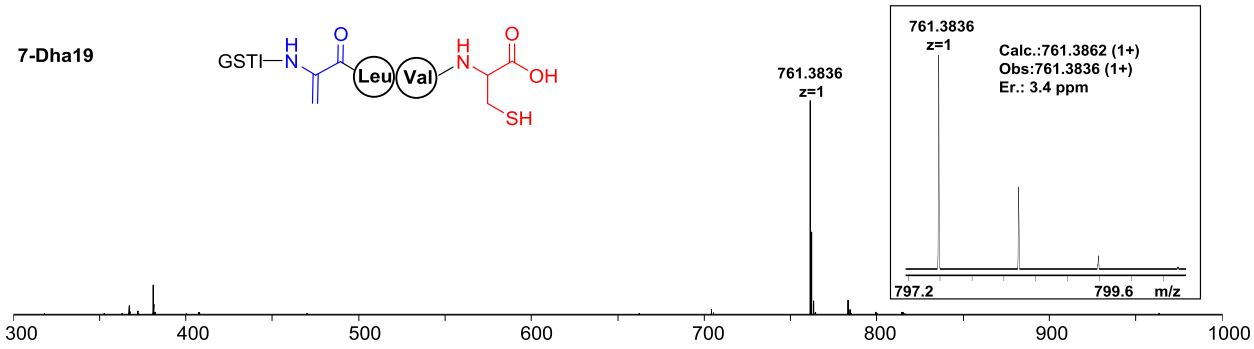

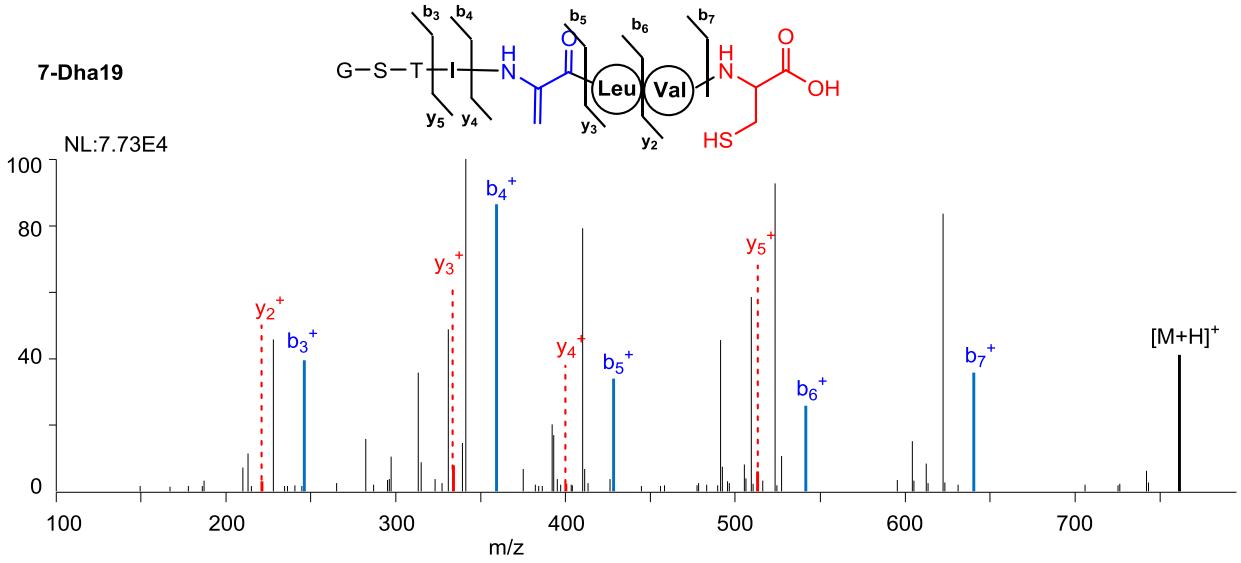

Ions	Calcd.	Obs.	Er. (ppm)
b_3	246.1090	246.1082	3.3
b_4	359.1931	359.1923	2.2
b_5	428.2145	428.2140	1.2
b_6	541.2986	541.2972	2.6
b_7	640.3670	640.3655	2.3
y_2	221.0960	221.0949	5.0
y_3	334.1801	334.1785	4.8
y_4	403.2015	403.2013	0.5
y_5	516.2856	516.2870	2.7

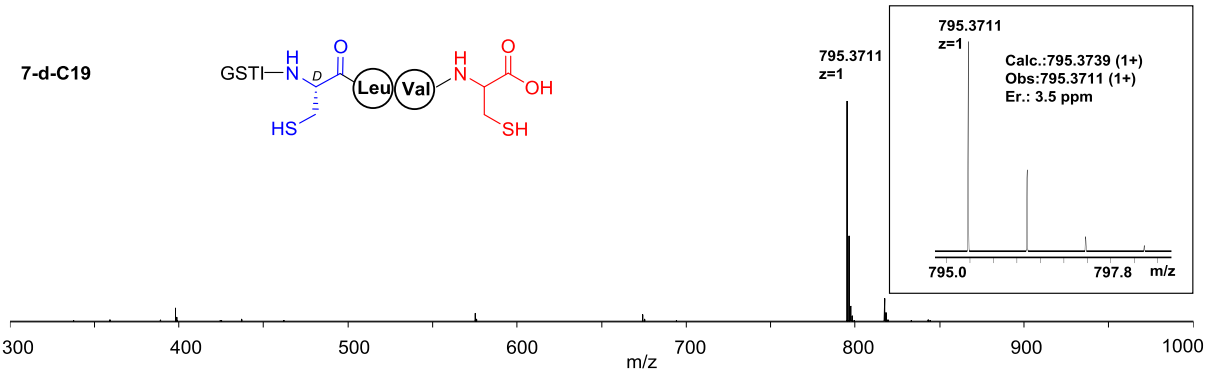
7-d-C19
GSTI
Leu
Val
OH
HS
SH
795.3711
z=1
Calc.:795.3739 (1+)
Obs:795.3711 (1+)
Er.: 3.5 ppm
795.0
797.8
m/z
300
400
500
600
700
800
900
1000
m/z

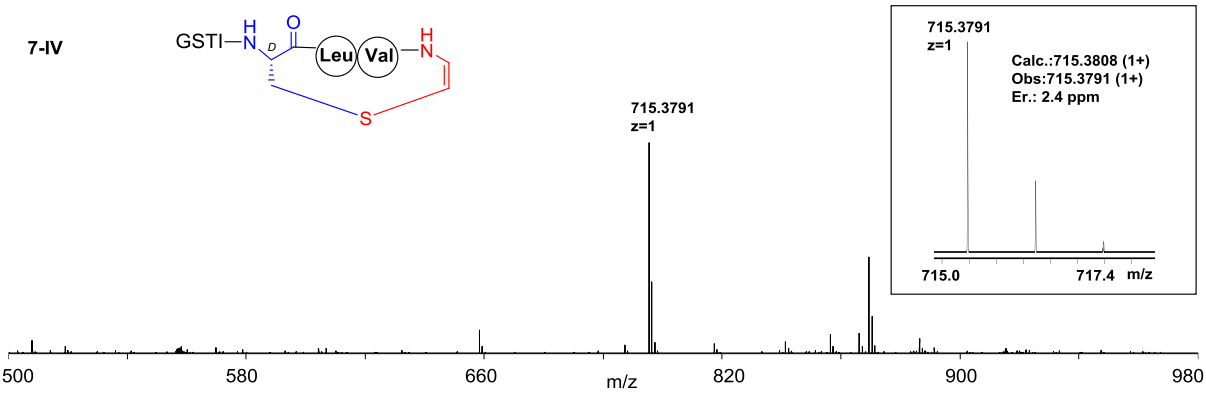
7-IV
GSTI
Leu
Val
S
715.3791
z=1
Calc.:715.3808 (1+)
Obs:715.3791 (1+)
Er.: 2.4 ppm
715.0
717.4
m/z
500
580
660
820
900
980
m/z

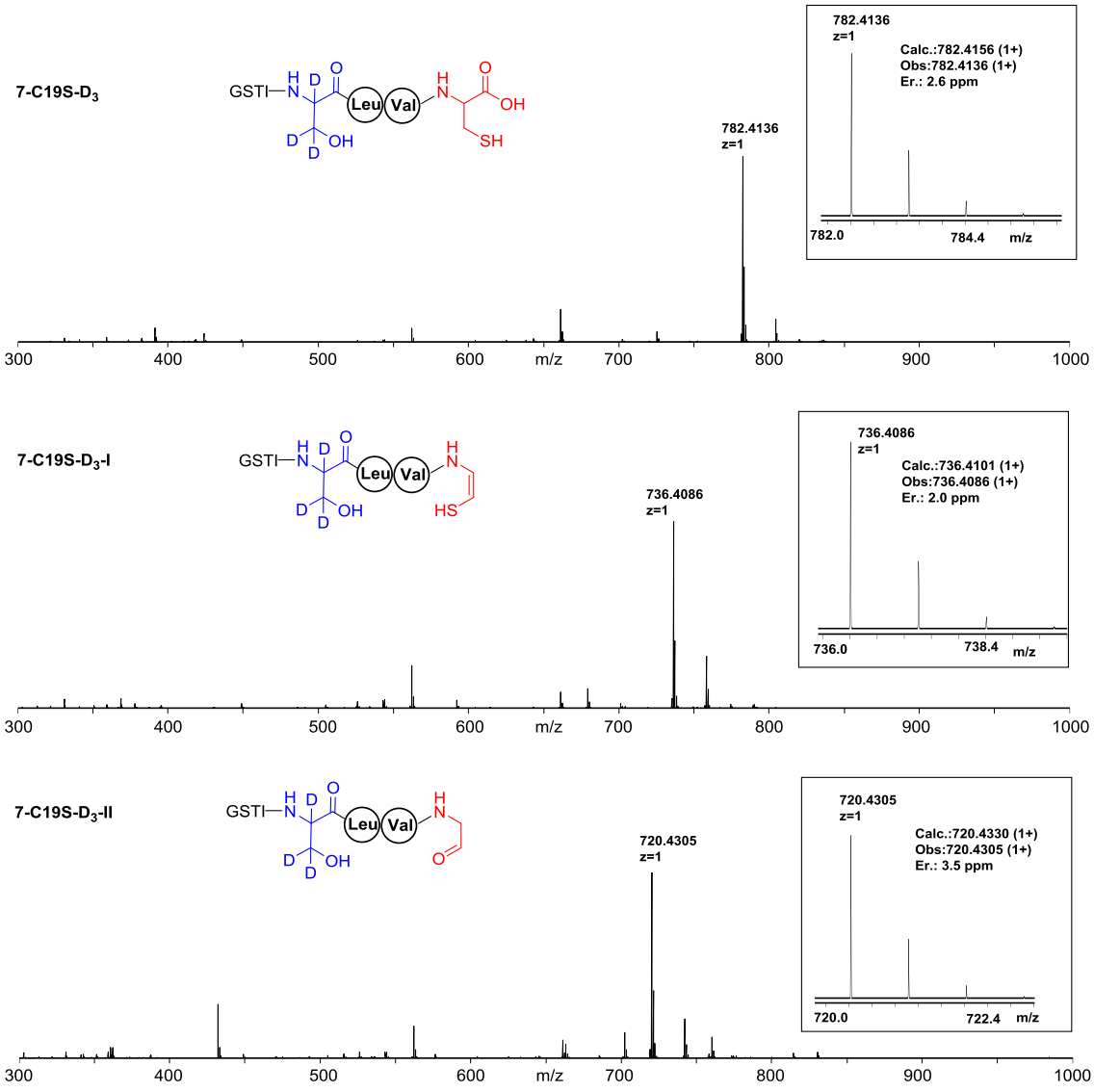
7-C19S-D3
GSTI
Leu
Val
OH
SH
782.4136
z=1
Calc.:782.4156 (1+)
Obs:782.4136 (1+)
Er.: 2.6 ppm
782.0
784.4
m/z
7-C19S-D3-I
HS
736.4086
z=1
Calc.:736.4101 (1+)
Obs:736.4086 (1+)
Er.: 2.0 ppm
736.0
738.4
7-C19S-D3-II
O
720.4305
z=1
Calc.:720.4330 (1+)
Obs:720.4305 (1+)
Er.: 3.5 ppm
720.0
722.4
300
400
500
600
700
800
900
1000

Supplementary Table 5. The ^{1}H and ^{13}C NMR data of **7** in DMSO-d_6.

Substructure	δ_C	δ_H, mult. (*J*, Hz)
Gly	165.9 s	
	40.2 t	3.60 m (overlap) 3.60 m (overlap)
Ser	169.9 s	
Ser-NH		8.55 d (7.8)
	54.8 d	4.56 q (6.7)
	61.9 t	3.59 m (overlap) 3.59 m (overlap)
Thr	169.7 s	
Thr-NH		8.05 d (8.3)
	58.3 d	4.25 m (overlap)
	66.3 d	4.05 m (overlap)
	19.8 q	1.05 d (6.4)
Ile	170.8 s	
Ile-NH		7.70 d (8.6)
	56.8 d	4.25 m (overlap)
	36.9 d	1.71 m (overlap)
	24.1 t	1.60 m (overlap) 1.43 m (overlap)
	15.2 q	0.82 m (overlap)
	11.2 q	0.79 m (overlap)
Cys1	169.4 s	
Cys1-NH		8.20 m (overlap)
	55.1 d	4.40 m (overlap)
	25.9 t	2.75 m (overlap) 2.65 m (overlap)
Leu	171.7 s	
Leu-NH		8.16 m (overlap)
	51.3 d	4.33 m (overlap)
	40.6 t	1.46 m (overlap) 1.46 m (overlap)
	24.1 d	1.06 m (overlap)

	21.5 q	0.82 m (overlap)
	23.1 q	0.87 m (overlap)
Val	170.9 s	
Val-NH		7.75 d (8.8)
	57.4 d	4.20 m (overlap)
	30.7 d	1.99 m (overlap)
	19.1 q	0.87 m (overlap)
	18.0 q	0.83 m (overlap)
Cys2	171.4 s	
Cys2-NH		8.18 m (overlap)
	54.4 d	4.37 m (overlap)
	25.4 t	2.87 dd (13.7, 4.5) 2.75 m (overlap)

Supplementary Table 6. Key data in the 2D-TOCSY f2-slice at f1 experiments in DMSO-d_6.

	2D-TOCSY f2-slice at f1 experiments (correlation signals)	
Residue (subunits)	Selective proton (δ_H in ppm, J in Hz)	Target proton (δ_H in ppm, J in Hz)
Ser	-NH, δ_H 8.50	H2, δ_H 4.54
Thr	-NH, δ_H 8.04	H2, δ_H 4.25 H3, δ_H 4.22 H4, δ_H 1.21
Ile	H2, δ_H 4.10	H3, δ_H 1.62 H4a, δ_H 1.33, H4b, δ_H 1.32 H5, δ_H 0.84 H6, δ_H 0.81
Leu	-NH, δ_H 8.21	H2, δ_H 4.36 H3a, δ_H 1.48, H3b, δ_H 1.47 H4, δ_H 1.24 H5, δ_H 0.83 H6, δ_H 0.81
Val	-NH, δ_H 7.00	H2, δ_H 4.04 H3, δ_H 2.10 H4, δ_H 0.84 H5, δ_H 0.82
-S-CH=CH-NH-	-NH, δ_H 7.16	H1, δ_H 5.53 (J = 7.3 Hz) H2, δ_H 7.14 (J = 7.3 Hz)

Supplementary Table 7. Statistics of X-ray crystallographic data collection and model refinements of $TvaF_{S-87}$ and CypD in their apo-forms.

Data set	SeMet-TvaF	SeMet-CypD	CypD
Data collection			
Wavelength (Å)	0.97915	0.97890	0.97891
Space group	*I*23	*I*4	*I*4
Cell dimensions			
a, b, c (Å)	193.96, 193.96, 193.96	140.11, 140.11, 197.53	139.62, 139.62, 197.21
α, β, γ (°)	90, 90, 90	90, 90, 90	90, 90, 90
Resolution range (Å)	96.98 - 2.27 (2.33 - 2.27)	50.00 - 2.38 (2.42 - 2.38)	50.00 - 2.40 (2.44 - 2.40)
R_{merge} (%) [a]	11.5 (79.3)	9.1 (124.0)	21.0 (81.3)
$I / \sigma I$	29.60 (7.30)	30.20 (2.00)	11.00 (2.44)
Completeness (%)	100.00 (100.00)	100.00 (92.60)	99.60 (100.00)
Redundancy	20.0 (21.7)	13.8 (14.3)	12.6 (13.3)
Refinement			
Resolution (Å)	19.59 - 2.27 (2.35 - 2.27)	44.31 - 2.38 (2.46 - 2.38)	34.88 - 2.40 (2.49 - 2.40)
No. reflections	55718	75830	72525
R_{work} / R_{free} (%) [b]	17.82 (21.83) /20.37 (25.30)	18.03 (23.12) /20.14 (21.85)	18.07 (20.25) /20.19 (26.80)
No. of atoms	5694	8890	8917
Protein	5347	8203	8172
Ligand	124	318	364
Water	223	369	381
Average B-factor (Å^2)	32.06	40.02	39.38
R.m.s.deviations			
Bond lengths (Å)	0.009	0.010	0.009
Bond angles (°)	1.230	1.370	1.260
Ramachandran plot [c]			
Favored region (%)	97.45	98.44	97.48
Allowed region (%)	2.55	1.56	2.52
Outliers (%)	0	0	0

[a] $R_{merge} = \sum|I_i - I_m|/\sum I_i$, where I_i is the intensity of the measured reflection and I_m is the mean intensity of all symmetry related reflections.

[b] $R_{work} = \Sigma||F_{obs}| - |F_{calc}||/\Sigma|F_{obs}|$, where F_{obs} and F_{calc} are observed and calculated structure factors.

$R_{free} = \Sigma_T||F_{obs}| - |F_{calc}||/\Sigma_T|F_{obs}|$, where T is a test data set of about 5% of the total reflections randomly chosen and set aside prior to refinement.

[c] Defined by Molprobity.

Numbers in parentheses represent the value for the highest resolution shell.

Supplementary Table 8. Statistics of X-ray crystallographic data collection and model refinement of CypD in complex with the **ISLVS** peptide

Data set	CypD/ISLVS peptide complex
Data collection	
Wavelength (Å)	0.97891
Space group	*F*23
Cell dimensions	
a, b, c (Å)	228.74，228.74，228.74
α, β, γ (º)	90, 90, 90
Resolution range (Å)	50.00 - 2.30 (2.34 - 2.30)
R_{merge} (%) [a]	24.5 (56.4)
$I / \sigma I$	18.45 (8.14)
Completeness (%)	99.30 (99.30)
Redundancy	37.4 (34.6)
Refinement	
Resolution (Å)	44.02 - 2.30 (2.38 - 2.30)
No. reflections	44029
R_{work} / R_{free} (%) [b]	20.34 (20.06) /22.25 (23.18)
No. of atoms	3106
Protein	2820
Ligand	106
Water	180
Average B-factor (Å^2)	31.91
R.m.s.deviations	
Bond lengths (Å)	0.009
Bond angles (°)	1.26
Ramachandran plot [c]	
Favored region (%)	98.29
Allowed region (%)	1.71
Outliers (%)	0

[a] $R_{merge} = \sum|I_i - I_m|/\sum I_i$, where I_i is the intensity of the measured reflection and I_m is the mean intensity of all symmetry related reflections.

[b] $R_{work} = \Sigma||F_{obs}| - |F_{calc}||/\Sigma|F_{obs}|$, where F_{obs} and F_{calc} are observed and calculated structure factors.

$R_{free} = \Sigma_T||F_{obs}| - |F_{calc}||/\Sigma_T|F_{obs}|$, where T is a test data set of about 5% of the total reflections randomly chosen and set aside prior to refinement.

[c] Defined by Molprobity.

Numbers in parentheses represent the value for the highest resolution shell.

Supplementary References

(1). T. Kieser et al., Practical Streptomyces Genetics (John Innes Foundation, 2000).

(2). Weber T, Blin K, Duddela S, Krug D, Kim HU, Bruccoleri R, *et al*. antiSMASH 3.0-a comprehensive resource for the genome mining of biosynthetic gene clusters. *Nucleic Acids Res.* **43,** W237-243 (2015).

(3). Ishikawa J, Hotta K. FramePlot: a new implementation of the frame analysis for predicting protein-coding regions in bacterial DNA with a high G + C content. *FEMS Microbiol. Lett.* **174,** 251-253 (1999).

(4). States DJ, Gish W. Combined use of sequence similarity and codon bias for coding region identification. *J. Comput. Biol.* **1,** 39-50 (1994).

(5). Gouet P. ESPript/ENDscript: extracting and rendering sequence and 3D information from atomic structures of proteins. *Nucleic Acids Res.* **31,** 3320-3323 (2003).

(6). Braunschweiler L, Ernst RR. Coherence transfer by isotropic mixing: Application to proton correlation spectroscopy. *J. Magn. Reson.* **53,** 521-528 (1983).

(7). Davis DG, Bax A. Simplification of proton NMR spectra by selective excitation of experimental subspectra. *J. Am. Chem. Soc.* **107,** 7197-7198 (1985).

(8). Subramanian S, Bax A. Generation of pure phase NMR subspectra for measurement of homonuclear coupling constants. *J. Magn. Reson.* **71,** 325-330 (1987).

(9). Kessler H, Oschkinat H, Griesinger C, Bermel W. Transformation of homonuclear two-dimensional NMR techniques into one-dimensional techniques using Gaussian pulses. *J. Magn. Reson.* **70,** 106-133 (1986).

(10). Gy. Batta, K.E. K6ver and Cs. Szantay, Jr. Methods for Structure Elucidation by High-Resolution NMR, (1997).

(11). Espindola AP, Crouch R, DeBergh JR, Ready JM, MacMillan JB. Deconvolution of complex NMR spectra in small molecules by multi frequency homonuclear decoupling (MDEC). *J. Am. Chem. Soc.* **131,** 15994-15995 (2009).

(12). Wu J, Lorenzo P, Zhong S, Ali M, Butts CP, Myers EL, *et al*. Synergy of synthesis, computation and NMR reveals correct baulamycin structures. *Nature* **547,** 436-440 (2017).

(13). Wang, Z. et al. Automatic crystal centring procedure at the SSRF macromolecular crystallography beamline. *J. Synchrotron. Radiat.* **23,** 1323-1332 (2016).

(14). Otwinowski, Z. & Minor, W. Processing of X-ray diffraction data collected in oscillation mode. Macromolecular Crystallography, *Pt. A.* **276,** 307-326 (1997).

(15). Storoni, L.C., McCoy, A.J. & Read, R.J. Likelihood-enhanced fast rotation functions. *Acta. Crystallographica Section D-Biological Crystallography* **60,** 432-438 (2004).

(16). Emsley, P. & Cowtan, K. Coot: model-building tools for molecular graphics. A*cta. Crystallographica Section D-Biological Crystallography* **60,** 2126-2132 (2004).

(17). Murshudov, G.N., Vagin, A.A. & Dodson, E.J. Refinement of macromolecular structures by the maximum-likelihood method. *Acta. Crystallographica Section D-Biological Crystallography* **53,** 240-255 (1997).

(18). Adams, P.D. et al. PHENIX: building new software for automated crystallographic structure determination. *Acta. Crystallographica Section D-Biological Crystallography* **58,** 1948-1954 (2002).

(19). Davis, I.W. et al. MolProbity: all-atom contacts and structure validation for proteins and nucleic acids. *Nucleic Acids Res.* **35,** W375-W383 (2007).